The Dissertation Committee for Devinder Kaur Ubhi Certifies that this is the approved version of the following dissertation:

Structural Analysis and Discovery of Lead Compounds for the Fungal Methionine Synthase Enzyme

Committee:

Jon D. Robertus, Supervisor

Eric V. Anslyn

Dean R. Appling

Walter L. Fast

Adrian T. Keatinge-Clay

Structural Analysis and Discovery of Lead Compounds for the Fungal Methionine Synthase Enzyme

by

Devinder Kaur Ubhi, B.A.&S.

Dissertation

Presented to the Faculty of the Graduate School of

The University of Texas at Austin

in Partial Fulfillment

of the Requirements

for the Degree of

Doctor of Philosophy

The University of Texas at Austin

December 2013

Dedication

To my wonderful family and friends who have supported and encouraged me.

Acknowledgements

I would like to thank Dr. Robertus for taking me into his lab and giving me the opportunity to experience the highs and lows of crystallography and drug discovery. I appreciate his patience, kind support and guidance. I would also like to thank Dr. Kathryn Kavanagh who provided me with excellent training, guidance and support. I would also like to thank the members of my supervisory committee, Dr. Anslyn, Dr. Appling, Dr. Fast, and Dr. Keatinge-Clay, for their guidance and insight.

I greatly appreciate the help and advice of Dr. Art Monzingo, Dr. Josh Beckham and former members of the Robertus lab: Grace Kago, Lawrence Manzano and Beth Eisenhut. I would also like to thank Natalie Potts for seamlessly taking care of financial and bureaucratic matters.

Finally, it has been a privilege to attend graduate school and to have had the support and encouragement of my family and friends. I would like to especially thank Steven R. Ritchie for his unwavering support, encouragement and exchange of ideas.

Structural Analysis and Discovery of Lead Compounds for the Fungal Methionine Synthase Enzyme

Devinder Kaur Ubhi, Ph.D.

The University of Texas at Austin, 2013

Supervisor: Jon D. Robertus

Methionine synthases catalyze methyl transfer from 5-methyl-tetrahydrofolate (5-methyl-THF) to L-homocysteine (Hcy) in order to generate methionine (Met). Mammals, including humans, use a cobalamin dependent form, while fungi use a cobalamin independent protein called Met6p. The large structural differences between them make Met6p a potential anti-fungal drug target.

Met6p is a 90 kDa protein with the active site located between two $(\beta\alpha)_8$ barrels. The active site has a catalytic Zn^{2+} and binding sites for the two substrates, Hcy and folate. I present the crystal structures of three engineered variants of the Met6p enzyme from *Candida albicans*. I also solved Met6p in complex with several substrate and product analogs, including Hcy, Met, Gln, 5-methyl-THF-Glu_3 and Methotrexate-Glu_3 (MTX-Glu_3), and the bi-dentate ligand S-adenosyl homocysteine. Also described is a new fluorescence-based activity assay monitoring Hcy. Lastly, a high-throughput Differential Scanning Fluorimetry (DSF) assay was used to screen thousands of compounds in order to identify ligands which bind Met6p.

My work details the mode of interaction of Hcy and folate with the Met6p protein. Several residues important to activity were discovered, like Asn 126 and Tyr 660, and proven to be important by site directed mutagenesis. Structural analysis

revealed an important aspect of the mechanism. When Hcy binds to its pocket it makes strong ion pairs with the enzyme. In particular, 614 moves toward the substrate amine and triggers a rearrangement of active site loops; this draws the catalytic Zn^{2+} toward the Hcy thiol where a new ligand bond is formed, activating the thiol for methyl transfer.

The work presented here lays the groundwork for structure based drug design and makes the development of Met6p specific bi-dentate ligands feasible. The fluorescence based activity assay I developed was successfully used to test the folate analog MTX-Glu_3, which inhibits with an IC_{50} of ~4 mM. I also discovered our first bi-dentate ligand in the form of S-adenosyl homocysteine.

Table of Contents

List of Tables

List of Figures

CHAPTER 1

INTRODUCTION AND BACKGROUND

INTRODUCTION

In mammals the amino acid methionine (Met) cannot be synthesized de novo and must be acquired through diet, either as Met or as Homocysteine (Hcy). Plants, bacteria and yeast are equipped to biosynthesize Met through the sulfur assimilation pathway. However, all organisms metabolize Met and recycle the end-product, Hcy, either through the methionine synthase, betaine homocysteine methyltransferase (BHMT) or S-methylmethionine Hcy S-methyltransferase (HMT) enzymes. The methionine synthases can be further divided into two groups, one that uses the cobalamin cofactor and another which is cobalamin-independent. Organisms such as mammals and some bacteria contain the cobalamin-dependent methionine synthase referred to as MetH. Organisms such as fungi, plants, archae and insects are deficient in vitamin B12 and thus contain the cobalamin-independent methionine synthase known as MetE. Certain bacteria have both enzymes.

MetE and MetH are zinc dependent enzymes that generate methionine by catalyzing the transfer of a methyl from 5-methyl-tetrahydrofolate-glutamate (5-methyl-THF-Glu) to Hcy (Figure 1.1). Although both carry out the same overall reaction, these proteins are dissimilar in sequence and structure. MetH from *E.coli* has been extensively characterized by biochemical/biophysical methods and X-ray crystallography. It is a large 140 kDa enzyme which consists of 4 modules that bind Hcy and Zn^{2+}, 5-methyl-THF-Glu_n, vitamin B-12, and S-adenosyl methionine (AdoMet), respectively (Figure 1.2). The B12-module mediates the methyl transfer reaction between the folate and Hcy through a methylcobalamin intermediate. MetE has also been well characterized from *E.*

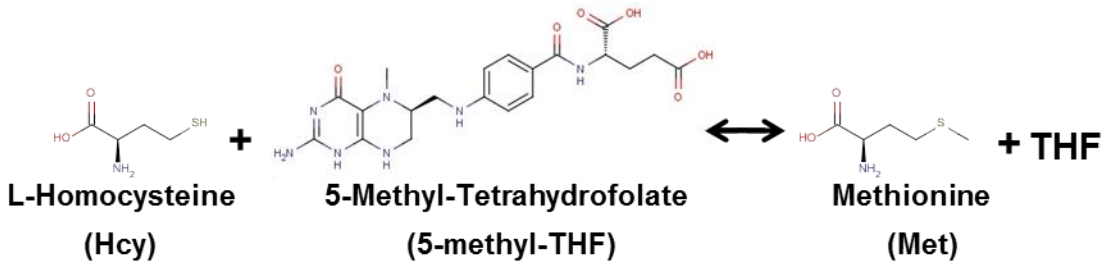

Figure 1.1 Overall reaction catalyzed by methionine synthase. Both the cobalamin-independent (MetE) and cobalamin-dependent (MetH) methionine synthase enzymes bind Hcy and 5-methyl-THF and mediate an alkylation reaction to generate Met and by-product THF.

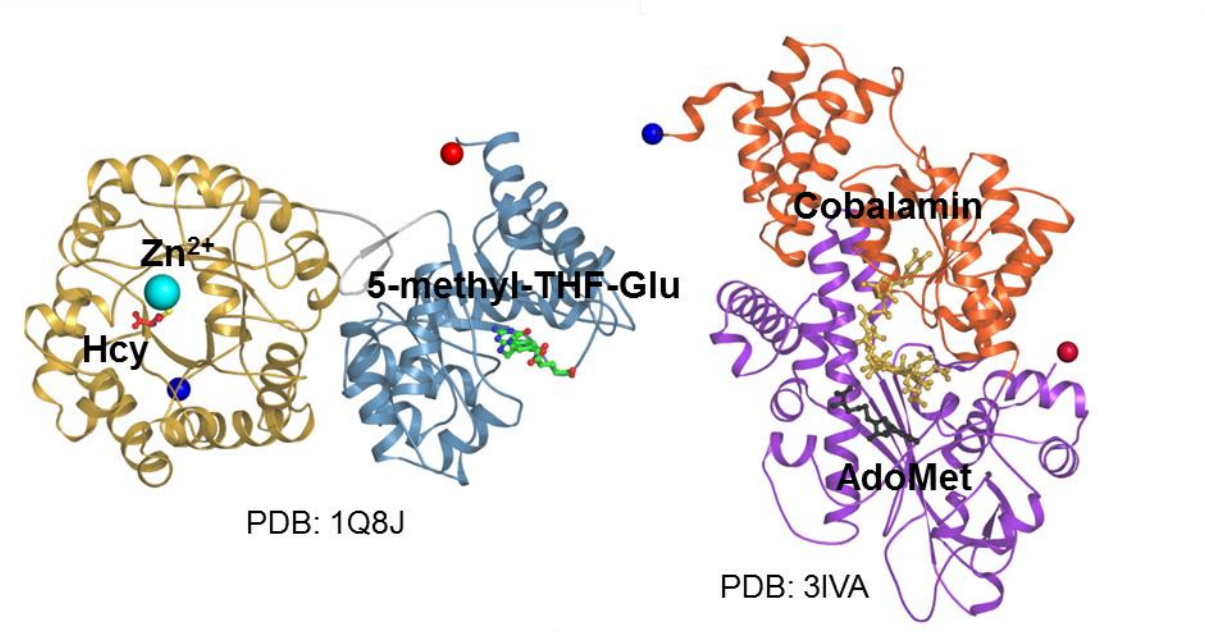

Figure 1.2 Structure of the cobalamin-dependent methionine synthase (MetH). The Hcy, 5-methyl-THF-Glu, AdoMet, and cobalamin are shown as sticks and colored red, green, grey, and golden, respectively. The Zn^{2+} is shown as a cyan sphere. The N and C-terminal residues are marked as blue and red spheres, respectively.

coli through biochemical/biophysical methods with X-ray structures solved from a variety of organisms. MetE is about half the size of MetH (90 kDa) with just two domains that are connected by a flexible linker (Figure 1.3). The active site is located in a cleft between the two domains and binds a Zn^{2+}, Hcy, and 5-methyl-THF-Glu_3. MetE catalyzes a direct methyl transfer reaction between the Hcy thiolate and the N^5 methyl group of 5-methyl-THF-Glu_3.

The Robertus and Appling groups have long been interested in the cobalamin-independent methionine synthase gene from *Candida albicans* (MET6) as a potential anti-fungal drug design target. Fungal pathogens are a health concern, particularly to immuno-compromised individuals, and the *Candida* species are associated with the highest mortality rate. In particular *C. albicans* leads in the number of patients diagnosed with fungal nosocomial bloodstream infections (Edmond, Wallace et al. 1999). The MET6 gene encodes the Met6p enzyme which shares ~40-50% sequence identity with the *E. coli* MetE. In fungi, Met6p carries out the last step in methionine biosynthesis and is a point in the metabolic map where the one-carbon folate metabolism cycle converges with the methyl cycle (Figure 1.4). Methionine is used to generate S-adenosyl methionine (AdoMet) which is the major source for one-carbon units vital for biosynthesis. A defective Met6p is expected to have lethal consequences as a result of flawed DNA/RNA synthesis, AdoMet mediated methylation reactions, and protein synthesis. In theory, the structural differences between the MetH of the mammalian host and the fungal Met6p enzyme make it possible to selectively target and inhibit the pathogenic enzyme.

The Robertus and Appling groups have investigated the importance of the *C. albicans* MET6 gene for fungal growth and have characterized the Met6 protein by steady state kinetics. Suliman cloned, expressed, purified and characterized the

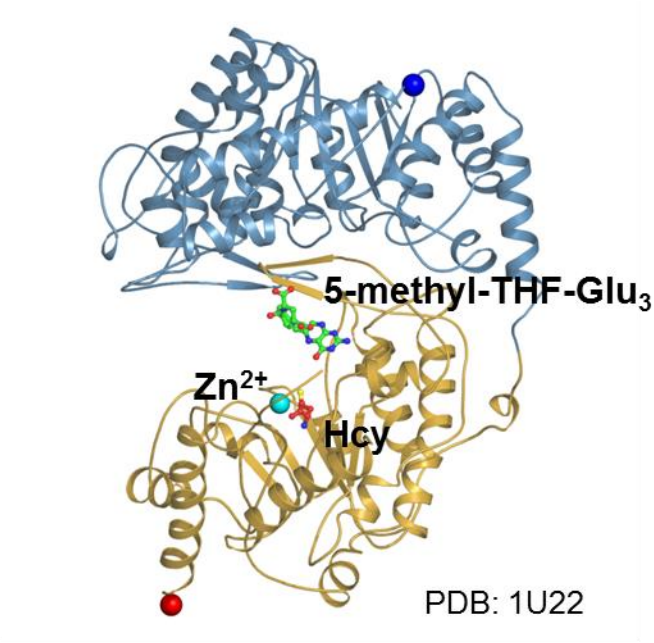

Figure 1.3 Structure of the cobalamin-independent methionine synthase (MetE). The Hcy and 5-methyl-THF are shown as sticks and colored red and green, respectively. The Zn^{2+} is shown as a cyan sphere. The N and C-terminal residues are marked as blue and red spheres, respectively.

methionine synthase from *C. albicans* and *S. cerevisiae* (Suliman, Sawyer et al. 2005). The MET6 gene from either yeast was able to complement the other and had similar substrate specificities. Both were able to utilize the 5-methyl-THF-Glu_n with at least a di-glutamate tail at K_M values of around 100 μM and k_{cat} of around 25/min. The K_M for Hcy was ~14 μM. Suliman also used homologous recombination techniques to test the growth of the diploid *Candida albicans* strains missing one or both MET6 genes; she also created another strain containing one functional MET6 gene under a regulatable GAL promoter (Suliman, Appling et al. 2007). A single MET6 gene knockout had little effect on fungal growth, however a double gene knockout was found to be lethal, even if the growth media was supplemented with methionine. As expected, the conditional mutant

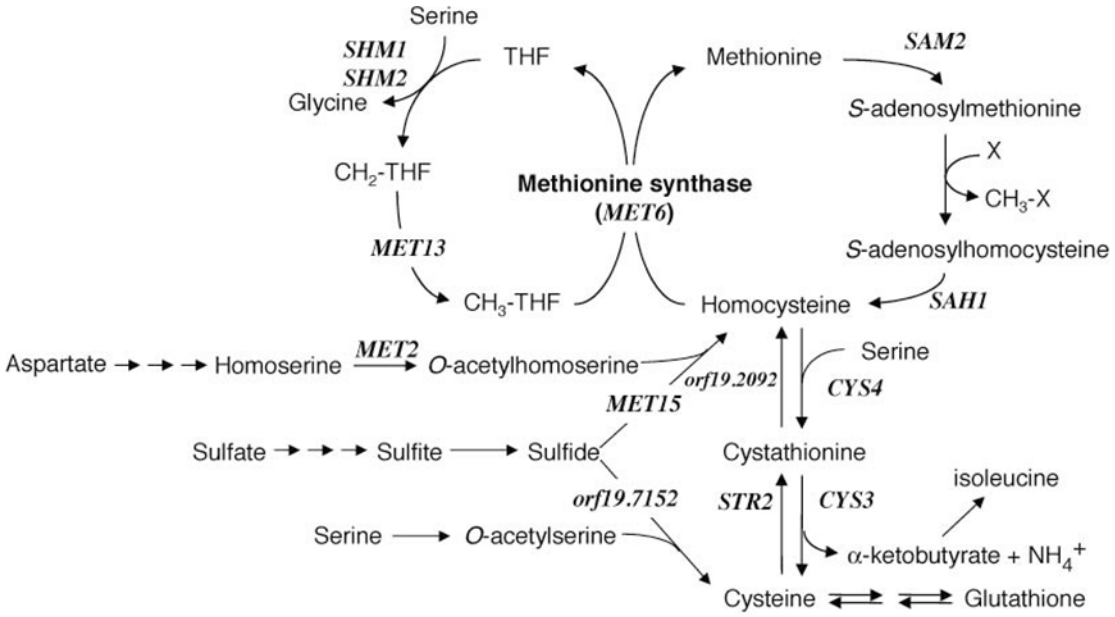

Figure 1.4 Methionine metabolism. The MET6 gene sits at a point of convergence between the folate mediated one-carbon metabolism and methionine biosynthesis. The methionine metabolism cycle generates Hcy which can enter the transsulfuration pathway.

grew as well as the wild-type under inducing conditions, zero growth was observed under repressing conditions, and colonies were observed under repressing conditions supplemented with exogenous methionine. This growth was due to a leaky GAL promoter. This work showed that the MET6 gene from the pathogen *C. albicans* is essential for fungal growth and that some amount of Met6p must be present in order to rescue fungal growth.

Although attempts made to crystallize the wild-type Met6p failed, Prasannan was able to create a Met6p model using the existing MetE structures and used site directed mutagenesis to identify a number of key catalytic and substrate binding residues (Prasannan, Suliman et al. 2009). She found that the ionic interaction observed between the side-chain of Asp614 and the Hcy ammonium group in MetE homologs is essential

for enzyme activity and *C. albicans* growth. Asp504 is another conserved residue that uses its side chain to bind and orient the folate ring. Mutants of Asp504 were also kinetically inactive and each strain failed to grow. Lastly, the aromatic ring of Trp576 is believed to make non-specific hydrophobic interactions with the folate ring and according to this mutagenesis study, could be replaced by phenylalanine but not alanine.

In continuing this research project, I used X-ray crystallography, a novel fluorescence-based activity assay and the biophysical method known as differential scanning fluorimetry (DSF) to study the Met6p protein structure and mechanism, and to identify novel fungistatic compounds. Since the native Met6p enzyme could not be crystallized using traditional high-throughput screens, the surface entropy reduction technique (Cooper, Boczek et al. 2007) was used to create three fully active variants that formed useful crystals which diffracted to at least 2.7 Å (Ubhi, Kavanagh et al. 2011). In these variants, Lys103, Lys104, and Glu107 were all converted to Tyr (Met6pY), Thr (Met6pT), and Ala (Met6pA).

Met6pA was used to obtain enzyme-ligand complexes due to its high diffraction resolution and possession of just one molecule in the asymmetric unit. Several X-ray structures were solved with Met6pA in a binary or ternary complex with: Hcy, Met, Glutamine (Gln), 5-methyl-THF-Glu_3, Methotrexate-$Glutamate_3$ (MTX-Glu_3), and S-adenosyl homocysteine (SAH). These structures provided a wealth of information with respect to substrate binding pockets, structural dynamics and potential drug design strategies.

A novel fluorescence based assay was developed to monitor Met6p activity, to characterize various mutants, and to test potential inhibitors, such as MTX-Glu_3. The commercially available compound Measure-iT^{TM} was used in the fluorescence-based activity assay to selectively measure the concentration of unused Hcy in a Met6p

reaction. Lastly, the DSF method was used to screen for ligands which bound and raised the melting temperature (Tm) of the wild-type Met6p enzyme. The method was optimized for high-throughput 96-well format with excellent repeatability, low standard deviation, and a Z' factor of 0.5-1 per plate. Compounds (cmnds) were screened from three diverse libraries: NIH Clinical Collection (731 cmnds), ChemBridge Fragment (4000 cmnds) and ChemBridge KINASet libraries (4000 cmnds). The observed hits were further evaluated using the absorbance based kinetic assay and X-ray crystallography.

BACKGROUND

Folate-Mediated One-Carbon Metabolism

Many processed foods are fortified with the synthetic B-vitamin, folic acid, while green leafy vegetables contain a number of natural folate derivatives (Figure 1.5). These derivatives include: dihydrofolate (DHF), tetrahydrofolate (THF), 5-methyl-THF, 10-formyl-THF, and 5,10-methylene-THF. These dietary sources provide us with an essential vitamin which can best be described as a carrier of one carbon units in folate-mediated one-carbon metabolism. Folate-dependent one-carbon metabolism is compartmentalized in the cytoplasm, mitochondria, nucleus and chloroplast and involves numerous enzymes and impacts the overall metabolic balance at the cellular level (Figure 1.6) (Appling 1991, Tibbetts and Appling 2010, Stover and Field 2011).

The overall picture of folate metabolism includes the one-carbon generating enzymes, the folate-interconverting enzymes, the folate-dependent biosynthetic enzymes and folate binding proteins (Appling 1991, Scott 1999, Litwach 2008). There is competition between these enzymes for free folate which appears to be tightly regulated by cells (Herbig, Chiang et al. 2002). Many of these enzymes have functionally independent domains, specialized for the generation of one-carbon units and for

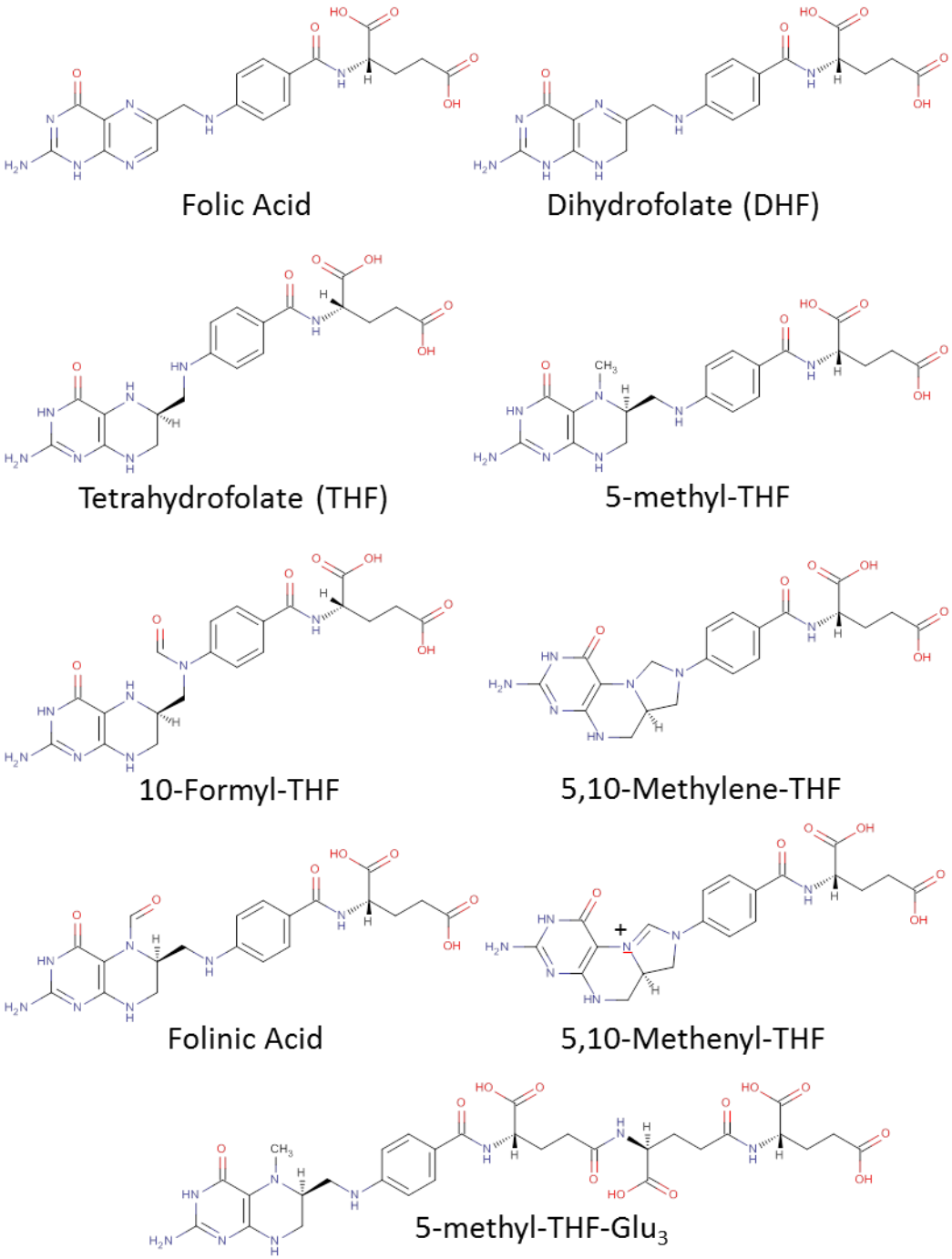

Figure 1.5 The synthetic B-vitamin Folic acid and various natural derivatives. The naturally occurring derivatives are reduced and often carry one carbon units.

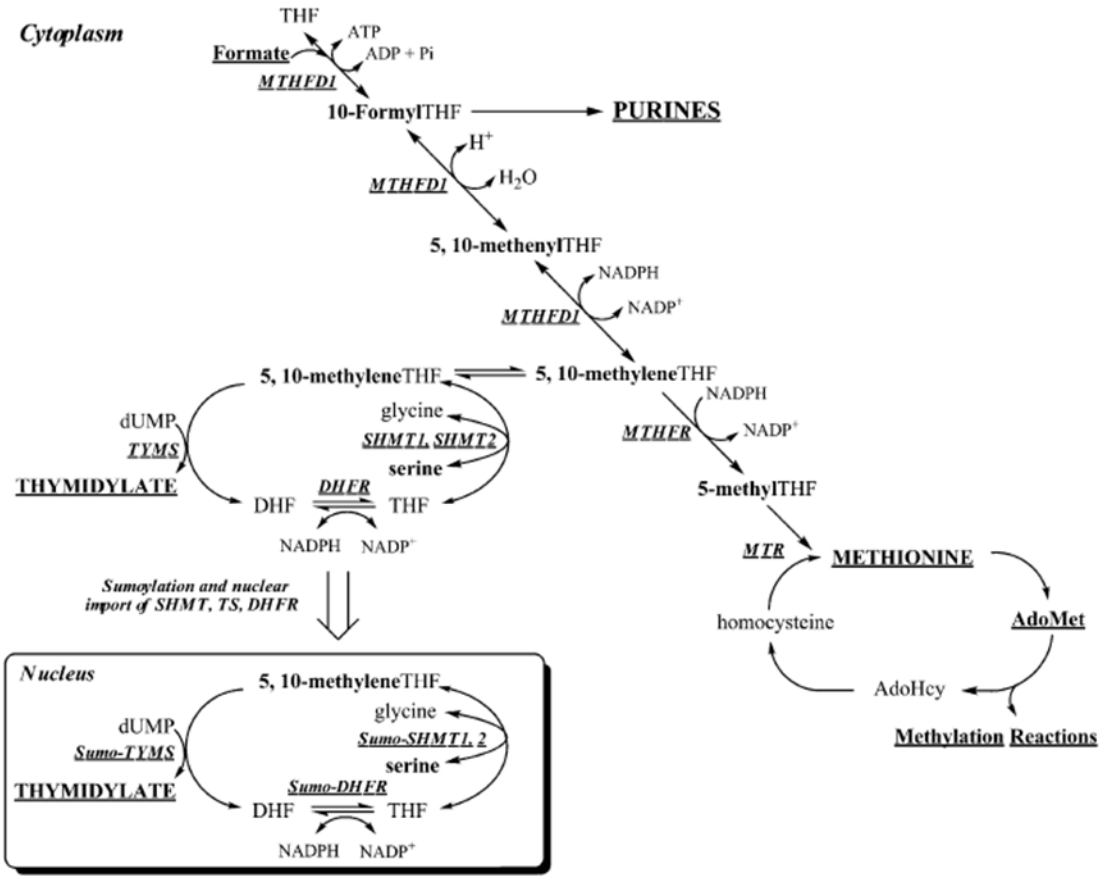

Figure 1.6 Folate-mediated one-carbon metabolism. Shown compartmentalized in the cytoplasm and nucleus. This figure is taken from Stover and Field 2011.

subsequent inter-conversion of the C1-folates. In order to enter the one-carbon metabolism cycle, the aromatic ring of folic acid must first be reduced in two steps by the enzyme dihydrofolate reductase (DHFR) to tetrahydrofolate (THF) (Schnell, Dyson et al. 2004). THF is then able to accept one carbon units in a range of oxidation states for use in a variety of biosynthetic reactions.

The one-carbon generating enzymes include serine hydroxymethyltransferase (SHMT), 10-formyltetrahydrofolate synthetase (FTHFS), and the bifunctional enzyme

complex of glutamate formiminotransferase and formimidoyltetrahydrofolate cyclodeaminase (Litwach 2008). In a reversible reaction, SHMT catabolizes the amino acid serine, making 5,10-methylene-THF and glycine (Rao, Talwar et al. 2000). The limited pool of methylene-THF can support thymidylate biosynthesis, methionine synthesis or purine biosynthesis. Formate is used as a source of carbon by FTHFS in order to synthesize 10-FormylTHF (McGuire and Rabinowitz 1978). The degradation of histidine generates formiminoglutamic acid which is processed by glutamate formiminotransferase to make 5-formiminoTHF (Kohls, Sulea et al. 2000). This intermediate is converted to 5,10-methenylTHF through the formimidoyltetrahydrofolate cyclodeaminase to be used for one-carbon transfer reactions.

The folate-interconverting enzymes include the 5,10-methenylTHF cyclohydrolase/dehydrogenase (MTHFC)/(MTHFD), 10-FormylTHF dehydrogenase (FDH), 5,10-MethenylTHF synthetase (MTHFS), and 5,10-MethyleneTHF reductase (MTHFR) (Litwach 2008). MTHFC carries out the reversible inter-conversion of 10-formylTHF and 5,10-methenylTHF. MTHFD carries out the reversible inter-conversion of 5,10-methenylTHF and 5,10-methyleneTHF (Eadsforth, Cameron et al. 2012). FDH catalyzes the irreversible hydrolysis of 10-formylTHF to THF and formate (Krupenko 2009). MTHFS carries out the irreversible conversion of 5-formylTHF to 5,10-methenylTHF (Holmes and Appling 2002). It is the only known enzyme to use folinic acid. MTHFR catalyzes the irreversible reduction of 5,10-methyleneTHF to 5-methylTHF and commits the C1-THF for methionine synthesis (Cathou and Buchanan 1963).

The folate dependent biosynthetic enzymes include thymidylate synthase (TS), methionine synthase (MS), the glycinamide ribonucleotide formyltransferase (GARFT) and 5-aminoimidazole-4-carboxamide ribonucleotide formyltransferase (AICARFT)

enzymes. TS uses 5,10-methyleneTHF to convert dUMP to dTMP, which is essential to DNA synthesis/replication and repair (Finer-Moore, Santi et al. 2003).

MS uses 5-methylTHF to methylate Hcy and produce Met (Gonzalez, Banerjee et al. 1992). MS thereby supports various methyl transfer reactions since it provides the precursor for the potent methyl donor, AdoMet. MS also removes Hcy, a toxic biomarker, from the cell and regenerates the THF to support folate-mediated one-carbon metabolism. GARFT and AICARFT use 10-formylTHF to add formate into the C8 and C2 positions of purine (Daubner, Schrimsher et al. 1985).

An intricate network of interdependent biosynthetic pathways drives folate metabolism. Folate mediated one-carbon metabolism is directly responsible for the synthesis of methionine, purines and thymidylate, and indirectly involved with amino acid and formate metabolism and DNA/protein methylation.

Folate deficiency results in seriously pathological phenotypes in mammals, including megaloblastic anemia, spina bifida, cardiovascular disease, neuropsychiatric disorders and increased sensitivity to oxidative stress (Litwach 2008). Mutations in the folate-mediated one-carbon pathway can lead to inborn errors in folate metabolism. Some of the most serious phenotypes are associated with mutations in the gene encoding methionine synthase. Enzymes currently targeted by anti-folates for the treatment of cancer, parasitic infection, malarial infection, and rheumatoid arthritis include DHFR, TS, SHMT, MTHFR, and GARFT.

The chemical and physical properties of folates

A number of different folates exist in nature and share the same overall structure consisting of a covalently linked pterin ring, p-aminobenzoic acid (PABA) and a glutamate residue (Figure 1.7). Folates vary in the level of oxidation of the pterin ring,

the nature of the carbon moiety at the N5 and/or N10 position, and in the number of glutamates in the polyanionic tail. All biologically relevant derivatives have a reduced pyrazine ring and exist as THF scaffolds (Maden 2000). THF can undergo methylation at position N5 and formylation at positions N5 or N10 (Scott 1999). The length of the poly-γ-glutamate tail is modified by the enzyme folylpolyglutamate synthetase and varies by cell type as well as compartment. Tail length effects affinity for certain folate-dependent enzymes, mediates cellular retention of folates, functions in substrate channeling and regulation of one carbon metabolism (Chabner, Allegra et al. 1985, Appling 1991).

The chemical and physical properties of folates and pteridines/pterins have been under investigation since 1925 with the discovery of folate in spinach and of pteridine/pterin as the pigment in butterfly wings (Blakley 1969). The properties of folates are largely determined by the pteridine constituent. Pteridine provides the platform for numerous substituted pterins, the most important of which is pterin, a 2-amino-4-oxo pteridine. Such compounds are found not only in wings, but also the skin of reptiles, amphibians, and fish.

Pteridine consists of a bicyclic nitrogenous ring system (fused pyrimidine and pyrazine rings) which is soluble in water and organic solvents (Figure 1.7). Substitution of a keto group at position 4 and amino group at position 2 results in a pterin. Pterins are poorly soluble in water (but can be dissolved in 0.05 M NaOH) and are very stable and resistant to oxidation. The UV spectra of pterins exhibit a maximum at wavelengths greater than 300 nm. Reduction takes place in the pyrazine ring to form 7,8-dihydropterins, 5,6,7,8-tetrahydropterins and 6-substituted tetrahydropterins but these derivatives are unstable and readily oxidized (Basu and Burgmayer 2011).

Folic acid can also be described as a 6-alkylpterin but is completely oxidized and therefore relatively stable at physiological pH under anaerobic conditions. However,

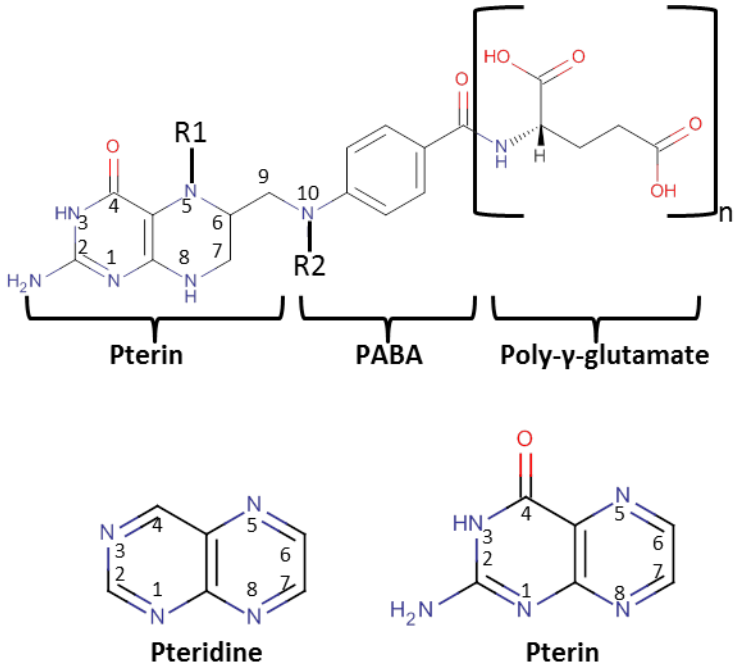

Figure 1.7 The general structure of folate. Folates consist of a pterin ring covalently linked to a p-aminobenzoic acid (PABA) and a glutamate residue. The naturally occurring folates have a reduced pyrazine ring. Folates can be substituted at positions R1 and R2 and have 1-6 glutamates.

alkaline hydrolysis under aerobic conditions or photodecomposition by sunlight will yield p-aminobenzoylglutamic acid and a pteridine. Folic acid has a UV absorbance maxima at neutral pH (ε_{282} = 27.6 mM^{-1}). Reduction of folic acid results in the biologically relevant 7,8-dihydrofolate (DHF) and 5,6,7,8-tetrahydrofolates (THF). These compounds are labile and must be protected from light and air and if possible stored with reducing agents and ascorbate. Naturally occurring THFs have an asymmetric center at the C-6 position corresponding to the S configuration (Fontecilla-Camps 1979). The THF dissociation constants have been reported: N1, pK_a 1.24; N5, pK_a 4.82; N10, pK_a -1.25; amide, pK_a 10.5; gamma-carboxyl, pK_a 4.8; alpha-carboxyl, pK_a 3.5 (Kallen and Jencks 1966).

The sulfur containing compounds: Homocysteine and Methionine

The element sulfur is present in a number of organic compounds including the amino acids cysteine (Cys) and methionine (Met), the vitamins biotin and thiamin, the cofactors S-adenosyl methionine (AdoMet), coenzyme A and lipoic acid, and the anti-oxidants glutathione and taurine (Takahashi, Kopriva et al. 2011). These molecules are synthesized through various pathways which can all be traced back to a sulfur assimilation event. The vast amounts of inorganic sulfur present in the atmosphere and soil is assimilated by plants, fungi, and some bacteria through their respective sulfur assimilation pathways (Figure 1.8). Plants and bacteria reduce the readily available sulfate ($SO4^{-2}$) into cysteine (Cys) (Hatzios and Bertozzi 2011, Takahashi, Kopriva et al. 2011). Yeast or fungi assimilate the inorganic sulfate into the organic molecule Hcy (Thomas and Surdin-Kerjan 1997). Cys and Hcy enter the transsulfuration or the Hcy methylation cycles to make other necessary organic molecules. In organisms that assimilate sulfate, the sulfur containing amino acids like Met or Cys are synthesized de novo. Most microorganisms also have transporters for Met. Mammals on the other hand depend on their diet to acquire the sulfur-containing amino acids, although they can interconvert them once acquired.

Hcy is similar in structure and reactivity to the amino acid Cys and in *S. cerevisiae* both are interconverted through the transsulfuration pathway (Figure 1.8). Both have an amino acid backbone and sulfur containing hydrocarbon side chains of different lengths (Figure 1.9). Under physiological conditions, the sulfur exists as a thiol/sulfhydryl group. The amino acid Cys can form disulfide bonds that stabilize protein structure. The amino acid can also mediate enzyme catalysis as a general acid or by serving as a mechanistic nucleophile. The thiolates also serve as metal ligands in

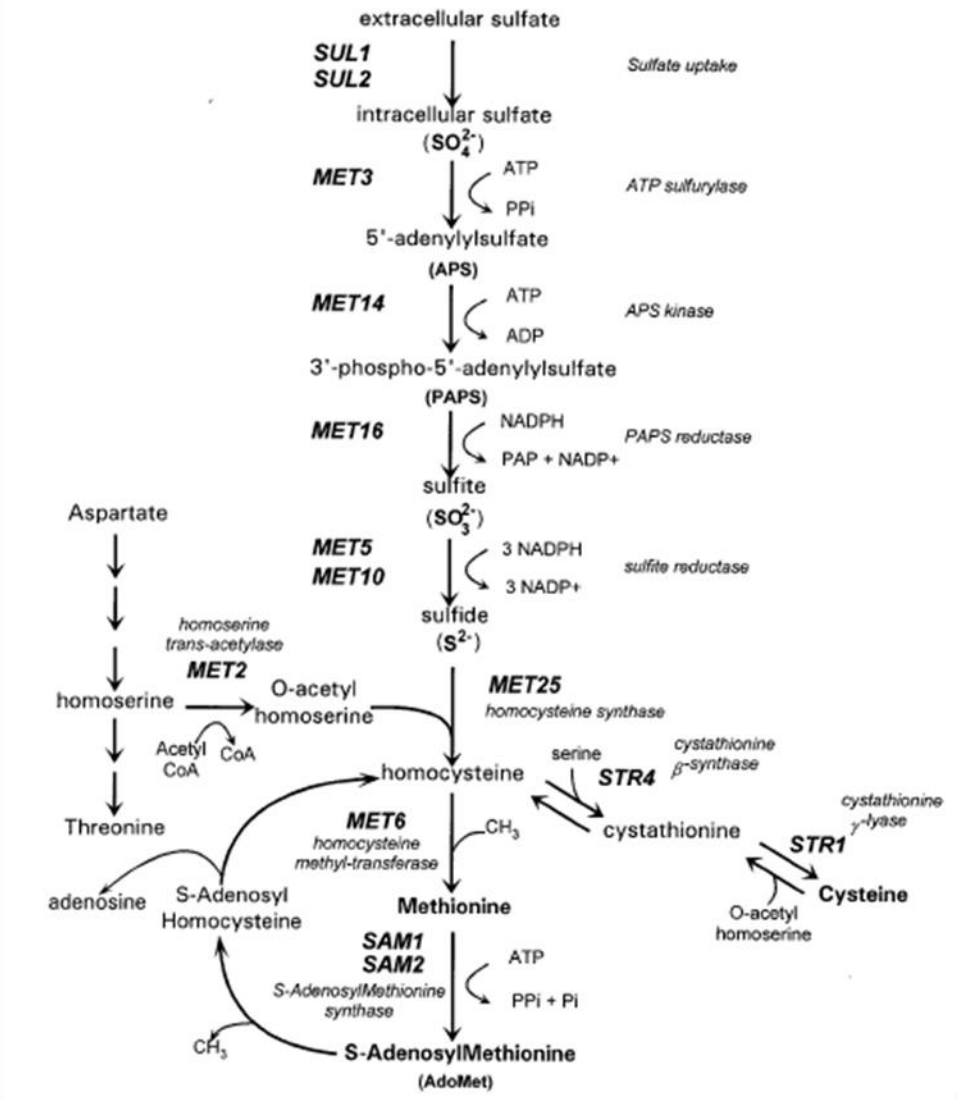

Figure 1.8 The sulfur assimilation pathway in *S. cerevisiae*. Yeast assimilate inorganic sulfur into the organic molecule Hcy. Hcy can enter the transsulfuration pathway in order to make cysteine or the methylation/remethylation cycle to generate methionine. This figure is taken from Thomas and Surdin-Kerjan 1997.

many proteins. The reactivity of the sulfhydryl group can be modified by the pH and the reducing or oxidizing environment.

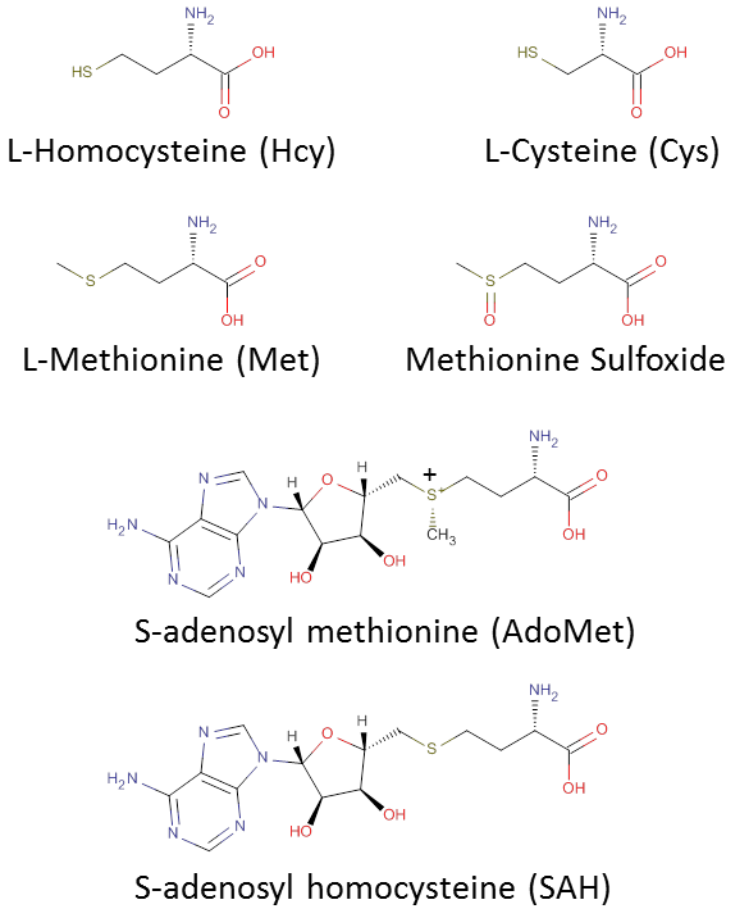

Figure 1.9 Organic molecules with sulfur. The sulfur containing amino acids include Hcy, Cys, and Met. Met can undergo oxidation and become methionine sulfoxide. AdoMet is the product of methionine metabolism and a widely used methyl donor. Numerous methyltransferases utilize AdoMet and generate the by-product SAH.

Hcy is a non-protein amino acid with similar properties as Cys. It is a metabolite, which either gets recycled through the folate-mediated one-carbon metabolism (or BHMT, HMT) to form methionine, or enters the transsulfuration pathway to make Cys. A high concentration of Hcy is a biomarker for disease in fungi, bacteria and mammals (Selhub 1999, Roe, O'Byrne et al. 2002, Pascon, Ganous et al. 2004). Accumulation of

Hcy is indicative of inborn errors in metabolism and leads to oxidative stress, toxicity and eventual death (McCully 2009).

The amino acid Met is heavily utilized by all organisms due to its role as a building block of proteins and as an intermediate in numerous transmethylation reactions. Unlike the reactive sulfhydryl group in Hcy and Cys, the sulfur in Met is a relatively inert thioether (Figure 1.9). In eukaryotes, Met successfully initiates translation by acting as a hydrophobic bridge between the initiator tRNA-Met and eIF-2 (Brosnan and Brosnan 2006). In proteins, Met is frequently found in the hydrophobic core or the membrane spanning domains, and to a lesser extent on the protein surface or at the active site. In solvent exposed regions, it can act as an endogenous antioxidant and form methionine sulfoxide (Figure 1.9). In its free form, Met is metabolized by the enzyme methionine adenosyl-transferase (MAT) to its active form S-adenosyl methionine (AdoMet). AdoMet is a powerful methylating agent and the second most widely used enzyme substrate after ATP (Figure 1.9) (Fontecave, Atta et al. 2004). AdoMet impacts a variety of cellular events such as gene expression and is implicated in fetal development and brain function. Numerous AdoMet dependent methyltransferases (MTases) use AdoMet as a methyl donor to methylate DNA, protein, hormones, neurotransmitters and phospholipids. This reaction produces the byproduct S-adenosyl homocysteine (SAH) which is reversibly cleaved by the enzyme AdoHcy hydrolase to form Hcy and adenosine (Figure 1.9). The remethylation of Hcy to Met completes the methylation metabolism cycle. The Hcy and Met metabolism pathways are linked through the commonly shared intermediate Hcy (Figure 1.8).

The role of Zinc in polypeptides

In living cells, the metal ion composition consists primarily of calcium (Ca^{2+}), magnesium (Mg^{2+}), sodium (Na^{1+}) and potassium (K^{1+}) while transition metals like iron (Fe^{2+}), zinc (Zn^{2+}), nickel (Ni^{2+}), cobalt (Co^{2+}) and copper (Cu^{2+}) are quite rare (Gillespie 1998). Of these, the rare transition metals are most likely to participate in enzymatic reactions. Enzymes interact with the metal based on its size, its ability to coordinate with available residues, and its coordination chemistry. A metal can have a catalytic and/or structure role and its behavior depends on whether it is a soft, hard or borderline metal. A hard metal is characterized by a small atomic radius, high nuclear charge and low polarizability. A soft metal is associated with a large atomic radius, low electronegativity, and high polarizability (Ho, Ho et al. 1978). According to the hard and soft acids and bases (HSAB) principle, hard acids react preferentially with hard bases and soft acids with soft bases while borderline acids are more flexible.

Zinc is a borderline metal and has unique properties that are ideal for a dynamic catalytic site or a rigid structural role in proteins. Zn^{2+} is the only member of the first row of transition metals with filled *d*-shell orbitals. Unlike the other reactive members which are often involved in redox reactions, Zn^{2+} can act as a redox-stable Lewis acid (McCall, Huang et al. 2000). Zn^{2+} is a stable ion which can also easily alternate between multiple coordination geometries with no energy penalty. Over 3,000 Zn^{2+} proteins are encoded in the human genome and belong to six different classes of enzymes (Andreini, Bertini et al. 2011). Over 200 Zn^{2+}-bound protein structures are available. The metal coordinates with 3, 4, 5 or 6 ligands through geometry resembling distorted tetrahedral, trigonal-bipyramidal or octahedral (Figure 1.10) (Auld 2001). Structural sites favor a stable tetrahedral geometry while catalytic sites benefit from a more dynamic metal coordination geometry. Zinc can coordinate with both hard and soft ligands such as

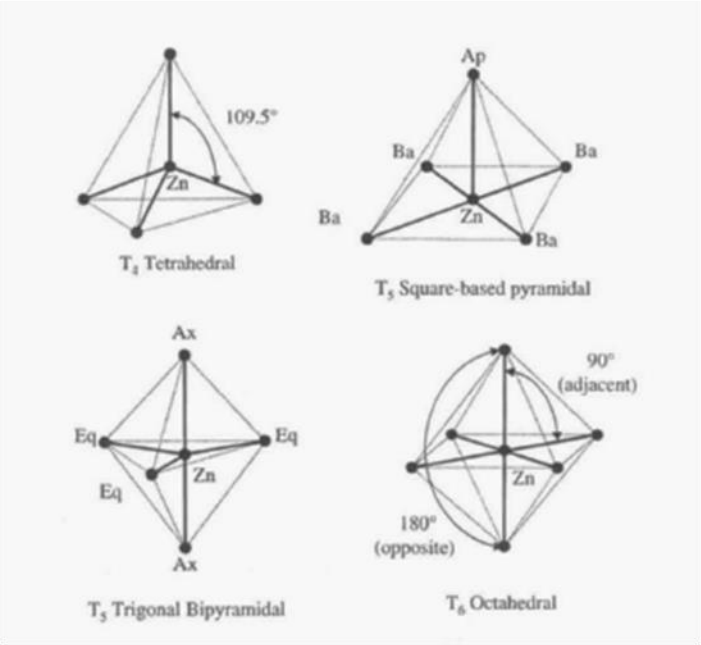

Figure 1.10 Zinc coordination geometry. Zinc can coordinate with 3-6 ligands through geometry resembling tetrahedral, square-based pyramidal, trigonal bipyramidal and octahedral. This figure is taken from Alberts, Nadassy et al. 1998.

oxygen (hard), nitrogen or sulfur (soft). In proteins Zn^{2+} is often coordinated by a combination of protein side chains including the nitrogen of histidine, oxygen of aspartate or glutamate, and the sulfur of cysteine. Less frequently observed ligands include the hydroxyl of tyrosine, the carbonyl of protein backbone, and the side chain carbonyls of asparagine or glutamine (McCall, Huang et al. 2000). The reactivity or function of Zn^{2+} depends on the first coordination sphere which dictates the oxidation state of Zn^{2+} and the second coordination sphere which orients and stabilizes the Zn^{2+} ligands and establishes the dielectric medium (Lee and Lim 2008, Maret and Li 2009, Andreini, Bertini et al. 2011). In other words, the chemistry of Zn^{2+} can be modulated by

different classes of enzymes in order to have desired stability constants, reactivities and functions (Vallee and Auld 1990).

The catalytic role of Zn^{2+} depends on its function as a Lewis acid, its ability to access different coordination geometries and fast ligand exchange. A catalytic Zn^{2+} binding site is generally "pre-organized" in the absence of metals. The metal is typically coordinated by three protein ligands, an exchangeable water, and/or a ligand (Maret and Li 2009). Histidine is the most commonly found protein ligand to coordinate the Zn^{2+} followed by glutamate, aspartate and cysteine. Four histidine ligands would retain an oxidation state of Zn^{2+}, making the metal a powerful Lewis acid. A water is almost always a ligand in the catalytic sites. Some enzymes like carbonic anhydrase use the metal to ionize the water while others like carboxypeptidase A use it to polarize the water (Rees, Lewis et al. 1981, Lindskog 1997). In either case, the metal helps to generate a hydroxyl nucleophile (Alberts, Nadassy et al. 1998). In the case of alcohol dehydrogenase, water is an exchangeable member of Zn^{2+}'s coordination sphere (Kleifeld, Frenkel et al. 2003). In coordination sites containing a cysteine or a non-protein sulfur ligand, as in the different protein prenyltransferases, or the Ada protein, the metal enhances the nucleophilicity of the free thiol by converting it to the active thiolate at neutral pH (McCall, Huang et al. 2000, Maurer-Stroh, Washietl et al. 2003, Maret and Li 2009). The Zn^{2+}/Thiol reactivity can be modified by adjusting the pH or the oxidizing/reducing environment. The sulfur reactivity is employed by the "Zn^{2+} switches" found in voltage gated K^+ channels (Wang, Strang et al. 2007).

A cocatalytic site has more than one Zn^{2+} and while one Zn^{2+} is often involved in making or breaking bonds, the others (bridged through water or protein residues) enhance its reactivity (Auld 2001). The metal can also stabilize negative charge.

A purely structural role of zinc is observed in a number of enzymes with functions ranging from Zn^{2+} sensing to transcription regulation. Structural Zn^{2+} binding sites can usually be distinguished from catalytic ones based on the type of metal ligands, lack of water, coordination geometry and general hydrophobicity (Andreini, Bertini et al. 2011). Coordination geometry is predominately tetrahedral and consists of CYS_4, CYS_3HIS_1 or CYS_2HIS_2 while Asp or Glu are rarely found in the coordination sphere. Cysteine residues dominate because Zn^{2+}-S complexes have high stability constants similar to those observed in disulfides (Vallee and Auld 1990). This allows Zn^{2+} to organize small domains, such as the zinc-finger containing metallothioneins or larger proteins like 3-methyladenosine DNA glycosylase I (Coyle, Philcox et al. 2002, Kwon, Cao et al. 2003, Maret and Li 2009). Metallothioneins are enriched with the classic CYS_2HIS_2 zinc-finger motif also found in a number of DNA and RNA binding proteins as well as between protein-protein binding domains (Laity, Lee et al. 2001).

The metal-ligand bond lengths and angles were recently evaluated from the zinc-replete structures available in the PDB (Alberts, Nadassy et al. 1998, Lee and Lim 2008). The zinc coordination numbers of 4 (T_4), 5 (T_5), and 6 (T_6) were observed in catalytic sites with frequencies of 48, 44 and 6%, respectively, and in structural sites with frequencies of 79, 6 and 12%, respectively. All T_4 sites have tetrahedral coordination while the majority of T_5 sites have trigonal bipyramidal geometries. In *catalytic* T4 sites, the average metal to ligand distance for Zn^{2+}-$N_{Histidine}$ is ~2.07 Å, Zn^{2+}-O_{water} is ~2.12 Å, Zn^{2+}-$O_{Glu/Asp/Asn/Gln}$ is ~2.04 Å, Zn^{2+}-S_{Cys} is ~2.21 Å. In *catalytic* T5 sites, the metal to ligand distance for Zn^{2+}-$N_{Histidine}$ is ~2.11 Å, Zn^{2+}-O_{water} is ~2.09 Å, Zn^{2+}-$O_{Glu/Asp/Asn/Gln}$ is ~2.16 Å, Zn^{2+}-S_{Cys} is ~2.30 Å. In *structural* T4 sites, the metal to ligand distance for Zn^{2+}-$N_{Histidine}$ is ~2.09 Å, Zn^{2+}-O_{water} is ~2.15 Å, Zn^{2+}-$O_{Glu/Asp/Asn/Gln}$ is ~1.95 Å, Zn^{2+}-S_{Cys} is 2.35 Å. In crystal structures, the angles observed between the zinc and the four ligands

in T4 or T5 sites often deviate from ideality. The ideal angles for a metal with tetrahedral geometry are 109.5° and with trigonal bipyrimidal geometry are 90° (Eq-Zinc-Ax), 120° (Eq-Zinc-Eq) or 180° (Ax-Zinc-Ax).

Table 1.1 Structures of cobalamin-independent methionine synthase (MetE)

Organism	Author	Condition	PDB ID
Thermatoga maritima	Pejchal	Substrate-free (-Zn), pH 4.6	1T7L
		Hcy (+Zn), pH 4.6	1XDJ
		5-methyl-THF-Glu3 (+Zn), pH 4.6	1XPG
		5-methyl-THF-Glu3 (-Zn), pH 4.6	1XR2
Arabidopsis thaliana	Ferrer	5-methyl-THF-Glu5 and Methionine (+Zn), pH 6.5	1U1J
		Methionine (+Zn), pH 6.5	1U1H
		Substrate-free (+Zn), pH 6.5	1U1U
		Pteroyl-Glu5 and Hcy (+Zn), pH 6.5	1U22
Thermatoga maritima	Pejchal	Hcy (+Zn), pH 8.5	3BQ5
		Substrate-free (+Zn), pH 8.5	3BQ6
Streptococcus mutans	Fu	Substrate-free (-Zn), pH 7.5	3L7R
		Substrate-free (+Zn), pH 7.5	3T0C
Streptococcus mutans	Fedorov	Substrate-free (-Zn), pH 5.5	2NQ5

Cobalamin-independent Methionine Synthases (EC 2.1.1.14)

The cobalamin-independent methionine synthase enzyme (MetE) binds Hcy and 5-methyl-THF-Glu_3 and catalyzes a Zn^{2+}-mediated alkylation reaction to generate methionine. This is the last step in the *de novo* methionine biosynthesis pathway in plants and microorganisms, and a means to recycle Hcy in all organisms. In the last 10 years, crystal structures of the Zn^{2+}-bound apo and substrate-replete MetE homologs from *Arabidopsis thaliana*, *Streptococcus mutans*, and *Thermatoga maritima* have been solved by various groups (Table 1.1) (Ferrer, Ravanel et al. 2004, Pejchal and Ludwig 2005,

Koutmos, Pejchal et al. 2008, Fu, Almqvist et al. 2011). Extensive kinetic characterization of MetE has also been done by the Matthews group using the *E. coli* homolog (Matthews, Smith et al. 2003, Taurog, Jakubowski et al. 2006, Taurog and Matthews 2006). MetE gene expression and enzyme properties were reported from the higher plant *Catharantus roseus* by the Schroder group (Eichel, Gonzalez et al. 1995, Eckermann, Eichel et al. 2000). Gene deletion studies and steady state kinetics were done using the fungal homolog from *Candida albicans* and *Saccharomyces cerevisiae* by the Robertus group (Suliman, Sawyer et al. 2005, Suliman, Appling et al. 2007, Prasannan, Suliman et al. 2009). The role of MetE in establishing virulence by *Streptococcus pneumoniae* and *Cryptococcus neoformans* was tested by McCusker and Brown, respectively (Pascon, Ganous et al. 2004, Basavanna, Chimalapati et al. 2013).

Structure of cobalamin-independent Methionine Synthase

The MetE protein from the plant *A. thaliana* was first crystallized and solved by Ferrer in 2004 (Ferrer, Ravanel et al. 2004). One year later, the bacterial structure from *T. maritima* was published by Pejchal (Pejchal and Ludwig 2005). The structure of MetE from the pathogenic bacterium *Streptococcus mutans* was also recently solved (Fu, Almqvist et al. 2011). In general, the MetE from these organisms is ~90 kDa. The amino acid sequence is only 40-50% similar but all three structures align with an RMSD < 2 Å.

The MetE enzyme consists of two $(\beta\alpha)_8$ TIM barrels that are connected by a linker and arranged face to face such that the extended surface loops form an inter-domain interface near the linker (Figure 1.11). The active site Zn^{2+} is coordinated by residues located on the top of the C-terminal barrel and facing the inter-domain interface. Inductively coupled plasma-atomic emission spectrometry was initially used by the

Matthews group to calculate one equivalent of Zn^{2+} per monomer and circular dichroism was used to confirm its non-structural role (Gonzalez, Pearlso et al. 1996). EDTA treatment was also found to inhibit MetE activity. Extended X-ray absorption fine structure (EXFAS) and site-directed mutagenesis were used to establish the three essential metal ligands His641, Cys643 and Cys726 (in *E. coli*), and a fourth exchangeable water or glutamate (Zhou, Pearlso et al. 1999).

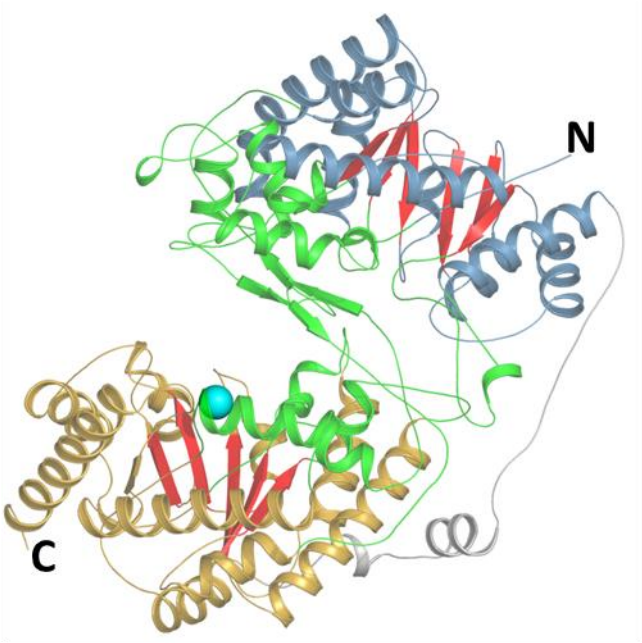

Figure 1.11 The overall structure of MetE from *Arabidopsis thaliana* (1U1U). The N and C-terminal $(\beta\alpha)_8$ TIM barrels are shown in blue and golden, respectively. The linker which connects both domains is shown in grey and the extended surface loops are shown in green. The zinc is shown as a cyan sphere.

The Hcy and Met bound structures of MetE from *A. thaliana* and *T. maritima* identified a small substrate/product binding pocket adjacent to the active site metal (Ferrer, Ravanel et al. 2004, Pejchal and Ludwig 2005). In both homologs, the backbone amino group is secured by a Glu462, Asp577, and carbonyl of Ile409 (Figure 1.12) (*T.*

maritima). The carboxylate group forms hydrogen bonds with the backbone amide and side chain OH of Ser411 (*T. maritima*). Prasannan used site directed mutagenesis to show that the Asp577 equivalent in *C. albicans* is essential for enzyme activity (Prasannan, Suliman et al. 2009). The entry of Hcy or L-selenohomocysteine into the active site has also been evaluated by the Matthews group using EXFAS (Peariso, Zhou et al. 2001). They found that the active site Zn^{2+} retains tetrahedral geometry and coordinates with four ligands in both the apo and Hcy/selenohomocysteine bound enzymes. However, the coordination environment around the Zn^{2+} changes from 2S + 2 (N/O) to 2S + 1N + 1Se/S. These results showed that Zn^{2+} easily switches between coordination geometries and ligands, and suggests that it acts as a Lewis acid to deprotonate and activate the Hcy. However, the Zn^{2+}-S_{Hcy} distances reported from the *A. thaliana* and *T. maritima* structures are too long at 4.1 Å and 3.2 Å, respectively.

In the substrate-free and substrate-bound plant structures, the metal does not coordinate with the Hcy thiol and instead remains tetrahedrally coordinated to Cys649, Cys733, His647 and a water molecule (Figure 1.12). In *T. maritima* the metal is coordinated by Cys620, Cys704, His618 and Glu642 in the apo structure but ends up moving 0.75 Å towards the substrate in the Hcy-bound structure (Figure 1.12). This results in two elongated bonds between Zn^{2+}-O_{642} and Zn^{2+}-S_{Hcy} and metal geometry somewhere between trigonal planar and trigonal bipyramidal. In a more recent paper published by Matthews and Ludwig, the *T. maritima* MetE was solved with and without Hcy at pH 8.5 (Koutmos, Pejchal et al. 2008). Under these conditions the results were consistent with the EXFAS data; the ligands around Zn^{2+} changed from S_{620}, S_{704}, H_{618}, O_{642} in the apo structure to S_{620}, S_{704}, H_{618}, S_{Hcy} in the substrate bound structure with the complete inversion of tetrahedral geometry (Figure 1.12).

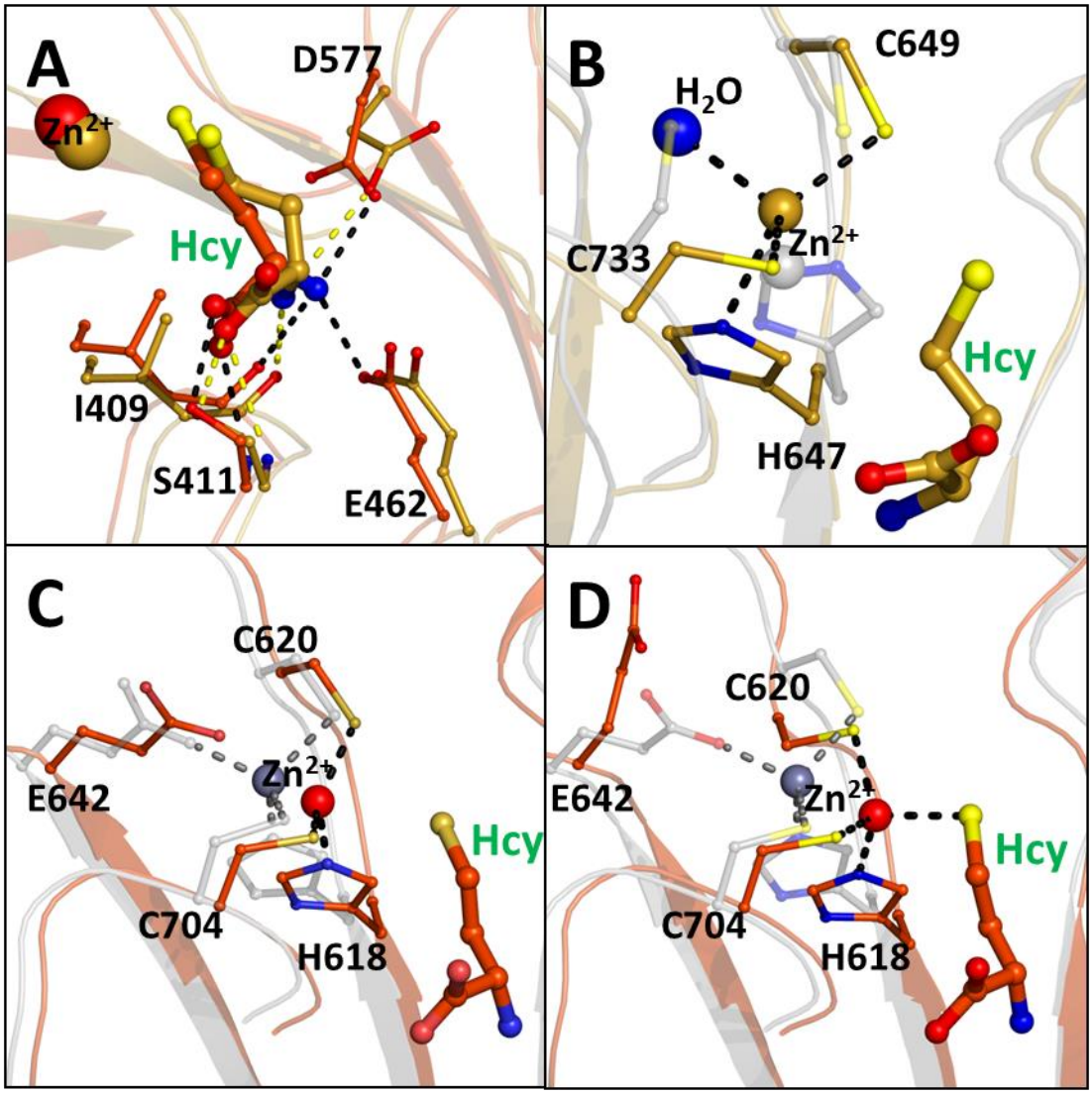

Figure 1.12 The zinc and ligand bound C-terminal barrel of MetE. A) Overlay of the plant (1U22; golden) and bacterial (1XDJ; orange) homologs bound with zinc and Hcy. Bonds are shown as black (bacterial) and yellow (plant) dashes. The *maritima* residues are labeled. B) Overlay of the Hcy-free (1U1U; grey) and Hcy-replete (1U22; golden) plant structures. Water is shown as a blue sphere. C) Overlay of the Hcy-free (1XPG; grey) and Hcy-replete (1XDJ; orange) bacterial structures. D) Overlay of the Hcy-free (3BQ6; grey) and Hcy-replete (3BQ5; orange) bacterial structures crystallized at pH 8.5.

So far both the natural substrate 5-methyl-THF-Glu_5 and substrate analog pteroyl-Glu_5 have been used to characterize the folate binding site of MetE. Unlike the well-defined Hcy/Met pocket in the C-terminal barrel, the folate binds at the inter-domain interface near the linker. Few folate bound MetE structures have been solved and the available structures are incomplete and somewhat inconsistent.

In the *A. thaliana* protein bound with Met and 5-methyl-THF-Glu_5 or Hcy and pteroyl-Glu_5, the reduced (THF) or aromatic (pteroyl) pterins form non-specific stacking interactions with a conserved Trp567, and the first glutamyl of the polyglu tail forms ionic or hydrogen bonds with Arg521 and Lys18, or Cys522, respectively (Figure 1.13) (33). In the superimposed structures, the polyglu tails and PABA moieties align relatively well but the pterins appear to slide around on the Trp567 ring. Each pterin is loosely secured through hydrogen bonds with the side-chain residues in its surroundings. These structures were the first to show that the folate binds at the inter-domain interface by folding into an 'L' configuration, where the base of the letter corresponds to the pterin.

In the *A. thaliana* structures, the N5 methyl group is ~7 Å away the Hcy thiolate. In the *T. maritima* homolog, 5-methyl-THF-Glu_3 binds in the same location primarily through stacking interactions between the pterin and Trp539 and hydrogen/ionic bonds between side chains of Lys18, Cys494, and Arg493 and the first glutamyl residue of the polyglu tail (Figure 1.13) (34). However, unlike the *A. thaliana* structures in which the folate folds onto itself and resembles the letter 'L', in *T. maritima* it binds in an extended configuration. Compared to the 'L', the pterin in the extended form rotates ~180°, forming an inverted L, and drops another ~45°. As a result, the N5 methyl group undergoes a rotation of ~180° and translation of ~3 Å, placing it 11 Å away from the Hcy thiolate. The authors believe that this is an intermediate conformation that later changes

to resemble the *A. thaliana* complex. Site-directed mutagenesis done by Prasannan identified the two essential folate binding residues Asp467 and Trp539 in *T. maritima*, and the Asp495 and Trp567 in the *A. thaliana* homolog (Prasannan, Suliman et al. 2009).

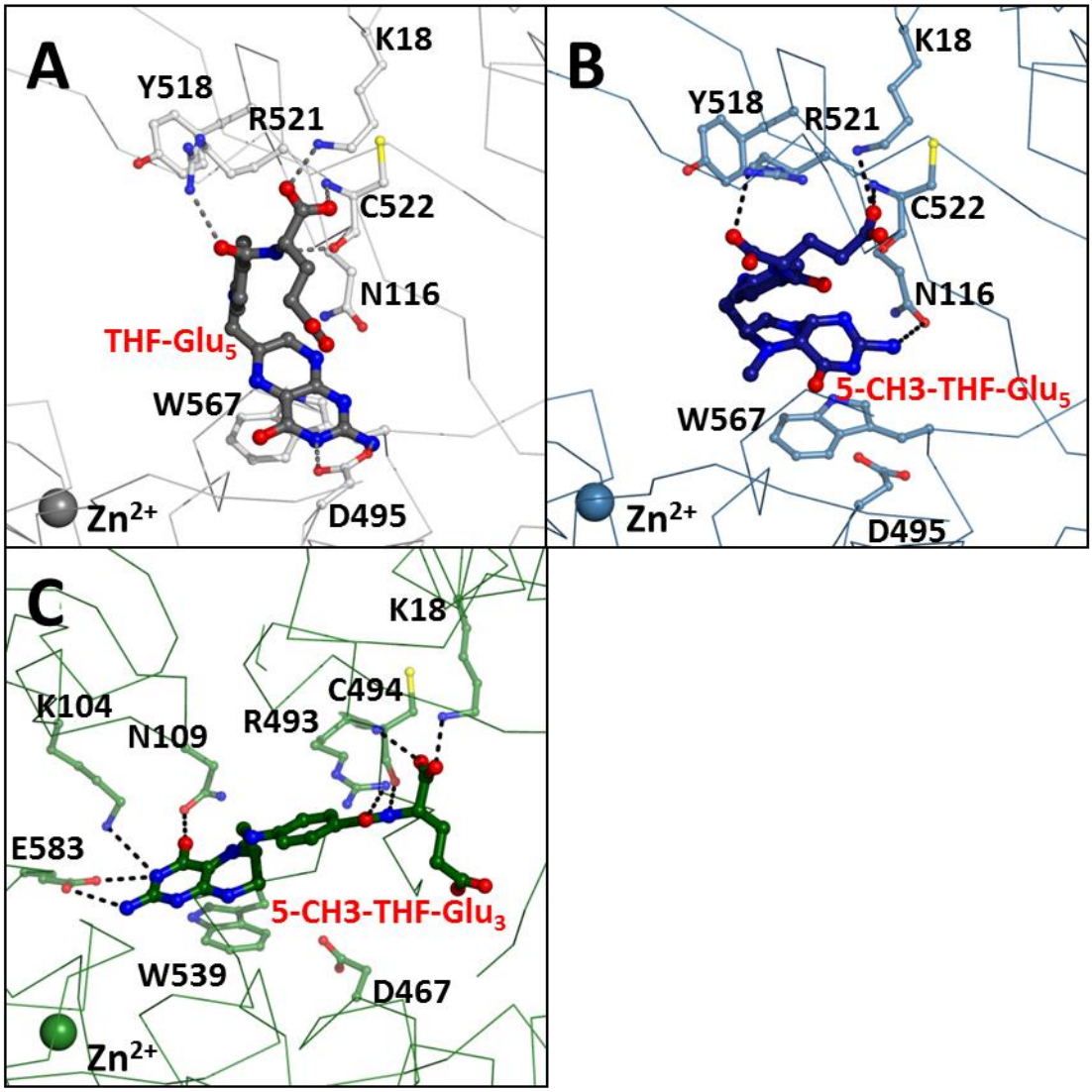

Figure 1.13 The folate-bound MetE enzyme. A) The plant homolog bound with Pteroyl-Glu_5 (1U22). B) The plant homolog bound with 5-methyl-THF-Glu_5 (1U1J). C) The bacterial MetE bound with 5-methyl-THF-Glu_3 (1XPG).

The substrate-free and substrate-bound MetE structures solved so far crystallize in an 'open' enzyme configuration. Since the methyl donor and acceptor are too far apart for a productive transfer reaction, a transient 'closed' configuration is expected to exist.

Proposed mechanism

MetE was initially purified from *E. coli* and evaluated for folate binding and catalysis by Whitfield and Weissbach (Whitfield, Steers et al. 1970, Whitfield and Weissbach 1970). They identified the requirement for polyglutamated 5-methyl-THF-Glu, Hcy, phosphate and Mg^{2+} for optimal MetE catalysis. The MetE homolog from the plant *Catharanthus roseus* was purified in 1995 and found to be similar in size to the bacterial homolog and shared a sequence identity of 49.5% (Eichel, Gonzalez et al. 1995). The plant enzyme only required phosphate, Hcy and 5-methyl-THF-Glu_3 for maximal activity (Eckermann, Eichel et al. 2000). The homologs from *Candida albicans* (CaMet6p) and *Saccharomyces cerevisiae* (ScMet6p) are about 48% identical to the *E. coli* MetE and were characterized in 2005 by Suliman (Suliman, Sawyer et al. 2005). Both were tested with phosphate and Mg^{2+} and found to be fully active with 5-methyl-THF-Glu_2.

The Matthews group has had a longstanding interest in the chemistry of methyl transfer; the chemically difficult direct transfer from 5-methyl-THF to Hcy has been particularly intriguing. They determined the kinetic constants and equilibrium dissociation constants for Hcy and 5-methyl-THF-Glu_3 (Taurog, Jakubowski et al. 2006). A substrate binding scheme is shown in Figure 1.14 and the rate constants and equilibrium binding constants are shown in Table 1.2. Since MetE carries out a bi-substrate reaction, they first tested the order in which each substrate enters the active site. They found that each binary complex (MetE*5-methyl-THF-Glu_3 and MetE*L-Hcy) is

chemically and kinetically competent for methyl transfer, and that either of the available substrates can be the first to bind free MetE. In either event, the second substrate was reported to bind 30-fold more tightly due to possible cooperatively and cross-talk between the substrate pockets. Each ternary complex then undergoes a methyl transfer

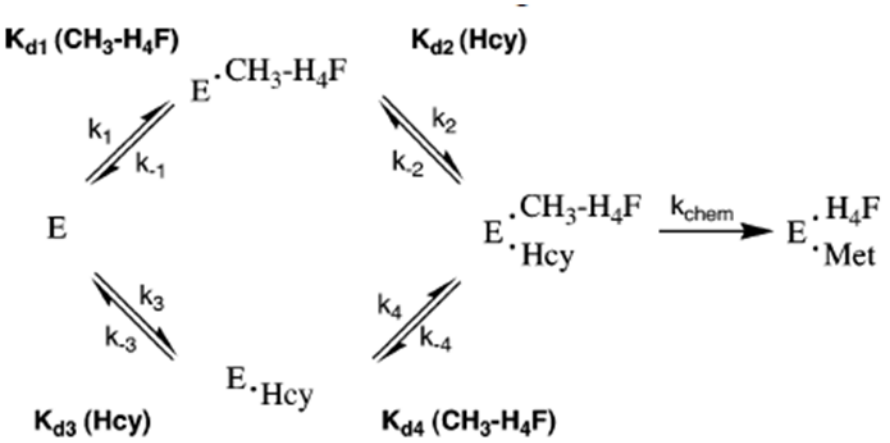

Figure 1.14 The substrate binding scheme for MetE proposed by Matthews. This figure is taken from Taurog, Jakubowski et al. 2006.

Table 1.2 Rate and equilibrium constants for substrate binding in MetE

K_{d1} (E + CH_3-H_4PteGlu$_3$) (μM)	10 ± 1	k_1 ($\mu M^{-1}s^{-1}$)	0.5 ± 0.3
		k_{-1} (s^{-1})	5 ± 3
K_{d2} (E·CH_3-H_4PteGlu$_3$ + Hcy) (μM)	1.4 ± 0.5	k_2 ($\mu M^{-1}s^{-1}$)	1.1 ± 0.6
		k_{-2} (s^{-1})	1.5 ± 0.6
K_{d3} (E + Hcy) (μM)	39 ± 3	k_3 ($\mu M^{-1}s^{-1}$)	16 ± 14
		k_{-3} (s^{-1})	600 ± 500
K_{d4} (E·Hcy + CH_3-H_4PteGlu$_3$) (μM)	0.4 ± 0.2	k_4 ($\mu M^{-1}s^{-1}$)	6 ± 4
		k_{-4} (s^{-1})	2.1 ± 0.8
		K_{chem} (s^{-1})	0.25 ± 0.09
		K_{cat} (s^{-1})	0.12 ± 0.03

This table is taken from Taurog, Jakubowski et al. 2006.

reaction with a reported k_{cat} of 0.12 ± 0.03 s^{-1} and K_{chem} of 0.25 ± 0.09 s^{-1} (at 25 °C). A separate paper by the same group demonstrated the existence of a "mixed" ternary complex MetE*THF-Glu_3*Hcy, and suggested that the release of byproduct THF-Glu_3 from either the binary or ternary complex is partially rate limiting (Taurog and Matthews 2006). This was supported by the observed k_{cat} and K_M, which show that something other than chemistry is rate limiting.

Steady state enzyme kinetic experiments have also been done by various groups. The MetE from *E.coli*, *C. roseus*, *S. cerevisae* and *C. albicans* is reported to have a 5-methyl-THF-Glu_3 K_M of 4.7 μM, 80 μM, 84 ± 8 μM, and 129 ± 25 μM, respectively (Whitfield, Steers et al. 1970, Eckermann, Eichel et al. 2000, Suliman, Sawyer et al. 2005). Hcy is reported to have a K_M of 14 ± 2.3 μM and 13 ± 2.6 μM in the *C. albicans* and *S. cerevisiae* homologs, respectively, with an overall turnover or k_{cat} of 25/min (Suliman, Sawyer et al. 2005).

The cobalamin-independent methionine synthase catalyzes an otherwise unfavorable direct methyl transfer reaction by first activating the Hcy thiol and 5-methyl-THF-Glu_3. The enzyme uses Zn^{2+} to deprotonate the Hcy thiol, converting it into a thiolate anion; the thiolate becomes the fourth metal ligand (Matthews, Smith et al. 2003). In MetE, this zinc-thiolate complex [$Zinc(S_{cys})_3(N_{His})_1$] has a net charge of -1. According to model studies done by Wilker and Lippart, this set of ligands and overall charge are essential in enhancing the thiolate reactivity towards alkylation by facilitating the dissociation from the zinc complex followed by alkylation (Matthews and Goulding 1997, Wilker and Lippard 1997). The question of whether alkylation takes place while the thiolate is Zn^{2+} bound or free is still under investigation. Model studies designed specifically to replicate the MetE catalyzed alkylation reaction suggest that a Zn^{2+} bound thiolate attacks the methyl group followed by product (Met) dissociation (Brand,

Rombach et al. 2001). Other zinc-containing enzymes that also catalyze thiol alkylation contain cysteine sulfur ligands and a net negative charge (Zhou, Peariso et al. 1999). The nucleophilicity of a zinc-thiolate is critical for alkylation reactions, and appears to be modified by the zinc ligands, the hydrogen bonds or environment, and net charge (Picot, Ohanessian et al. 2008).

A successful thiolate mediated alkylation reaction is possible only if the 5-methyl-THF-Glu_3 is also activated by protonation (Smith and Matthews 2000). Although the Zn^{2+} activated thiolate is an excellent nucleophile, the resulting THF-Glu_3 anion is a poor leaving group and must be activated prior to the removal of the N5 methyl group. In solution, protonation is associated with a pK_a of 5.05 and can occur on the nitrogen (N5) or on a conjugated carbon (C8a or C2). The Matthews group monitored folate absorbance under various conditions and found that 5-methyl-THF-Glu_3 binds MetE in the unprotonated form (Taurog and Matthews 2006). The formation of this complex does not involve a proton uptake or release and the UV-visible absorbance spectrum is associated with the folate entering a hydrophobic environment. They found that protonation only occurs in a ternary complex prior to the methyl transfer reaction (Smith and Matthews 2000, Taurog and Matthews 2006). It is not rate limiting and occurs at the N5 position. The proton donor remains unidentified; however, the active site of MetE in the ternary complex is expected to stabilize the protonated folate. It is expected to be in a hydrophobic (> 80% acetonitrile) environment and bind ~7 Å away from the Hcy thiolate anion. A non-specific stacking interaction is also expected to exist between the charged pterin and a conserved tryptophan. This cation-pi interaction is theorized to raise the pK_a of the protonated 5-methyl-THF-Glu_3 so that in the ternary complex, the folate pK_a is well above 7 (Matthews, Smith et al. 2003).

Lastly, Whitfield and Weissbach tested the ability of the *E. coli* MetE to bind the individual components of the 5-methyl-THF-Glu_3 substrate. They found that neither the pteroic acid nor γ-L-glutamylglutamic acid can independently bind MetE or inhibit catalysis. In order to bind and inhibit MetE, the folate required an oxidized or reduced pterin connected by a PABA moiety to at least two glutamates (Whitfield, Steers et al. 1970, Whitfield and Weissbach 1970).

Cobalamin-Dependent Methionine Synthases (EC 2.1.1.13)

The methionine synthase found in mammals and some bacteria catalyzes the Zn^{2+} mediated transfer of a methyl group from 5-methyl-THF-Glu_1 to Hcy in a cobalamin-dependent reaction, producing Met and THF-Glu_1. In prokaryotes, this is the last step in methionine biosynthesis and Hcy regeneration but in mammals it is the only means of regenerating methionine from Hcy. The cobalamin-dependent methionine synthase enzyme (MetH) is encoded by the metH gene. The enzyme is best characterized from *E. coli* and *T. maritima*, which share a sequence identity of ~55% (Gruber and Kratky 2001). Eubacteria like *E. coli* can express both MetE and MetH but the two are used under different growth conditions and have different enzyme requirements (Banerjee and Matthews 1990). MetH requires vitamin B12, AdoMet, and a reducing system; it can use a mono or polyglutamated folate. In contrast, the bacterial MetE requires magnesium (or manganese), phosphate ions and a polyglutamated folate. In addition, the MetE and MetH amino acid sequences are unrelated, meaning the proteins have arisen by convergent evolution (Gonzalez, Banerjee et al. 1992).

Structure of cobalamin-dependent methionine synthase

The metH gene encodes a large 136 kDa modular enzyme (1227 residues) that contains a 38 kDa Hcy-binding domain, 33 kDa 5-methyl-THF-binding domain, 27 kDa

cobalamin-binding domain, and a 38 kDa activation domain (Gruber and Kratky 2001). The four modules are connected in this order by three polypeptide linkers. The enzyme has been successfully crystallized by dividing it in parts: 1-566 (Hcy & Folate), 744-1227 (Cobalamin & activation domain), 651-896 (Cobalamin), and 901-1227 (Activation domain) (Table 1.3). A model of the overall MetH structure has been created by combining together the existing crystal structures. The MetH activity can be evaluated by using four segregated modules or the entire holoenzyme (Drennan, Matthews et al. 1994).

Table 1.3 Structures of cobalamin-dependent methionine synthase (MetH)

Organism	Author	Condition	PDB ID
Thermatoga maritima	Evans/ Ludwig	Fragment 1-566, Substrate-free, (-Zn), pH 5.7	1Q7Q
		Fragment 1-566, Substrate-free, (+Cd), pH 5.7	1Q7Z
		Fragment 1-566, L-Hcy, 5-CH3-THF-Glu1, (+Cd), pH 5.7	1Q8J
Escherichia coli	Koutmos/ Ludwig	Fragment 1-566, Substrate-free, (+Zn), pH 7.0	3BOL
		Fragment 1-566, L-Hcy, (+Zn), pH 7.0	3BOF
Escherichia coli	Datta/ Matthews	Fragment 649-1227, Cobalamin, pH 7.2	3BUL
Escherichia coli	Drennan/ Ludwig	Fragment 651-896, Cobalt-MethylCobalamin	1BMT
Escherichia coli	Dixon/ Ludwig	Fragment 901-1227, S-Adenosylmethionine (SAM), pH 7.2	1MSK
Escherichia coli	Bandarian/Ludwig	Fragment 649-1227, Cobalamin, pH 6.5	1K98
Escherichia coli	Koutmos/ Matthews	Fragment 651-1226, Cobalamin, S-Adenosyl-L-Hcy, pH 7	3IVA
		Fragment 651-1226, Cobalamin, pH 7	3IV9

The N-terminal half of MetH consists of the Hcy and 5-methyl-THF-Glu_1 binding domains. Each domain is a $(\beta\alpha)_8$ TIM barrel, like the barrels found in the cobalamin-independent methionine synthase, MetE. Unlike MetE, in which the barrels are arranged face-to-face, in MetH the barrels are arranged side-to-side with their axes perpendicular to one another (Evans, Huddler et al. 2004). The Hcy and folate binding sites are located on the face of each barrel and set ~50 Å apart from each other. The two barrels are tethered through a linker and no direct communication exists between the two active sites. Each domain is believed to be an independent entity, containing within it the binding and activation determinants for each respective substrate.

The Hcy binds in a pocket located on the top of the C-terminal barrel and adjacent to the active site Zn^{2+} (residues 1-353) (Evans, Huddler et al. 2004). The backbone carboxylate of Hcy forms ionic interactions with side chain residues Glu146 and Asp105 and the backbone amino group forms hydrogen bond with the mainchain amides of Tyr22 and Gly23 (Figure 1.15). The Hcy sulfur coordinates with the active site Zn^{2+} and this side-chain is sequestered from the solvent by surrounding residues Phe66 and Thr147. In the Hcy-free structure (3BOF), Zn^{2+} is tetrahedrally coordinated by four conserved ligands, Cys207, Cys272, Cys273, and Asn234 with Zn^{2+}-S_{207}, Zn^{2+}-S_{272}, Zn^{2+}-S_{273}, Zn^{2+}-O_{234} bonds of 2.23 Å, 2.37 Å, 2.29 Å, and 2.12 Å, respectively (Figure 1.15). The entry of Hcy (3BOL) results in the displacement of Zn^{2+} by 1.97 Å towards the Hcy thiol. The Zn^{2+}-O bond is broken while a Zn^{2+}-S_{Hcy} bond of 2.34 Å is made with complete inversion of tetrahedral geometry (Peariso, Zhou et al. 2001).

The folate binding pocket is also located on the face of the C-terminal barrel consisting of residues 345-649. In MetH, the 5-methyl-THF-Glu_1 binds in an extended mode, unlike the L- or V-configurations adopted by folates in DHFR, TS and MetE (Evans, Huddler et al. 2004). The methylated N5 pterin is secured through an extensive

network of hydrogen bonds between its proton donors/acceptors and the side chains of surrounding residues Asp390, Asn411, Asp473 and Asn508 (Figure 1.15). The PABA moiety stacks against Glu320 side chain and its backbone carbonyl donates a hydrogen bond to Arg516. These interactions help to point the N5 methyl in the direction of the incoming cobalamin.

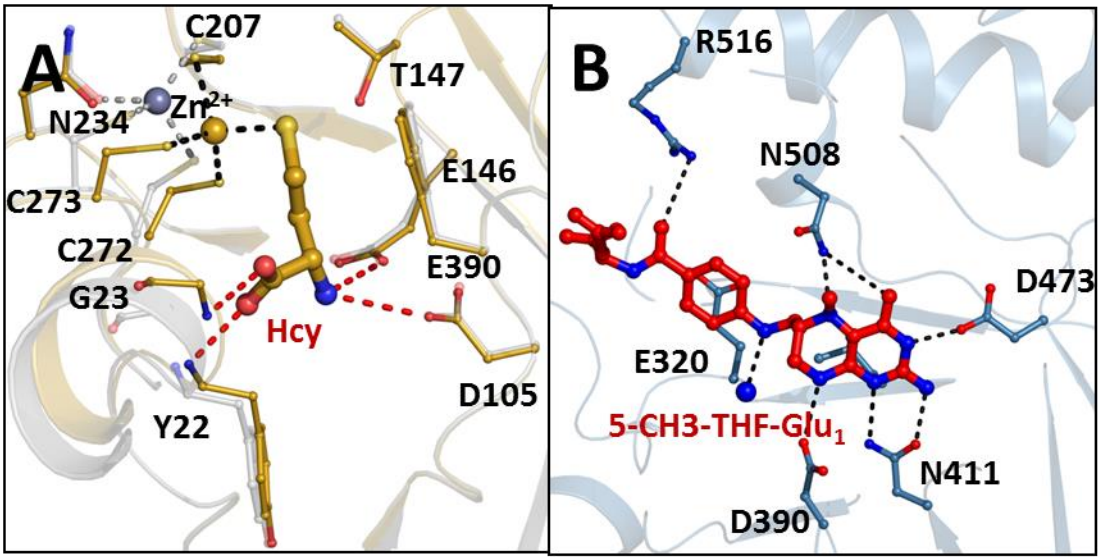

Figure 1.15 The Zn^{2+}, Hcy and folate bound MetH enzyme. A) Overlay of the Hcy-free (1BOL; grey) and Hcy-replete (1BOF; golden) N-terminal module (residues 1-353). The zinc atoms are shown as spheres. B) The second module (residues 345-649) bound with 5-methyl-THF-Glu_1 (1Q8J). Water is shown as a blue sphere.

The cobalamin prosthetic group is embedded in the third module, in between a helical bundle and a α/β domain (Drennan, Huang et al. 1994, Drennan, Matthews et al. 1994). This module is expected to cycle between the folate and Hcy pockets which are separated by ~70 Å (Evans, Huddler et al. 2004). The cobalt (Co) in the cobalamin corrin ring has six possible coordination sites out of which two are exchangeable. One of these sites carries the methyl group (from folate) and the other can make or break an

interaction with a residue (His759) in the activation domain. Cobalamin chemistry allows it to be a supernucleophile (cobalamin (I)) and this reactivity is controlled by the making and breaking of the Co-His_{759} interaction (Banerjee 1997, Gruber and Kratky 2001). During a catalytic cycle, the enzyme bound cobalamin (I) first reacts with the 5-methyl-THF-Glu_1 to form an intermediate methyl-cobalamin (III). This docking event has been modeled by Evans using the substrate bound folate module and a free cobalamin (Figure 1.16) (Evans, Huddler et al. 2004). The methyl-cobalamin (III) bound domain then migrates to the Hcy module in order to complete the second methyl transfer reaction from methyl-cobalamin (III) to the Hcy thiolate. Once again, the Evans group created a model showing the possible interactions between a free methyl-cobalamin and a substrate bound Hcy module (Figure 1.16).

Lastly, in the event that the highly reactive cobalamin (I) is oxidized to cobalamin (II), the C-terminal activation domain carries out reductive reactivation using flavodoxin and subsequent re-methylation using S-adenosyl methionine (AdoMet) (residues 897-1227). The activation domain consists of a mixed $\alpha + \beta$ structure with an overall shape resembling the letter C (PDB: 1MSK). It is unlike the AdoMet binding domains found in DNA or RNA-methyltransferases which resemble the Rossman-type α/β fold (Dixon, Huang et al. 1996, Gruber and Kratky 2001). AdoMet binds near the center of the concave C and comes in contact with cobalamin (II) in the cobalamin-activation domain docking event (Koutmos, Datta et al. 2009).

Proposed mechanism

The overall reaction catalyzed by MetH superficially resembles the reaction carried out by MetE. However, the chemical strategy used by each enzyme is unique. The strategy used by MetH is highly efficient with a turnover number of 1500 min^{-1}. By

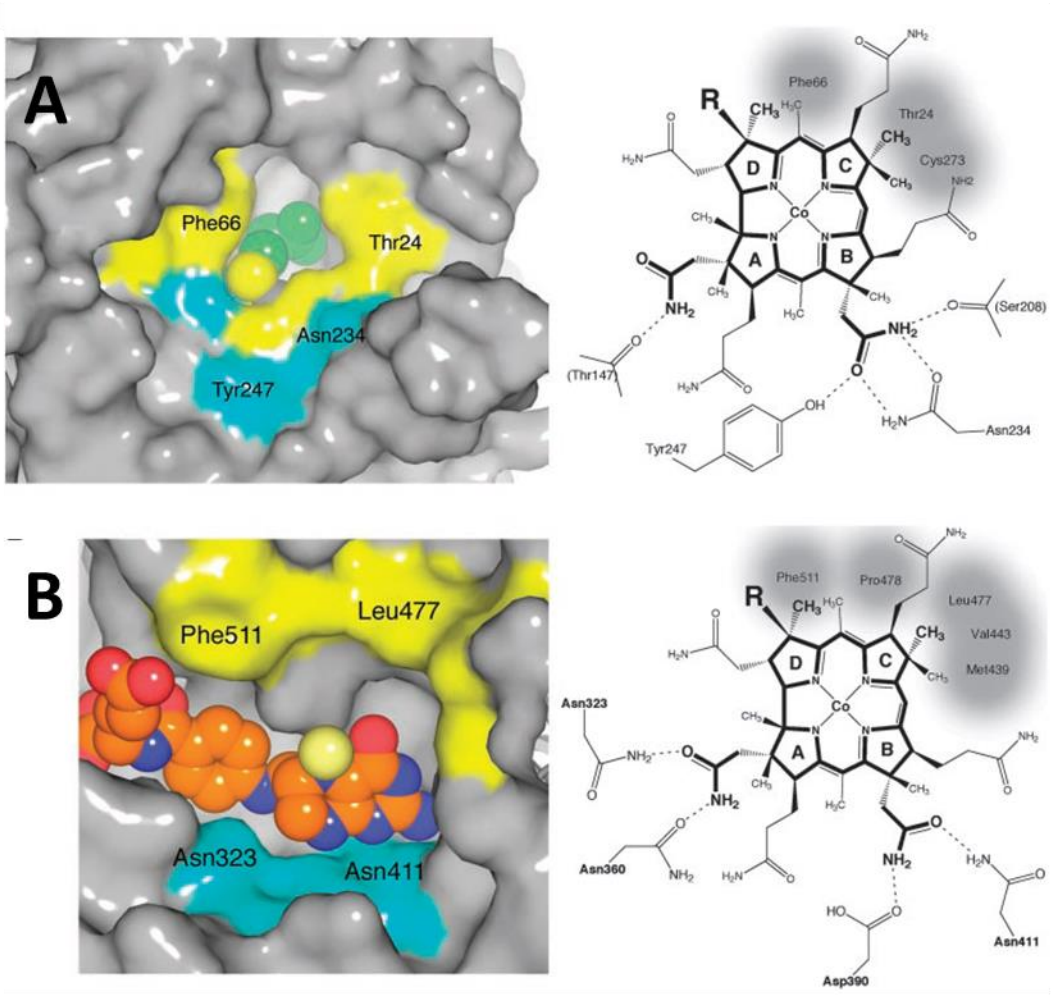

Figure 1.16 A model of cobalamin bound to the Hcy and folate modules. Model was created by Evans (Figure 7 in Evans, Huddler et al. 2004). A) The top of the Hcy module is shown on the left with hydrophobic patches shown in yellow and hydrophilic in cyan. The Hcy is shown as van der Waals spheres. Cobalamin is expected to dock on this surface. The possible interactions between the cobalamin and residues of the Hcy domain are shown on the right. B) The top of the folate module is shown on the left with hydrophobic patches (yellow) and hydrophilic patches (cyan) and the folate (spheres). Cobalamin is expected to dock on this surface by potentially making interactions shown on the right.

comparison, MetE is sluggish with a turnover number of just 12.3 min^{-1} (Gonzalez, Banerjee et al. 1992). Despite being a large modular enzyme, MetH has a significant advantage over the smaller MetE because it uses the supernucleophile cobalamin. The domain rearrangements are expected to be the slow steps in substrate turnover (Evans, Huddler et al. 2004). As in MetE, the Hcy is activated by the active site zinc to create a thiolate nucleophile and the folate is thought to be activated by protonation at the N5 amine carrying the methyl. The protonation event is only observed in the ternary complex containing MetH, 5-methyl-THF-Glu_1, and cobalamin (I) through an unknown mechanism (Smith and Matthews 2000, Matthews, Smith et al. 2003).

The MetH catalyzed methyl transfer reaction can be divided into two half reactions. In the first reaction, the cobalamin (I) nucleophile is expected to attack the folate methyl group located on a quaternary N5 amine, generating methylcobalamin (III) and the byproduct THF-Glu_1. This event has an observed rate constant of 250 s^{-1} and the folate K_M of ~27.8 uM (Banerjee, Frasca et al. 1990). In the second half reaction, the B12-module carrying the methylcobalamin (III) first docks against the Hcy-module followed by a nucleophilic attack by the Hcy thiolate on the CH_3-cobalamin (III). This reaction is essentially irreversible and generates the final product methionine and cobalamin (I) with an observed rate constant of 140 s^{-1} and an estimated Hcy K_M of ~1 uM. The Matthews group also evaluated catalysis using free cobalamin (I) and the substrate bound folate and hcy modules, or a free methylcobalamin (III) in the presence of the substrate bound Hcy module (Goulding, Postigo et al. 1997). Both conditions were found to be catalytically competent, meaning the hcy and folate binding modules are independently active.

Once every 1000-2000 turnovers the cobalamin (I) is oxidized to the inactive cobalamin (II) (Liptak, Datta et al. 2008). Reductive remethylation takes place in a

complex formed by the enzyme flavodoxin and the B12-binding and activation domains (AdoMet) of MetH (Hall, Jordan-Starck et al. 2000). In this complex, flavodoxin provides the electrons used to reduce the cobalamin metal and AdoMet donates a methyl to create the catalytically competent methylcobalamin (III) intermediate.

Betaine Homocysteine Methyltransferase (BHMT)

The enzyme BHMT (EC 2.1.1.5), is a Zn^{2+} dependent thiolmethyltransferase which generates methionine by catalyzing the transfer of a methyl group from betaine to homocysteine (Figure 1.17) (Pajares and Perez-Sala 2006). In mammals and some bacteria, BHMT is one of the two major enzymes (MetH is the other) which convert homocysteine to methionine. In solution and in crystal structures, BHMT exists as a tetramer of 45 kDa subunits (407 residues). Each monomer has a $(\beta\alpha)_8$ barrel (residues 1-318) followed by an extended structure called the dimerization arm. Surprisingly, BHMT is 40% similar in sequence to the N-terminal region of MetH (Evans, Huddler et al. 2002). Although the MetH and BHMT do not share any sequence identity with MetE, all three of these enzymes have structurally similar $(\beta\alpha)_8$ barrels which bind Zn^{2+} and Hcy. In fact, the Hcy/Met binding pockets in all three enzymes (MetH: 3BOF, MetE: , BHMT: 1LT8) use at least one negatively charged residue to anchor the amino group, use backbone nitrogens to stabilize the carboxylate group, and have a hydrophobic pocket to sequester the thiol containing side-chain. All three also exploit the nucleophilicity of the adjacent Zn^{2+} ion to deprotonate the Hcy thiol (pK_a =10) under physiological conditions, converting it into a thiolate anion (Millian and Garrow 1998). In rat BHMT, the Zn^{2+} is coordinated by four conserved residues, Cys217, Cys299, Cys300 and Tyr160 (Gonzalez, Pajares et al. 2004). In the presence of Hcy, the zinc is expected to have a net charge of -2, which is identical to the net charge in MetH.

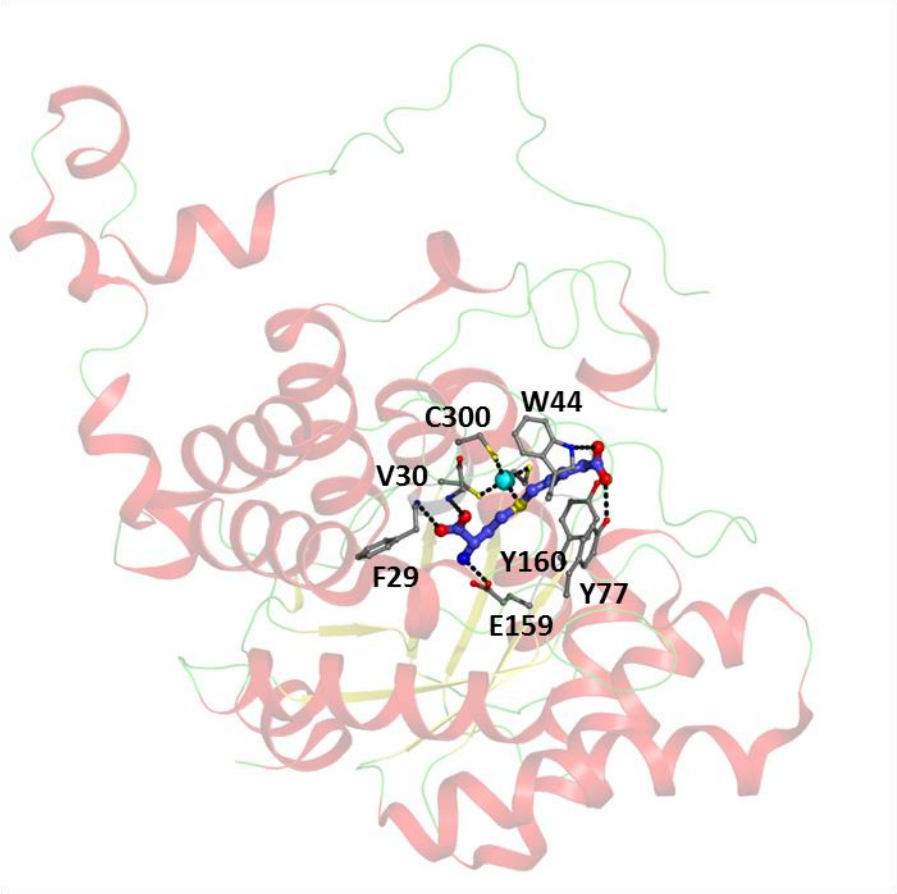

Figure 1.17 The zinc and S-(δ-carboxybutyl)-L-homocysteine (CBHcy) bound BHMT. Zinc is shown as a cyan sphere and is coordinated by three cysteines and the sulfur of CBHcy (purple). The hydrogen and ionic bonds between the CBHcy and protein residues are shown as black dashes.

Unlike MetE and MetH, which dedicate an entire domain to bind and activate 5-methyl-THF, BHMT is much smaller and its compact structure accommodates the much smaller methyl donor betaine. Betaine bound BHMT structures are currently unavailable but mutational studies along with a BHMT bound transition state bi-substrate analog S-(δ-carboxybutyl)-L-homocysteine (CBHcy), have identified a ring of aromatic residues which participate in betaine binding (Pajares and Perez-Sala 2006). The substrates enter

the active site in order of Hcy followed by betaine (Castro, Gratson et al. 2004). Substrate binding induces conformational changes that are expected to bring the two substrates in proximity. A direct methyl transfer reaction is expected to proceed between a thiolate nucleophile and a methyl group attached to the quaternary amine of betaine.

S-Methylmethionine Hcy S-Methyltransferase (HMT)

The enzyme HMT (EC 2.1.1.12) is a zinc metalloenzyme which generates methionine by catalyzing the transfer of a methyl group from L-*S*-methylmethionine (SMM) to homocysteine (Ranocha, Bourgis et al. 2000). SMM is a major sulfur containing metabolite in plants, created and depleted through the SMM cycle. Organisms such as bacteria, yeast and mammals can obtain SMM through diet and use it to make methionine via the HMT enzyme.

Enzymes with HMT activity have been isolated from *Homo sapiens* (BHMT-2) and *E. coli* (YagD) (Thanbichler, Neuhierl et al. 1999, Szegedi, Castro et al. 2008). The bacterial enzyme, YagD shares some sequence similarity with the amino-terminal domain of MetH and to BHMT. It synthesizes methionine using SMM or S-adenosyl methionine and Hcy. The mammalian enzyme, BHMT-2 encodes a 40 kDa protein which is 73% identical to the BHMT protein. BHMT-2 uses SMM and to a lesser degree AdoMet as a methyl donor. A model of BHMT-2 was built by Garrow and colleagues using BHMT as a scaffold (Swiss model software). Like the amino-domain of MetH, BHMT, and the C-terminal domain of MetE, BHMT-2 consists of a $(\beta\alpha)_8$ barrel with conserved cysteine residues which coordinate with a zinc.

Folate and anti-folate bound enzymes deposited in the PDB

The majority of folate and anti-folate bound structures available in the PDB are of Dihydrofolate reductase (DHFR) and Thymidylate synthase (TS). DHFR has long been a

target of anticancer and antibiotic drugs due to its role as the sole provider of THF. THF is an essential intermediate for purine and thymidylate synthesis and indirectly effects cell growth and proliferation (Schnell, Dyson et al. 2004). Thymidylate synthase is also a target for anticancer chemotherapy due to its role as the sole provider of de novo thymidylate, an essential precursor required for DNA replication and repair (Garg, Henrich et al. 2010). Although the two enzymes are structurally unique, a number of folate and antifolate scaffolds can bind both enzymes. Figure 1.18 shows each enzyme bound with methotrexate-Glu_1. Research over the last 50 years has generated a number of unique antifolate scaffolds with structural and mechanistic data (Wright and Anderson 2011).

A PDB ligand search with the folate/antifolate scaffolds of THF, folinic acid or methotrexate yields a number of ligand bound structures. As expected, the majority of structures are of DHFR or TS, but a fair number are other enzymes in which a folate binding site also exists (Table 1.4). The overall structures are quite different, but all manage to bind folate; many are proteins that contain a Rossman fold, $(\beta\alpha)_8$ barrel, alpha+beta fold of some sort resembling TS, and a three domain clover leaf. Some have extensive hydrogen bond and ionic bond interactions with all parts of the folate while others appear to anchor one particular moiety. For example, in the corrinoid iron-sulfur protein (CoFeSP) folate binds in an extended conformation with extensive hydrogen bonding and ion pair interactions with residues on the top of a $(\beta\alpha)_8$ barrel, very similar to the MetH bound structure (Figure 1.18). In others like pteridine reductase (PTR1) with a Rossmann fold (also found in DHFR), the PABA moiety folds back onto the pterin, much like the “V” or “L” conformation observed in MetE (Figure 1.18). The available folate analogs and inhibitors can be potentially useful when targeting the Met6p active site.

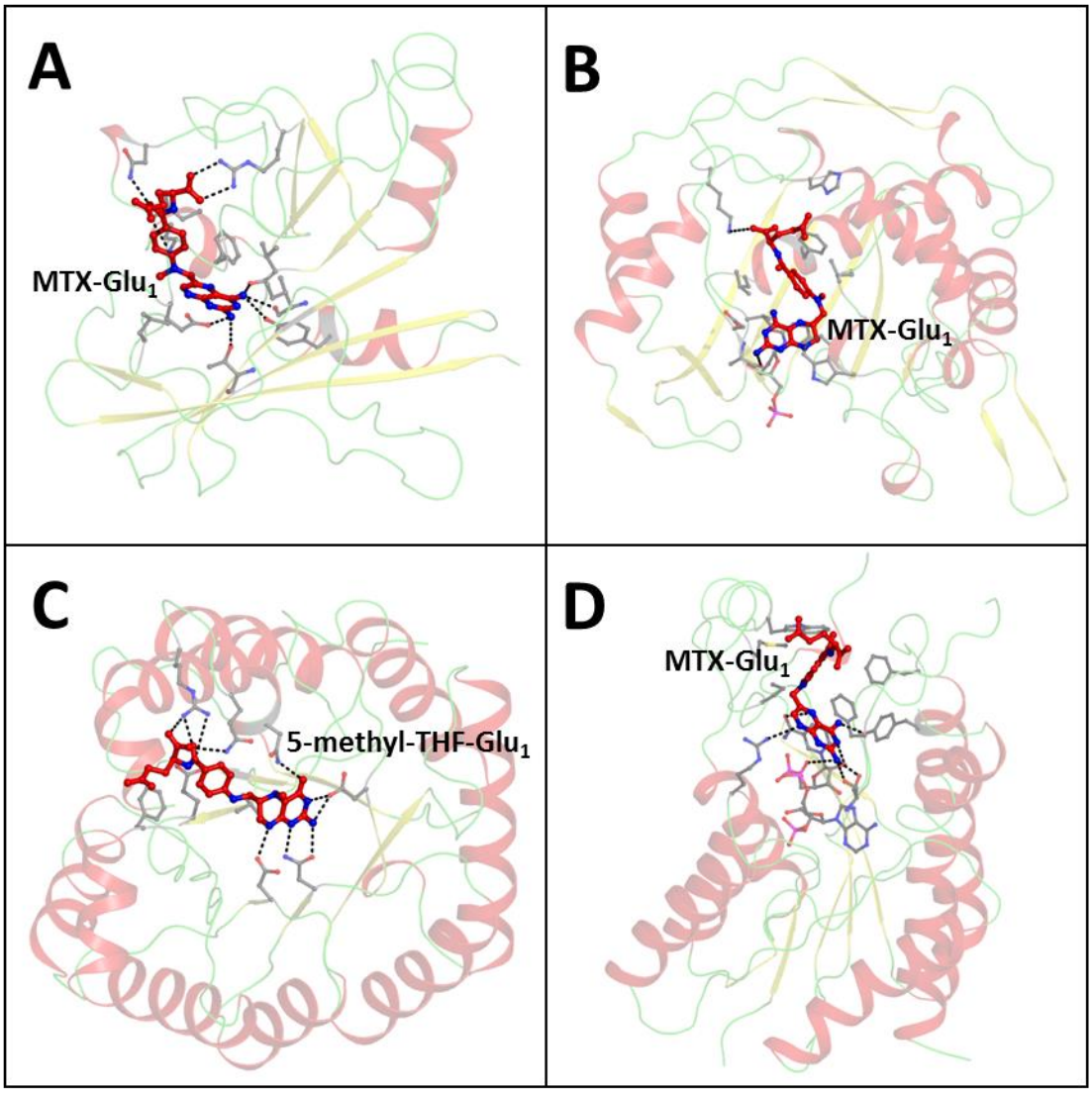

Figure 1.18 Few folate/anti-folate bound enzymes. A) DHFR (3EIG) bound with MTX-Glu_1. B) TS (1AXW) bound with MTX-Glu_1. C) CoFeSP (2YCJ) bound with 5-methyl-THF-Glu_1. D) PTR1 (2C7V) bound with MTX-Glu_1. Bonds are shown as black dashes.

Table 1.4 Folate/anti-folate bound proteins available in the protein data bank

Enzyme	Ligand	PDB ID
Dihydrofolate Reductase	6S-Folinic Acid (Glu1)	1JOL
Dihydrofolate Reductase	Inhibitors	3S7A, 1OHK, 2INQ, 3EIG, 1KLK, 3D80, 1BZF, 3TQ8, 3FRE, 2BFM, 1DIS, 3QFX, 3NTZ
Serine Hydroxymethyltransferase	Folinic Acid (Glu3)	1LS3
Glycinamide Ribonucleotide Transformylase (PurN)	5-methyl-THF-Glu1	3DCJ
N-Terminal formyltransferase domain of ARNA	6R-Folinic Acid (Glu1)	2BLN
Pteridine Reductase I	Inhibitors	3H4V, 2QHX, 2C7V, 2X9V, 2BFM
Thymidylate Synthase	5,10-Methylene-THF-Glu1, 6S-THF-Glu1	3BGX, 1KZI
Thymidylate Synthase	Inhibitors	2BBQ, 1JTQ, 1JTU, 1JUT, 1KCE, 1SYN, 1AXW
Formiminotransferase domain of formiminotransferase-cyclodeaminase	6R-Folinic Acid (Glu1)	1QD1
MnmE G protein	6R-Folinic Acid (Glu1)	3GEH
GTP-binding protein TrmE	6R-Folinic Acid (Glu1)	1XZQ
Cobalamin dependent methionine synthase	5-methyl-THF-Glu1	1Q8J
Cobalamin independent methionine syntase	5-methyl-THF-Glu3, THF-Glu3	1U1J, 1U22
Corrinoid iron-sulfur protein (CoFeSP)	5-methyl-THF-Glu1	2YCJ
T-Protein of Glycine Cleavage System	5-methyl-THF-Glu1, 6S-Folinic Acid (Glu1)	1WSV,1WOP
Heterotetrameric sarcosine oxidase	6R-Folinic Acid (Glu1)	1VRQ
Dimethylsulfoniopropionate-dependent demethylase	6S-THF-Glu1	3TFJ
D552A Dimethylgycine oxidase	6S-THF-Glu1, 6S-Folinic Acid (Glu1)	3GSI, 1PJ7
Nitric oxide synthase Heme protein	6S-THF-Glu1	1M7V
Nitric oxide synthase Heme protein	Quinonoid 7,8-tetrahydrobiopterin, 4-Aminobiopterin	1DWW, 2G6J
Glutamate Carboxypeptidase II	MTX analog	3BI1

Cobalamin-independent Methionine Synthase as a drug target

Structural perspective

The cobalamin-independent methionine synthase enzyme is a promising new anti-fungal drug target because structurally and mechanistically it is unlike the methionine synthase found in mammals (MetH). Although both enzymes bind the same substrates, prior to the alkylation reaction, these substrates are set 50 Å apart in MetH and only 7 Å apart in MetE. Both enzymes rely on large structural rearrangements to complete the methyl transfer reaction. In MetH, the B_{12} module cycles between the tops of the immobile $(\beta\alpha)_8$ barrels and the reaction takes place between a methylcobalamin intermediate and the Hcy. In contrast, MetE mediates a direct methyl transfer reaction by merging the two individual substrate pockets into one as it structurally transitions from the 'open' configuration to a 'closed' configuration.

A drug design strategy aimed at selectively binding and inhibiting the cobalamin-independent enzyme is feasible for both the open and closed MetE configurations. Clearly, both enzymes have evolved to bind an amino acid (Hcy) and a folate. Each site represents a potential target for inhibitor design, however a single bi-dentate substrate analog that spans both substrate binding pockets has great drug potential. From a practical standpoint, the binding affinity of such a ligand could be strong since the free energy of each component adds to the binding of the complete ligand. Also, the specificity is enhanced since no other protein binds both moieties in close proximity. The therapeutic window for such a compound would be large since the human enzyme is so different from the fungal one. That is, a bi-substrate inhibitor designed for MetE will be a poor ligand for the methylcobalamin-Hcy transition state pocket in MetH. A model of the methylcobalamin bound to the Hcy module was created by Evans in which a flat B_{12} corrin ring stacks against the top of the $(\beta\alpha)_8$ barrel (Figure 1.16) (Evans, Huddler et al.

2004). Hydrophobic interactions and specific hydrogen bonds help to create a unique Hcy-methylcobalamin binding site.

High quality substrate-bound structures of the fungal Met6p enzyme are very desirable in order to design decent bi-substrate inhibitors. So far the bacterial and plant MetE homologs have only been crystallized in the 'open' configuration and the available substrate-replete structures are of poor quality. Nevertheless, a MetE specific bi-substrate analog can be designed to bind and immobilize this 'open' configuration. Also, if the Met6p enzyme is successfully crystallized in the 'closed' form it may lead to more potent inhibitors of MetE that immobilize it in a closed configuration.

Biological perspective

The gene encoding the Met6p enzyme is absolutely required for *C. albicans* growth (Suliman, Appling et al. 2007). The Robertus and Appling labs have already shown that a diploid *C. albicans* strain lacking both copies of the MET6 gene is unable to grow in media supplemented with methionine. Since *C. albicans* can acquire methionine from the media via a number of amino acid transporters, the lethal phenotype cannot be explained by a simple methionine auxotrophy (Kaur and Mishra 1991, Sophianopoulou and Diallinas 1995, Wipf, Ludewig et al. 2002). When one MET6 locus was deleted and the second placed under a regulatable, but slightly leaky promoter, the mutant grew under inducing conditions. However, it would not grow under repressing conditions, unless supplemented with exogenous methionine. The conditional mutant is different from the double knockout strain because its growth was rescued with exogenous methionine while the double knockout is lethal. This is attributed to the low amount of MET6 expressed under repressing conditions by the leaky conditional promoter, and further supports the requirement of the Met6p protein for fungal growth.

Similar experiments have also been done in *Cryptococcus neoformans*, *Fusarium graminearum*, *Aspergillus nidulans*, *Saccharomyces cerevisiae*, and *Schizosaccharomyces pombe* (Kacprzak, Lewandowska et al. 2003, Pascon, Ganous et al. 2004, Seong, Hou et al. 2005, Suliman, Sawyer et al. 2005, Fujita, Ukena et al. 2006). Although the complete depletion of the MET6 gene is not lethal to the pathogenic fungus *C. neoformans* and the wheat scub fungus *F. graminearum*, it does result in a significant growth defect. In both fungi, the MET6 mutants also grew poorly in media supplemented with methionine. The doubling time for the mutant *C. neoformans* was ~3.5 hours compared to the ~1.6 hours observed for the wild-type strain. In *Aspergillus nidulans*, and *Saccharomyces cerevisiae* the MET6 gene is not essential and growth of a MET6 mutant can be fully rescued with exogenous methionine (Kacprzak, Lewandowska et al. 2003, Suliman, Sawyer et al. 2005). Interestingly, the MET6 mutant in *Schizosaccharomyces pombe* was rescued when both methionine and adenine were added to the growth media (Fujita, Ukena et al. 2006).

The slow growing MET6 mutant strains of *C. neoformans* and *F. graminearum* have also been evaluated for virulence in mice and plants, respectively. Pascon and coworkers discovered that when mice were infected with the wild type *C. neoformans* they died between 21-25 days post infection; in contrast, those infected with the MET6 mutant strain remained healthy until they were euthanized 70 days post-infection (Pascon, Ganous et al. 2004). When grown in cell culture, the MET6 mutant strain showed signs of compromised virulence including reduced capsule formation and lowered thermotolerance. The MET6 mutant was also more susceptible to the antifungal drugs fluconazole, FK506 and CsA. Likewise, plants infected with the MET6 mutant strain (msy1) of *F. graminearum* appeared healthy and viable, meaning the mutant failed

to establish wheat head infection. In cell culture, this mutant also produced very little aerial hyphae; an important virulence factor (Seong, Hou et al. 2005).

The complete disruption of the methionine synthase gene is lethal for *C. albicans*, *C. neoformans* and *F. graminearum,* even when supplemented with Met. It may be that high concentrations of the metabolite Hcy are toxic to the cells. A high level of Hcy is usually indicative of defects in enzymes responsible for remethylation (methionine synthase), trans-sulfuration (cystathionine β-synthase) or folate metabolism (Zimny, Sikora et al. 2006). However, in the case of methionine synthase, even if the mutation is compensated by adding the product methionine, the MET6 mutant is not fully rescued possibly because of the accumulating Hcy. A high concentration of Hcy is linked to toxicity in animals, yeast, and bacteria. Although the exact mechanism of toxicity is unknown, it might be linked to the conversion of Hcy to Hcy-thiolactone. If Hcy is not metabolized to Hcy-thiolactone, it can be incorporated into proteins to form toxic Hcy-proteins. On the other hand, the synthesis of Hcy-thiolactone consumes cellular energy in the form of ATP, and the resulting product is a reactive intermediate which damages proteins through protein homocysteinylation (Jakubowski 1999). Hcy-thiolactone is either excreted or hydrolyzed back to Hcy by a Hcy-thiolactonase. The accumulation of Hcy is also predicted to inhibit purine biosynthesis, and high levels of Hcy have been found to inhibit ergosterol synthesis in yeast (Hatanaka, Ariga et al. 1974, Parks and Casey 1995, Fujita, Ukena et al. 2006).

The concentration of Hcy was measured by HPLC in a wild-type and MET6 mutant strain of *Schizosaccharomyces pombe.* As expected, the total Hcy content in the methionine synthase mutant was 18 times higher than the wild-type strain (Fujita, Ukena et al. 2006). In *E. coli* both the Hcy and Hcy-thiolactone metabolites are known to

upregulate the mRNA and enzyme levels of methionine synthase (Kacprzak, Lewandowska et al. 2003).

The gene deletion studies have established that MetE is important for growth and virulence. This is in line with gene expression studies which show that MET6 is strongly expressed in plants, yeast and bacteria during growth, stress or infection. Methionine is an important metabolite since cells invest significant energy for its synthesis through methionine synthase or acquisition through the amino acid transporters. During growth and in the absence of cobalamin and methionine, the MetE enzyme is extremely abundant, constituting 3% of the total soluble protein in *E.coli* cells (Gonzalez, Banerjee et al. 1992). And during plant infection, the gene expression of MetE in the bacterium *Ralstonia solanacearum* was found to be specifically and strongly induced (10-fold more than MetH) (Plener, Boistard et al. 2012). During normal growth, fungi (*Cladosporium fulvum*, *Saccharomyces cerevisiae*, *Aspergilus nidulans*), plants (*Catharantus roseus*) and bacteria (*E. coli*) modulate the expression of MET6/MetE based on methionine availability (Weissbach and Brot 1991, Eichel, Gonzalez et al. 1995, Solomon, Nielsen et al. 2000). Starvation and high stress conditions experienced during host infection by the pathogen *C. fulvum* also appeared to increase MET6 gene expression (Solomon, Nielsen et al. 2000). When the plant cells of *C. roseus* or leaves of *Solanum tuberosum* were deprived of nutrients by using sucrose, a significant increase in the expression of MetE was observed (Eichel, Gonzalez et al. 1995, Zeh, Leggewie et al. 2002). Since methionine is a precursor of S-adenosyl methionine (AdoMet), the major methyl-group donor required for protein synthesis and gene expression, the synthesis or acquisition of methionine is understandably up-regulated for growth and survival.

Candidiasis and candidemia

Various microorganisms, including bacteria, fungi, yeast, archae and viruses, colonize the skin, oral cavity, respiratory pathways, stomach, the gastrointestinal tract, and the urinary and genital tracts of the human body (Tannock 1995). These microbes form complex communities and establish an ecosystem that can benefit the host (Rajilic-Stojanovic 2013). The highest microbe density is reported in the intestinal tract where the microbiota's collective genome contains 100 fold more genes than the host. The microbial activity is beneficial since it improves digestion, provides vitamins, inhibits pathogenic growth and stimulates the immune system.

However, an imbalance in the indigenous microbial composition leads to problems in metabolism and causes infections (Kim, Jeon et al. 2013). A few bacterial strains make up 99.9% of the ecosystem; the less abundant, but more diverse 0.1% 'rare biosphere' includes the fungal microbiome (Huffnagle and Noverr 2013). Aside from the known benefits of *Saccharomyces cerevisiae*, there is no strong evidence in favor of a mutual fungal-host relationship. Many fungal species such as those belonging to the genus *Candida* are members of the normal microbiome in the various mucosal surfaces and skin. However, in response to a compromised host immune system or alterations in the normal microbiota, the opportunistic *Candida* species becomes pathogenic and cause infection. *Candida* infections, or candidiasis, can be superficial or severe, as in systemic candidiasis. In fact, *Candida* infections are ranked as the 3rd or 4th most common cause of hospital-acquired bloodstream infections, called candidemia (Moyes and Naglik 2011).

Over the last two decades, the incidence of candidemia has increased significantly and can be attributed to the ever growing number of immuno-compromised individuals who undergo transplantations, chemotherapy or suffer from HIV infections (Pfaller, Jones et al. 1998, Falagas, Roussos et al. 2010, Das, Nightingale et al. 2011). The mode

of virulence is perhaps best characterized for *C. albicans* since it is the most prevalent and usually associated with the highest mortality (Pfaller, Jones et al. 1998). Normally, *C. albicans* grows as budding yeast and this growth is kept under control by the diverse microbe community and an effective immune system. The host-fungus interaction is quite complex and still under investigation. However, a few studies have shown that *Candida* is not a passive participant in the process of pathogenesis (Rizzetto and Cavalieri 2011, Sardi, Scorzoni et al. 2013). *Candida albicans*, in particular, is equipped with fitness attributes and virulence factors which are used to actively establish candidiasis and evade the host immune system. These include the ability to attach to host cells (using adhesins), growth as filamentous hyphae (yeast-hyphae transition), penetration of the host cell (using invasins and hydrolytic enzymes), formation of impregnable biofilms in host cells and catheters, adaptation to fluctuations in environmental pH, acquisition of nutrients, and survival under stress (heat, oxidation) (Mayer, Wilson et al. 2013). The ability to transition between yeast and hyphae and to form a biofilm is critical for establishing virulence, characteristics also possessed by the newly emerging pathogens *C. parapsilosis*, *C. tropicalis* and *C. glabrata*.

The current arsenal of anti-fungal drugs is limited due to the similarities between mammalian and fungal pathways. The first class consists of polyene derivatives which associate with the ergosterol in the cell membrane and promote cell leakage. The azole derivatives also target the cell membrane by inhibiting the fungal cytochrome P450 dependent conversion of lanosterol to ergosterol. Finally, the echinochandins weaken the cell wall by inhibiting 1,3-ß -glucan synthase (Lai, Tan et al. 2008).

Unfortunately, substantial adverse effects and limited anti-fungal activity are associated with the use of polyene and azole derivatives. Echinochandins target a uniquely fungal pathway and therefore have the lowest toxicity and the widest spectrum

of use. However, in order to treat the often drug-resistant biofilms, drugs from the different classes must be combined or the infected medical device must be removed (Sardi, Scorzoni et al. 2013). A major problem is that drug resistant *Candida* strains have already been isolated and include the mostly fluconazole resistant *C. glabrata* isolates (Krcmery and Barnes 2002).

Summary and Project Goals

The cobalamin-independent (Met6p) and dependent (MetH) methionine synthases are two very different enzymes which catalyze the same overall reaction in the pathogenic fungi and the human host, respectively. The methionine synthase enzyme in each organism is metabolically essential and sits at a point of convergence where folate-mediated one-carbon metabolism meets methionine synthesis. Defects in methionine synthase impact folate metabolism, AdoMet mediated methyl transfer reactions and Hcy metabolism. In fact, in the fungal species, *Candida albicans*, the MET6 gene which encodes the Met6p enzyme is absolutely required for fungal growth. This fungal species is one of the most prevalent causes of candedimia in the immunocompromised population around the world, and the primary fungal target in the Robertus lab.

We believe that the structural and biological attributes of the Met6p enzyme make it an ideal antifungal drug target and potent Met6p specific inhibitors should be able to control a fungal infection with minimal toxicity against the human host. The overall goal of this project is to discover a variety of drug-like scaffolds for the Met6p active site and to develop structural and kinetic methods to characterize the drug-Met6p interaction. The resulting lead compounds could then be derivatized into highly specific and potent Met6p inhibitors in collaboration with an organic chemist, and ultimately tested in mice infected

with *Candida albicans*. I successfully tested a part of this hypothesis by completing the following aims:

Aim 1: Crystallization of the Met6p enzyme using SER

The wild type Met6p protein could not be crystallized by traditional screening methods so Dr. Kate Kavanagh suggested we use a protein engineering strategy known as Surface Entropy Reduction (SER). Under her guidance I created three variants of Met6p in which three surface residues were replaced by alanines (Met6pA), threonines (Met6pT), or tyrosines (Met6pY). The X-ray structures and crystal packing arrangement of each crystal were reported in "Structure of *Candida albicans* methionine synthase determined by employing surface residue mutagenesis" (Ubhi, Kavanagh et al. 2011).

Aim 2: Characterization of the Met6p active site in the 'open' configuration

Met6p catalyzes a direct methyl transfer reaction by cycling between the 'open' configuration we observed in the Met6pA, Met6pT and Met6pY variants, to the yet unobserved 'closed' configuration. The 'open' configuration has two substrate binding pockets separated by ~7 Å and a metal coordination site. I solved a number of substrate or product bound binary and ternary complexes which were analyzed and compared to each other and the apo structure. Any interesting residues were mutated by site-directed mutagenesis and their function was evaluated using an activity assay.

Aim 3: Development of a fluorescence-based Met6p activity assay

The established absorbance based kinetic assay cannot be used to evaluate inhibitors which also absorb at 350 nm, so an alternative fluorescence based kinetic assay was created, optimized and used to test potential inhibitors. This assay uses the Measure-iT^{TM} thiol quantitation reagent to selectively measure the concentration of unused Hcy in a Met6p reaction.

Aim 4: Optimization of a high-throughput DSF assay used to screen diverse compound libraries

The high-throughput Differential Scanning Fluorimetry (DSF) method is frequently used in drug discovery programs to identify compounds which bind and increase the melting temperature (Tm) of a target protein. I optimized a 96-well DSF method for Met6p and used it to screen 731 compounds from the NIH clinical collection, 4000 compounds from the Fragment library (Chembridge) and 4000 compounds from the KINAset library (Chembridge). The hits were further evaluated by an activity assay and the IC_{50}s were determined using dose-response experiments.

Aim 5: Discovering lead compounds by rational drug design

The last strategy used to find potential Met6p inhibitors was based on principles of ligand-based and structure-based drug design. I searched for commercially available ligands which could occupy the folate, Hcy or both binding pockets simultaneously. These ligands include anti-folates like MTX-Glu_3, amino acids like Gln, or a folate-Hcy bi-substrate analog like S-adenosyl homocysteine. These ligands were tested for binding by X-ray crystallography and for inhibition by the fluorescence based activity assay.

CHAPTER 2: MATERIALS AND METHODS

Cloning and expression of Met6p in *E. coli*

The MET6 gene encoding the *Candida albicans* Met6p protein was amplified from Yep24-CaMET6 vector and cloned into the kanamycin resistant *E. coli* expression vector pNIC28-Bsa4 purchased from Addgene (Figure 2.1) (Suliman, Sawyer et al. 2005). We amplified the MET6 gene by using PCR primers with the extensions TACTTCCAATCCatg on the 5' end of the upstream primer and TATCCACCTTTACTGtca on the 5' end of the downstream primer. These extensions overlap the vector sequences that flank the cloning site in pNIC28-Bsa4 (Figure 2.1). A detailed cloning, annealing, and transformation protocol described by Savitsky was used to create the pNIC28-CaMET6 vector (Savitsky, Bray et al. 2010). In this vector the MET6 gene is fused with an N-terminal tag of 23 residues (MHHHHHHSSGVDLGTENLYFQSM) that contains a hexahistidine (His_6) site for Ni-NTA purification followed by a TEV protease cleavage site (ENLYFQS) (Fig 2.2). The fusion gene and protein sequences are shown in Figures 2.3 and 2.4, respectively.

The pNIC28-CaMET6 expression vector was transformed into One Shot BL21(DE3) *E. coli* cells and Met6p protein was expressed in 2-4 L LB media supplemented with 500 μM $ZnSO_4$ and 50 mg/L kanamycin. Cells were grown at 37 °C until the OD600 reached 0.8. The cultures were shifted to 25 °C and expression was induced with 500 μM IPTG and allowed to continue for 4 hours. Cells were harvested by centrifugation and the pellets were stored at -80 °C.

A

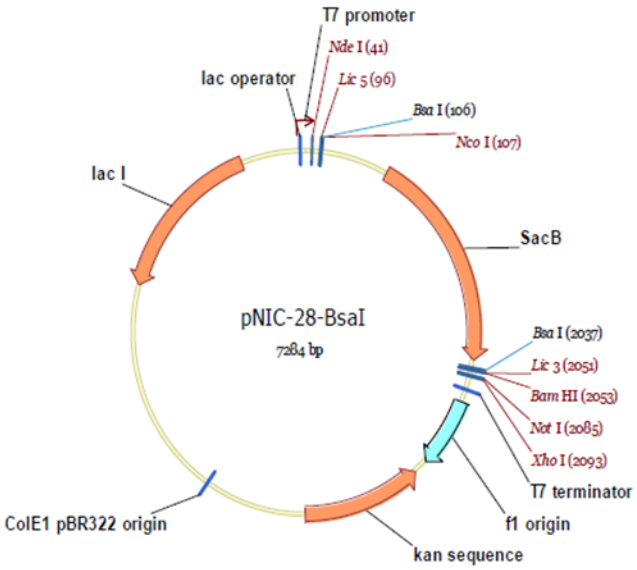

B

Vector Name	**pNIC28-Bsa4**
Source	Opher Gileadi
Sequence accession/link	(SGC)

Description	pET expression vector with His_6 tag in 22-aa N-terminal fusion peptide, with TEV protease cleavage site. Includes sites for LIC cloning, and a "stuffer" fragment that includes the SacB gene, allowing negative selection on 5% sucrose

Antibiotic resistance	Kanamycin, 50 μg/ml
Promoter	T7 - lacO
Cloning	LIC. (vector treated with BsaI, then with T4 DNA polymerase in presence of dGTP)
Initiation codon	Supplied in PCR primer
N-terminal fusion – seq.	MHHHHHHSSGVDLGTENLYFQ*SM (* - TEV cleavage site)
N-terminal fusion – MW	2684.1 Da including Met (2465.8 Da removed by TEV cleavage)
Termination codons	supplied in PCR primer
Protease cleavage	TEV
Additional features	
Preferred host	DE3 hosts: BL21, Rosetta, etc. MUST express T7 RNA polymerase.
5' sequencing primer	pLIC-for: TGTGAGCGGATAACAATTCC
3' sequencing primer	pLIC-rev: AGCAGCCAACTCAGCTTCC

Figure 2.1 The pNIC-28-Bsa4 cloning vector. A) Cloning vector. B) Vector information sheet from Addgene (http://www.addgene.org/26103/).

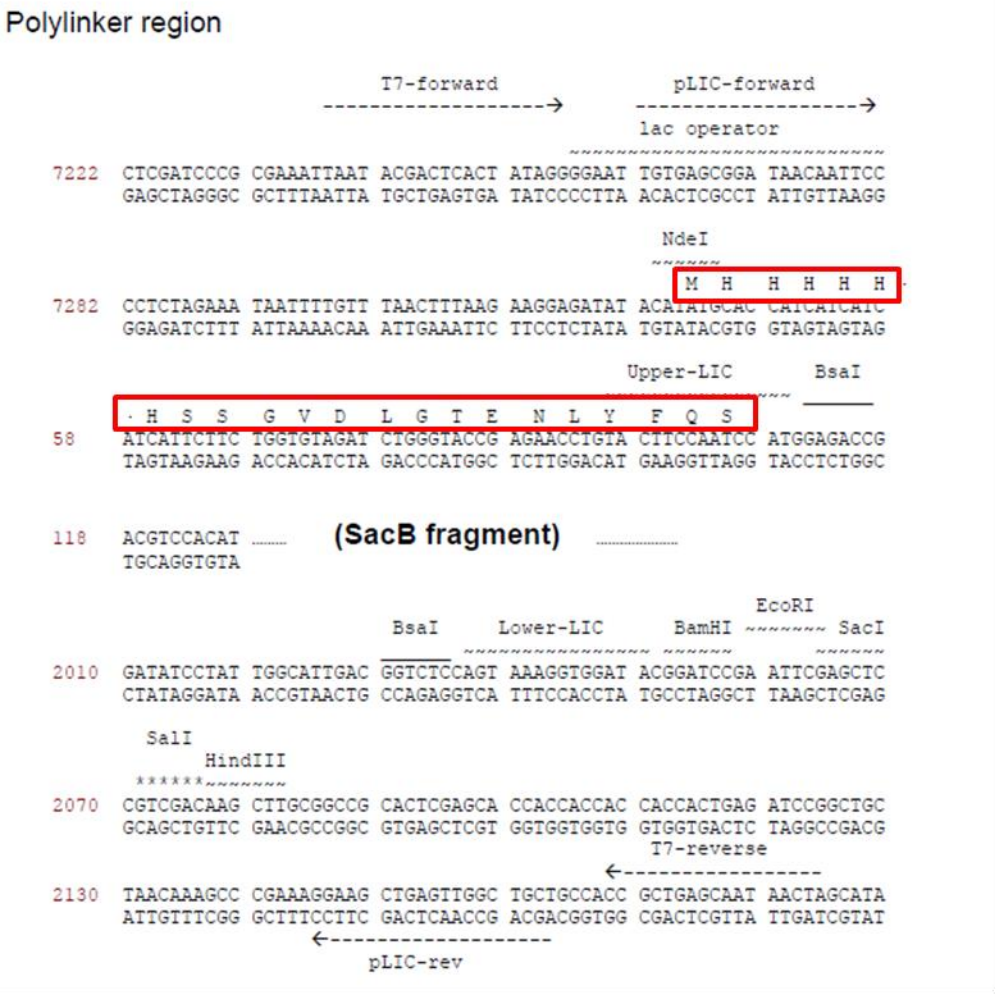

Figure 2.2 The polylinker region in the pNIC-28-Bsa4 cloning vector. The His_6 and TEV protease cleavage (ENLYFQS) sites are boxed in red. Available online at http://apps.thesgc.org/structures/MM/Vectors/pNIC28-Bsa4/pNIC28-Bsa4_Vector_sheet.pdf.

```
   1  ATGCACCATC ATCATCATCA TTCTTCTGGT GTAGATCTGG GTACCGAGAA CCTGTACTTC
  61  CAATCCATGG TTCAATCTTC CGTCTTAGGT TTCCCACGTA TTGGTGGTCA AAGAGAATTA
 121  AAAAAAATCA CTGAGGCCTA CTGGTCCGGT AAAGCTACTG TTGAAGAATT GTTAGCTAAA
 181  GGTAAAGAAT TGAGAGAGCA CAATTGGAAA TTACAACAAA AAGCTGGTGT TGATATCATT
 241  CCATCTAATG ATTTCTCCTA CTATGATCAA GTTTTAGATC TTTCTTTGTT GTTCAATGCT
 301  ATCCCAGAAA GATACACCAA ATTTGATTTG GCTCCAATTG ATGTTTTGTT TGCCATGGGT
 361  AGAGGTTTAC AAAAGAAAGC CACTGAAACT CAAGCTGCTG TTGATGTTAC TGCTTTGGAA
 421  ATGGTTAAAT GGTTTGATTC TAACTACCAT TATGTCAGAC CAACCTTTTC TCACTCTACT
 481  GAATTCAAAT TGAACACTGC TGCTGGTATC AAACCAGTTG ATGAATTCAA CGAAGCTAAA
 541  GCTTTGGGTG TTCAAACCAG ACCAGTCATC TTGGGTCCAG TTTCTTACTT GTATTTAGGT
 601  AAAGCTGACA AAGATTCCCT TGATTTGGAA CCAATTTCCT TGTTACCAAA GATCTTGCCA
 661  GTTTACAAGG AATTGTTGCA AAAATTGAAG GAAGCTGGTG CTGAACAAGT TCAAATTGAT
 721  GAACCAGTTT TGGTTTTGGA CTTGCCAGAA GCTGTTCAAT CCAAATTCAA AGAAGCTTAC
 781  GACGCTTTGG TTGGTGCTGA TGTCCCAGAA TTGATCTTGA CTACCTACTT TGGTGATGTC
 841  AGACCAAACT TGAAAGCCAT TGAAAACTTG CCAGTTGCTG GTTTCCACTT TGATTTCGTC
 901  AGAGTTCCAG AACAATTGGA CGAAGTTGCT TCTATCTTGA AAGATGGTCA AACTTTGTCT
 961  GCTGGTGTTG TCGATGGTAG AAACATTTGG AAGACTGATT TCGCCAAGGC TTCCGCTGTT
1021  GTCCAAAAAG CTATTGAAAA AGTTGGTAAA GATAAGGTTG TTGTTGCTAC TTCATCTTCA
1081  TTGTTGCACA CTCCAGTTGA TTTGGAATCT GAAACTAAAT TAGACGCTGT TATCAAGGAC
1141  TGGTTTTCCT TTGCTACTCA AAAATTGGAT GAAGTTGTTG TCATTGCCAA GAATGTTTCT
1201  GGTGAAGATG TTTCTAAACA ATTAGAAGCC AATGCTGCTT CCATCAAAGC TAGATCCGAA
1261  TCTTCTATCA CCAACGATCC AAAGGTTCAA GAAAGATTAA CTACCATTAA CGAAGCTTTG
1321  GCTACCAGAA AAGCCGCTTT CCCAGAAAGA TTAACTGAAC AAAAGGCTAA ATACAACTTG
1381  CCATTGTTCC CAACCACCAC CATCGGTTCT TTCCCACAAA CCAAAGACAT TAGAATCAAC
1441  AGAAACAAAT TTGCTAAAGG CCAAATTACT GCTGAAGAAT ACGAAGCTTT TATCAATAAA
1501  GAAATTGAAA CTGTTGTTAG ATTCCAAGAA GAAATTGGTT TGGATGTTTT AGTCCATGGT
1561  GAACCAGAAA GAAACGATAT GGTTCAATAC TTTGGTGAAC AATTGAATGG TTTTGCTTTC
1621  ACCACTAACG GTTGGGTCCA ATCTTATGGT TCTAGATATG TCAGACCACC AATTATTGTT
1681  GGTGATGTTT CCAGACCAAA AGCTATGACT GTTAAAGAAT CTGTCTATGC TCAATCTATT
1741  ACTTCTAAAC CAATGAAGGG TATGTTGACT GGTCCAGTCA CCATTTTGAG ATGGTCATTC
1801  CCAAGAGATG ATGTTTCTGG TAAAATCCAA GCTTTGCAAT TGGGTTTGGC TTTAAGAGAT
1861  GAAGTTAACG ACTTGGAAGG TGCTGGTATT ACTGTTATCC AAGTTGATGA ACCAGCTATC
1921  AGAGAAGGTT TGCCATTGAG AGCCGGTAAA GAAAGATCCG ACTATTTGAA CTGGGCTGCT
1981  CAATCATTTA GAGTTGCCAC TTCTGGTGTT GAAAACTCTA CTCAAATCCA CTCCCACTTC
2041  TGTTACTCCG ATTTGGATCC AAACCATATT AAAGCTTTGG ATGCTGATGT TGTTTCCATT
2101  GAATTCTCCA AGAAGGATGA TCCAAACTAT ATTCAAGAAT TCTCTGAATA TCCTAATCAC
2161  ATTGGTTTAG GTTTATTCGA TATCCACTCT CCAAGAATTC CATCTAAACA AGAATTTGTT
2221  TCCAGAATTG AAGAAATCTT GAAGGTTTAC CCAGCTTCTA AATTCTGGGT CAACCCAGAT
2281  TGTGGTTTGA AAACTAGAGG CTGGCCAGAA GTTAAGGAAT CATTGACCAA TATGGTTGAA
2341  GCTGCCAAAG AATTCAGAGC TAAATACTAA
```

Figure 2.3 The nucleotide sequence of the MET6 gene (in the pNIC28-CaMET6 vector). The nucleotides marking the start and end of the MET6 gene are shown in red.

Protein purification

Cell pellets were thawed and resuspended in lysis buffer (1X PBS, 20 mM Imidazole, 10 mM β-mercaptoethanol, pH 8.0) with protease inhibitors (Roche Complete EDTA-free, 1 tablet/50 mL). The cells were homogenized using a French pressure cell (3 passes, 1000 psi) and the cell debris removed by centrifugation for 1 hour at 25,000g and 4°C. The cell lysate was added to 2 mL of Ni-NTA resin and both were gently mixed for

MHHHHHHSSGVDLGTENLYFQSMVQSSVLGFPRIGGQRE
LKKITEAYWSGKATVEELLAKGKELREHNWKLQQKAGV
DIIPSNDFSYYDQVLDLSLLFNAIPERYTKFDLAPIDVLFA
MGRGLQKKATETQAAVDVTALEMVKWFDSNYHYVRPTF
SHSTEFKLNTAAGIKPVDEFNEAKALGVQTRPVILGPVSY
LYLGKADKDSLDLEPISLLPKILPVYKELLQKLKEAGAEQ
VQIDEPVLVLDLPEAVQSKFKEAYDALVGADVPELILTTY
FGDVRPNLKAIENLPVAGFHFDFVRVPEQLDEVASILKDG
QTLSAGVVDGRNIWKTDFAKASAVVQKAIEKVGKDKVV
VATSSSLLHTPVDLESETKLDAVIKDWFSFATQKLDEVVV
IAKNVSGEDVSKQLEANAASIKARSESSITNDPKVQERLT
TINEALATRKAAFPERLTEQKAKYNLPLFPTTTIGSFPQTK
DIRINRNKFAKGQITAEEYEAFINKEIETVVRFQEEIGLDV
LVHGEPERNDMVQYFGEQLNGFAFTTNGWVQSYGSRYV
RPPIIVGDVSRPKAMTVKESVYAQSITSKPMKGMLTGPVT
ILRWSFPRDDVSGKIQALQLGLALRDEVNDLEGAGITVIQ
VDEPAIREGLPLRAGKERSDYLNWAAQSFRVATSGVENS
TQIHSHFCYSDLDPNHIKALDADVVSIEFSKKDDPNYIQEF
SEYPNHIGLGLFDIHSPRIPSKQEFVSRIEEILKVYPASKFW
VNPDCGLKTRGWPEVKESLTNMVEAAKEFRAKYStop

Figure 2.4 The amino acid sequence of the Met6p protein (expressed using the pNIC28-CaMET6 vector). The start and end of the Met6 protein is shown in red.

30 min at 4 °C. This mixture was applied to a gravity flow column, washed with 20 mL lysis buffer and eluted with 6 mL of lysis buffer containing 500 mM imidazole. The eluted protein was first buffer exchanged into 20 mM Tris-HCL, 150 mM NaCl, 10 mM β-mercaptoethanol, pH 7.4 using a PD10 column and then further purified using a size exclusion column (S200 16/60) run at 1 ml/min on an Akta purification system. The fractions were analyzed by SDS-PAGE (8% gel) and those containing Met6p protein were pooled and concentrated using a Centricon filtration unit with 30 kDa MW cut-off. Protein purity was estimated to be >95% by SDS-PAGE gel (Figure 2.5). Protein concentration was measured using the absorbance at 280 nm and an extinction coefficient calculated from the protein sequence (ε = 90,760 M^{-1} cm^{-1}).

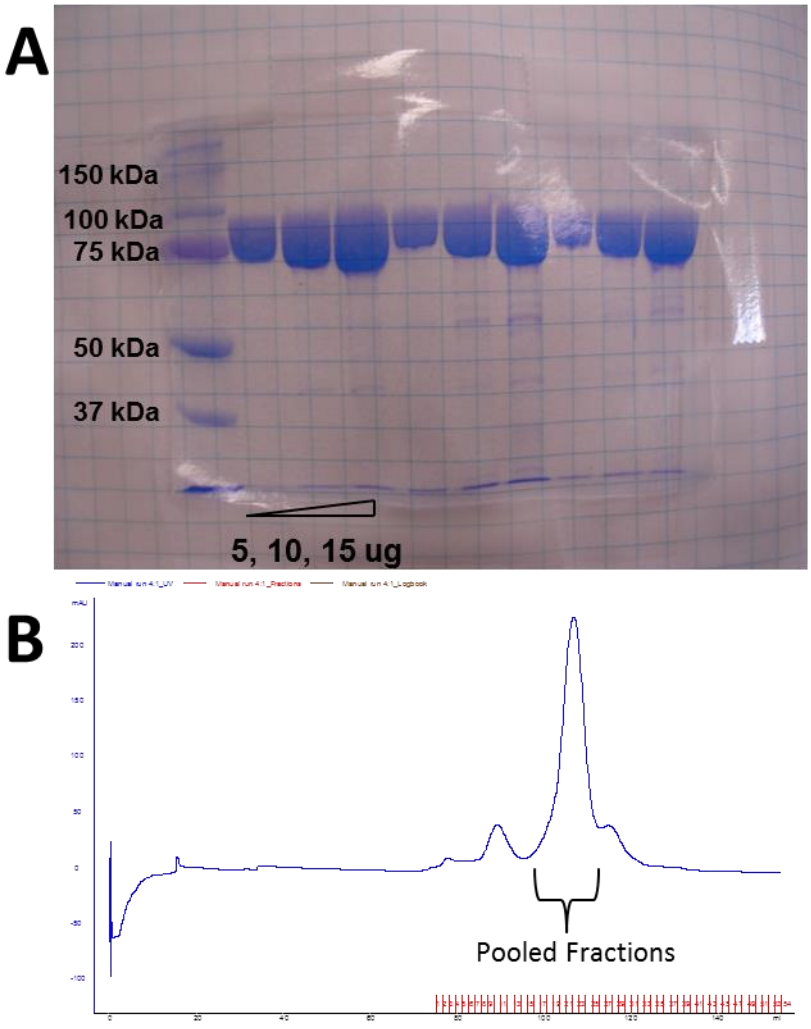

Figure 2.5 Met6p protein purification. A) An 8% SDS gel was loaded with 5, 10, and 15 µg of purified Met6p protein. The precision plus protein standard from Biorad was loaded in the first well on the left. B) A typical absorbance 280 nm spectra observed for Met6p by gel filtration (S200 16/60, GE Healthcare).

Surface Entropy Reduction (SER)

The SERp server (http://nihserver.mbi.ucla.edu/SER/) was used to identify potential residues for surface entropy reduction mutations (Goldschmidt, Cooper et al.

2007). The top scoring cluster, ^{103}LysLysAlaThrGlu^{107}, with the SERp score of 7.01 was then compared to known bacterial and plant structures and found to be on a loop that is ~10 residues longer in the fungal protein. This loop region was chosen for mutation. Based upon a previous study that looked at the role of different amino acids in promoting crystal contacts, the two lysine and one glutamate residues were mutated either all to Ala, all to Thr, or all to Tyr in variants labeled Met6pA, Met6pT, and Met6pY, respectively (Cooper, Boczek et al. 2007).

Site-directed mutagenesis

The desired mutations were introduced using PCR-based site-directed mutagenesis by following the instructions in the QuickChange™ Site-Directed Mutagenesis Kit (Stratagene, La Jolla, CA, USA) (Kim and Maas 2000). We used the online QuikChange Primer Design program (http://www.genomics.agilent.com/primerDesignProgram) to make each set of complementary PCR primers. The PCR primers used to create the SER mutants Met6pA, Met6pT and Met6pY, were designed to introduce multiple mutations in the wild-type MET6 gene (Figure 2.6). The PCR primers used to generate each point mutant Tyr660Ala, Tyr660Gln, Tyr660Phe, and Asn126Ala were shorter and introduced a single mutation in the gene encoding the Met6pA variant (Figure 2.6). The general PCR reaction conditions are listed in Figure 2.6. We used KOD Hot Start DNA polymerase (Novagen) for plasmid amplification and destroyed each parent vector with the enzyme *DpnI* (Biolabs). The gene mutations were verified by DNA sequencing. All mutant plasmids were transformed into BL21 cells followed by protein expression and purification using the methods described above.

A

Mutant	Tm	Primers
Met6pA	79°C	5'-gttttgtttgccatgggtagaggtttacaagcggcagccactgcaactcaagctgctgtt-3' 5'-aacagcagcttgagttgcagtggctgccgcttgtaaacctctacccatggcaaacaaaac-3'
Met6pY	79°C	5'-tttgtttgccatgggtagaggtttacaatattatgccacttatactcaagctgctgttgatgttactgc-3' 5'-gcagtaacatcaacagcagcttgagtataagtggcataatattgtaaacctctacccatggcaaacaaa-3'
Met6pT	79°C	5'-gttttgtttgccatgggtagaggtttacaaaccacagccactacaactcaagctgctgttgat-3' 5'-atcaacagcagcttgagttgtagtggctgtggtttgtaaacctctacccatggcaaacaaaac-3'
Met6pA Y660A	78°C	5'-aatccactcccacttctgtgcctccgatttggatccaaac-3' 5'-gtttggatccaaatcggaggcacagaagtgggagtggatt-3'
Met6pA Y660F	78°C	5'-aaatccactcccacttctgtttctccgatttggatc-3' 5'-gatccaaatcggagaaacagaagtgggagtggattt-3'
Met6pA Y660Q	78°C	5'-tcaaatccactcccacttctgtcagtccgatttggatcca-3' 5'-tggatccaaatcggactgacagaagtgggagtggatttga-3'
Met6pA N126A	79°C	5'-ggaaatggttaaatggtttgattctgcctaccattatgtcagaccaacctttt-3' 5'-aaaggttggtctgacataatggtaggcagaatcaaaccatttaaccatttcc-3'

B

Final Concentration	Components (Stock Conc.)	**50 µl RXN**
1X	PCR buffer (10x)	5
0.2 mM	dNTPs (2 mM)	5
1.0 mM	MgSO4 (25 mM)	2
0.3 µM	5' Primer (10 µM)	1.5
0.3 µM	3' Primer (10 µM)	1.5
20 ng DNA	Plasmid DNA (20 ng/µl)	5
	PCR grade water	29
1.0 U	KOD Polymerase (1U/µl)	1

Cycle(s)	Temperature (°C)	Time
1	95	**2 Min**
18	95	**30 Sec**
	(Primer Tm - 3°C)	**30 Sec**
	72	**8 Min**

Figure 2.6 PCR primers and reaction conditions. A) Complementary PCR primers were created to make each Met6p mutant. B) PCR conditions used to create each Met6p mutant.

Crystallization

The SER variant proteins were concentrated to ~20 mg/ml in 20 mM Tris, 150 mM NaCl, 10 mM β-mercaptoethanol, pH 7.4. Crystallization trials were set up with both apo protein solutions and protein solutions containing 10 mM Hcy using the JCSG$^+$ suite (Qiagen) and PEG/Ion HT (Hampton Research) 96-well screening kits. The plates were set up using a Phoenix crystallization robot (Art Robbins Instruments) and were incubated at 20 °C. Several conditions producing initial crystals were identified, and two were chosen for optimization: JCSG$^+$ G9 (30% [w/v] PEG-MME 2000, 0.1 M KSCN) and PEG/Ion A10 (20% [w/v] PEG3350, 0.2 M NaI). Crystal optimization experiments were set up with all three mutants in 96-well and 24-well formats.

Optimized crystals of the Met6pA mutant were rod-shaped with a maximum length of 800 μm (Figure 2.7). They were grown in hanging drops at 20 °C by mixing 1 μL of 20 mg/ml apo protein and 2 μL of a well solution consisting of 27 % (w/v) PEG 3350, 50 mM NaI and equilibrated against 500 μL of the well solution. Prior to data collection, a single crystal was cryo-protected in 30% (w/v) PEG 3350, 50 mM NaI and flash-cooled in liquid nitrogen.

Optimized crystals of the Met6pT mutant were large plates with dimensions 800 x 300 x 50 μm (Figure 2.7). They were grown in hanging drops at 20 °C by mixing 1 μL of 20 mg/ml apo protein with 2 μL of a well solution composed of 25% (w/v) PEG-MME 2000, 75 mM KSCN and equilibrated against 500 μL of well solution. Prior to data collection, a single crystal was cryo-protected in 30% (w/v) PEG-MME 2000, 75 mM KSCN, and plunged into liquid nitrogen.

Optimized crystals of the Met6pY mutant were rod-shaped with a maximum length of 200 μm (Figure 2.7). They were grown in hanging drops at 20 °C by mixing 0.7 μL of 20 mg/ml apo protein and 1.3 μL of a well solution consisting of 20% (w/v)

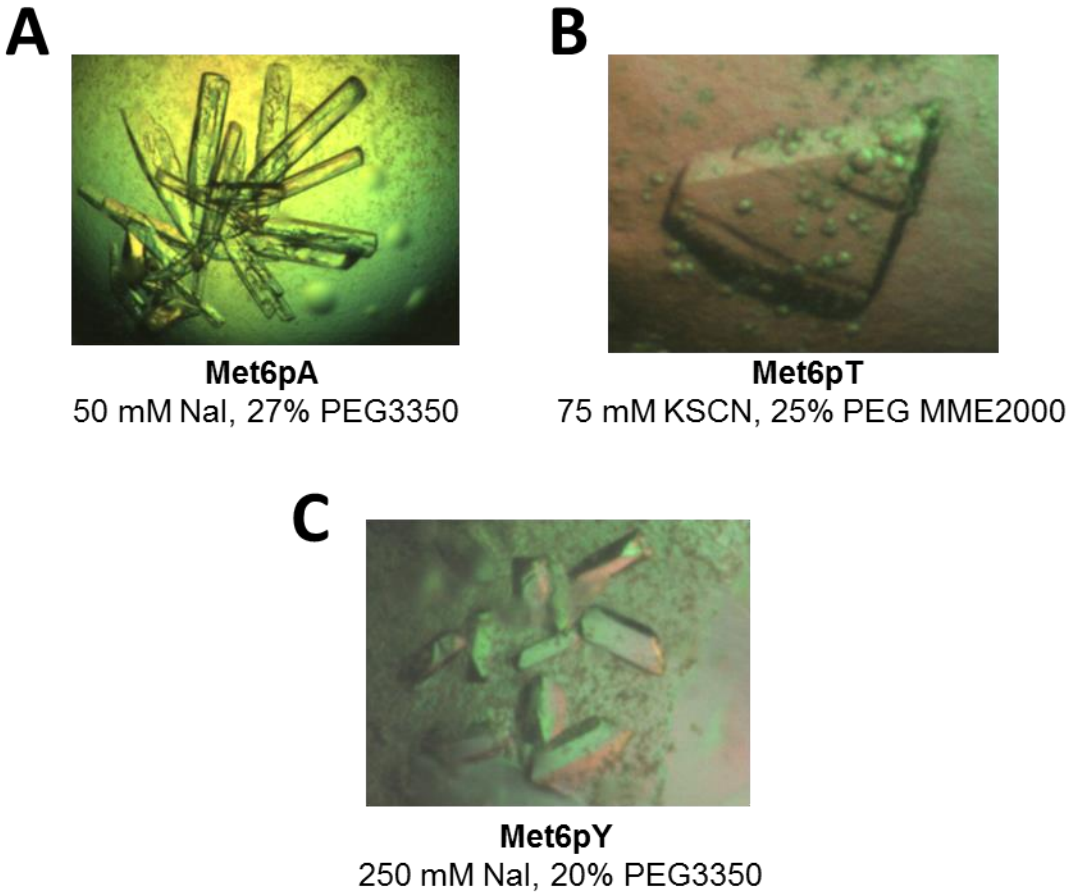

Figure 2.7 Protein crystals of the SER mutants. A) Met6pA variant. B) Met6pT variant. C) Met6pY variant.

PEG 3350, 250 mM NaI and equilibrated against 500 µL of the well solution. Prior to data collection, a single crystal was cryo-protected in 20:80 (v/v) ratio of PEG 400 to well solution and flash-cooled in liquid nitrogen.

Among the three mutant proteins, only Met6pY crystallized with Zn^{2+} at the active site while Met6pT and Met6pA both lost the Zn^{2+} during crystallization. While Met6pT crystals were fragile and difficult to reproduce, Met6pA formed large well-

diffracting crystals and were soaked in a Zn^{2+} containing solution in order to obtain a zinc-replete crystal. Met6pA crystals were first soaked in reservoir solution supplemented with 250 μM zinc sulfate and 500 μM DTT for 3 hours followed by a 8-12 hour soak in reservoir solution including 500 μM DTT. Met6pA crystals plus zinc were then cryo-protected in 30% (w/v) PEG 3350, 50 mM NaI and flash-cooled in liquid nitrogen.

Ligand-replete crystals

The SER variant Met6pA was used for all ligand bound experiments because Met6pA diffracts to high resolution and has a single molecule in the asymmetric unit. Large well-diffracting crystals were first soaked in a zinc containing solution in order to obtain zinc-replete crystals (described above). The zinc-replete crystals were then soaked for 4 hours in the crystallization condition with the ligand of choice.

The soaking experiments done to map out the substrate and product binding pockets included Met6pA in a binary complex with 5 mM Hcy, 10 mM Met, >70mM Gln, 5 mM 5-methyl-THF-Glu_3, and 10 mM SAH. Crystals were soaked with both 5 mM 5-methyl-THF-Glu_3 and 10 mM Met for the ternary substrate complex. A ternary inhibitor complex was prepared with 10 mM MTX-Glu_3 and 5 mM Hcy.

The soaking experiments done with compounds from the NIH clinical collection, Fragment library and KINAset library were limited to 5 mM. These compounds are normally dissolved in 100% DMSO and Met6pA crystals can only tolerate up to 5-7% DMSO for extended periods of time. Prior to data collection, a single crystal from each condition was cryo-protected in each respective soak condition containing 30% (w/v) PEG 3350 and flash-cooled in liquid nitrogen.

Data collection and processing

Diffraction data from the three SER variant crystals and most of the Met6pA-ligand complexes was collected at 100 K at the Advanced Light Source at the Lawrence Berkeley national Laboratory. Data for the SAH bound Met6pA crystal was collected at 100 K at the Macromolecular Crystallography Facility at UT Austin using the Rigaku MicroMax-007HF generator and the R-AXIS IV++ plate detector (Rigaku, The Woodlands, TX). The Met6pY and Met6pT data were integrated and scaled with Mosfilm and Scala (Leslie 1992). HKL2000 was used to process each Met6pA data set (Otwinowski 1997). A molecular replacement solution for the Met6pY crystal was determined with Phaser using the structure of *A. thaliana* methionine synthase (PDB ID: 1U1H) as the search model (Ferrer, Ravanel et al. 2004, McCoy 2007). A molecular replacement solution for Met6pT was found with Phaser. A solution for ligand-free Met6pA was found with MOLREP using the Met6pY structure as the search model, while Phaser was used for the ligand-bound Met6pA structures. The models were improved through iterative rounds of model building with COOT and refinement using Phenix and Refmac (Collaborative Computational Project 1994, Murshudov, Vagin et al. 1997, Emsley and Cowtan 2004, Adams, Afonine et al. 2010). Each structure was reviewed using MOLPROBITY (Lovell, Davis et al. 2003).

5-Methyl-THF-Glu_3 synthesis

(6-R,S) 5-CH3-THF-Glu_3 was synthesized from Pteroyl-Glu_3 by using a modified procedure (http://appling.cm.utexas.edu/methylTHF.pdf) originally developed by Yeo and Wagner (Yeo and Wagner 1992). The starting material Pteroyl-Glu_3, intermediate THF-Glu_3 and final product 5-CH_3-THF-Glu_3 absorb at wavelengths 282 nm (23.4 mM^{-1}), 298 nm (30 mM^{-1}), and 292 nm (31.7 mM^{-1}).

40 μmol Pteroyl-Glu_3 was first combined with 200 μL of 0.265 mM $Pb(NO_3)_2$ and dissolved by vortexing and slowly adding 15-35 μL of 5N NaOH until the final pH was ~7.5. Pteroyl-Glu_3 was reduced to THF-Glu_3 by adding 132 μmol $NaBH_4$ over 20 minutes. This was done at 4°C and pH was maintained at 8.5-8.8 using 20% (w/v) citric acid. The solution was flushed with N_2 and mixed for 2 hours in the dark at ~23°C. The vial was cooled to 4°C and the excess $NaBH_4$ was destroyed by reducing the pH to 5.0 using 5M acetic acid. The pH was adjusted back to 7.8 using 5 N NaOH. The intermediate product, THF-Glu_3, was then condensed with HCHO by adding 80 μmol of a 37% formaldehyde solution and mixing at 45°C for 15 minutes in the dark. This produced the intermediate CH_2-THF-Glu_3, which was subsequently reduced to 5-CH_3-THF-Glu_3 by adding 264 μmol $NaBH_4$. As before, the $NaBH_4$ was added slowly over 20 minutes and pH of 8.5-8.8 was maintained with 20% (w/v) citric acid. The solution was immediately flushed with N_2 and mixed for 1 hour in the dark at 45°C. The solution was cooled and 50 mM of the reducing agent BME was added. As before, excess $NaBH_4$ was destroyed by acetic acid and pH was adjusted to 7.5 using NaOH. The solution was flushed with N_2 and stored in the dark (with desiccant) at -80°C in 25 μL aliquots.

The concentration of 5-methyl-THF-Glu_3 was determined by measuring the absorbance at 298 nm. The yield was determined by diluting 2 μL of the product 1:4000 in 10 mM Tris pH 7.5. 400 μL of the dilution was combined with 100 μL of 5N HCL/60% Formate and heated for 10 minutes at 80°C. The reaction was cooled and the absorbance was measured over the 200-500 nm range. A peak at 350 nm is diagnostic of THF and lack of a peak is indicative of 5-methyl-THF-Glu_3.

Hcy synthesis

Hcy was synthesized from L-homocysteine thiolactone using a modified method originally described by Uerre & Miller (Uerre and Miller 1966). Prior to use, all solutions including the ddH_2O, 5 M acetic acid, and 5 N NaOH were flushed with N_2 for 2-5 minutes. 0.25 mmol L-Hcy thiolactone was dissolved in 750 µL 5 N NaOH and incubated at 37 °C for 5 minutes. The solution was neutralized with 750 µL of 5 M acetic acid. The Hcy was further diluted to ~100 mM by adding 1 mL ddH_2O, flushed with N_2, and divided up in 100 µL aliquots. All aliquots were flushed with N_2 and stored at -80 °C. The concentration of Hcy was determined by using the thiol quantitation reagent DTNB (Ellman 1959). DTNB reacts with a free thiol and generates the p-nitrothiophenol which absorbs at 412 nm and has an extinction coefficient of 13.6 mM^{-1}. A 2 mL reaction was prepared with 500 uM DTNB and 1 µL of Hcy in 100 mM $NaPO_4$ pH 8.0 buffer and incubated for 5 minutes at room temperature. The absorbance at 412 nm was converted to mM Hcy using the Beer's Law.

Absorbance based Met6p activity assay

The enzyme activity of wild-type or mutant Met6p was evaluated using a modified methionine synthase assay described by Drummond et al. (Drummond, Jarrett et al. 1995). The (6R,S)-5-methyl-tetrahydrofolate-Glu_3 substrate (5-methyl-THF-Glu_3) was synthesized from pterin with a three glutamate tail, $PteGlu_3$, using a modified procedure of Yeo and Wagner, and the Hcy was made by alkaline hydrolysis of L-homocysteine thiolactone (Yeo and Wagner 1992, Drummond, Jarrett et al. 1995, Suliman, Appling et al. 2007). When available, 5-methyl-THF-Glu_3 was purchased from Schircks Laboratories (catalog # 16.243).

Initially a 380 µL reaction containing 50 mM potassium phosphate (pH 7.0), 50 mM Tris-HCl (pH 7.4), 100 µM $MgSO_4$, 10 mM DTT, 140 µM 5-methyl-THF-Glu_3, and

400 μM Hcy was prepared and preheated to 37 °C. The reaction was initiated by adding 9 μg of enzyme (in a 20 μL volume) and allowed to proceed for 20 min at 37 °C. The reaction was terminated by adding 100 μL of 5 N HCl/60% formic acid and incubating for 10 min at 80 °C. During this high temperature step unmethylated THF-Glu_3 is converted to methenyl-THF-Glu_3 by the formic acid. The reaction mixture was incubated on ice for 3 min and centrifuged to remove any precipitate. Methenyl-THF-Glu_3 was quantified spectroscopically by measuring absorbance at 350 nm (ε = 26,500 M-1 cm-1).

The K_M and k_{cat} for the 5-methyl-THF-Glu_3 purchased from Schircks Laboratories (Jona, Switzerland) was determined by varying the concentration of 5-methyl-THF-Glu_3 in the presence of effectively saturating levels of Hcy (400 μM) over a 13 minute time course. All reactions were done in duplicates and SigmaPlot (Systat Software Inc, San Jose CA) was used to plot and fit experimental data to the Michaelis-Menten equation.

The IC_{50} of any potential inhibitor was determined by measuring the enzyme activity in the presence of varying inhibitor concentrations (0-1 mM). A routine activity assay was done with an enzyme plus + inhibitor pre-incubation step of 15 minutes at room temperature. Both substrates were added in last at concentrations equal to 1x the K_M. The μM Methenyl-THF-Glu_3 produced by the enzyme was converted to fractional activity and plotted against the concentration of inhibitor. When appropriate, a three-parameter logistic equation was used to calculate the IC_{50} (Copeland 2005).

Fluorescence based Met6p activity assay

I created a novel fluorescence based assay that can be used to measure enzyme activity; this can be used to characterize the enzymes catalytic parameters and to screen for potential inhibitors. The existing absorbance assay described by Drummond et al. (Drummond, Jarrett et al. 1995), was modified to selectively measure the concentration

of Hcy using the Measure-iT^{TM} thiol quantitation reagent from Invitrogen (M30550); steady state kinetics could be followed by monitoring the decrease in [Hcy] over time. For these assays, 5-methyl-THF-Glu_3 was purchased from the Schircks Laboratories (Jona, Switzerland) and re-suspended in 10 mM Tris pH 7.4. Hcy was made by alkaline hydrolysis of L-homocysteine thiolactone (Yeo and Wagner 1992, Drummond, Jarrett et al. 1995, Suliman, Appling et al. 2007). Both substrates were flushed with N_2 gas, protected from light and stored at -80 °C. Prior to use, reducing agent was removed from the Met6p protein aliquot using the Zeba^{TM} Micro Spin Desalting Column, 7K MWCO from Thermo Scientific (89878). All reagents and buffers were flushed with N_2 gas and if necessary kept on ice and protected from light.

In order to use this detection system to evaluate Met6p activity, we first tested for any interactions between the fluorescent probe and the individual components of the Met6p assay. Concentration gradients of the protein, Hcy, Met, 5-methyl-THF-Glu_3 and potential inhibitor Methotrexate-Glu_3 were tested for a fluorescence signal at excitation/emission wavelengths of 464/510 nm. A significant and linear increase in fluorescence was only observed for Hcy over a range of 0 to 200 μM.

Preliminary assay development suggested steady state kinetics could be reliably measured using about 100 nM wildtype enzyme and substrate concentrations of 100-200 μM Hcy and 500 μM 5-methyl-THF-Glu_3. Under these conditions the reaction is linear for up to 20 minutes. K_M and k_{cat} values for both substrates were measured by varying the concentration of each in the presence of effectively saturating levels of the other; the time course was adjusted to be sure the time course was linear for low substrate concentrations. All reactions were done in duplicates. SigmaPlot (Systat Software Inc, San Jose CA) was used to plot and fit experimental data to the Michaelis-Menten equation.

A standard 10 μL reaction, used to assess wild-type, mutant, and inhibitor activity, contains 50 mM potassium phosphate (pH 7.0), 50 mM Tris–HCl (pH 7.4), 500 uM 5-methyl-THF-Glu_3, and 200 uM Hcy. The reaction is initiated by adding 0.1 μg of enzyme (113 nM) to the test and buffer to the control and allowed to proceed for 10 min at 37 °C. The reaction is stopped by incubation on ice for 5 minutes and transferred to a 96 well polypropylene plate from Roche (Part # 4729692001) containing 100 μL of the 1:100 Measure-iT^{TM} thiol quantitation reagent per well. The plate is immediately sealed and centrifuged at 1000 RPM for 1 minute. The fluorescence is measured using the Roche LightCycler® 480 RT-PCR instrument (Roche, USA) with excitation/emission filters of 464/510 nm. The fluorescence reading is converted to concentration of Hcy using a standard curve. The concentration of Hcy consumed during the reaction is calculated as the difference between the control and test sample.

The IC_{50} for MTX-Glu_3 was determined by measuring the enzyme activity in the presence of 0-20 mM inhibitor. A routine activity assay was done with an enzyme plus + inhibitor pre-incubation step of 15 minutes at room temperature. Both substrates were added in last at concentrations equal to two times the K_M. The Hcy consumed by the enzyme was converted to fractional activity and plotted against substrate concentration in order to determine inhibitor parameters. IC_{50} and the Hill coefficient were computed using a three-parameter logistic equation appropriate for the inhibition curve (Copeland 2005).

The Met6pA mutant enzymes (Tyr660Ala, Tyr660Gln, Tyr660Phe, and Asn126Ala) were tested for activity using the standard assay described above but with 570 nM protein. Mutant activity was estimated as a simple fraction of wild type activity, normalized for concentration differences.

Differential scanning fluorimetry assay (DSF)

The DSF method was optimized to measure the melting temperature (Tm) of the fungal Met6p protein (Niesen, Berglund et al. 2007). Concentration gradients of the protein, Sypro® Orange dye (Life Technologies^{TM}, USA) and dimethyl sulfoxide (DMSO) were tested in a 25 µL reaction buffered with 100 mM hepes, 150 mM NaCl, pH 7.4. The condition that generated the best fluorescence signal and excellent repeatability (across a single 96 well plate) consisted of 750 nM protein, 5X Sypro® Orange dye and ≤ 2% DMSO. The observed protein Tm was 71 ≤ 0.07 °C. The addition of 500 uM Hcy raised the Tm to 72.5 ≤ 0.07 °C. This method was optimized for 96-well format in order to screen the thousands of commercially available compounds and potentially identify some that bind and shift the Tm of Met6p.

Thermal melting experiments were done in high throughput 96-well format using the Roche LightCycler® 480 RT-PCR instrument (Roche, USA). The TI3D facility at UT Austin provided the NIH Clinical Collection (Evotec, Germany), ChemBridge Fragment and the KINASet libraries (ChemBridge, USA) and prepared the compound dilution plates. Compounds were stored in 100% DMSO at ~10 mM. TI3D prepared an intermediate dilution plate with 0.8 µL of the library and 69 µL of the hepes reaction buffer (115 µM compound in 1.15% DMSO). The Janus dispensing robot (PerkinElmer, USA) was used to transfer 21 µL of the intermediate mix to the polypropylene reaction plate (Roche, part 4729692001). Compounds were dispensed in all but the first and last columns; column 1 was used for the negative control and column 12 was used for the positive control. A Phoenix crystallization robot (Art Robbins Instruments) was used to add 750 nM of protein per well. 500 µM of Hcy was added to the last column. The plate was briefly centrifuged at 1000 rpm and incubated for 25 minutes at room temperature to allow for equilibration. Sypro® Orange dye (2 µL of 62.5X) was added using a multi-

channel pipette, bringing the final reaction volume to 25 μL. The plate was sealed, briefly centrifuged and secured in the 96 well block inside the instrument. The thermal melt program first equilibrated the plate for 15 seconds at 25 °C followed by an increase in temperature at a ramp rate of 0.02 °C/s until it reached 95 °C. The excitation and emission filters used to measure the fluorescence produced by the Sypro® Orange dye were 465 and 580 nm, respectively. The program generated a plot of fluorescence vs. temperature and the protein melting software was used to calculate the exact Tm.

The positive and negative controls from each plate were used to calculate the z-factor. Inhibitors that shifted the Tm ≥ 0.3 °C were further tested only if the plate had a Z' factor of 0.5-1 (Zhang, Chung et al. 1999).

Atomic coordinates

The coordinates and structure factors of the refined models of Met6pA with and without zinc in the active site, Met6pT ($-Zn^{2+}$), and Met6pY ($+Zn^{2+}$) have been deposited in the PDB with entry codes 3PPG, 3PPF, 3PPH, and 3PPC, respectively. The coordinates and structure factors of the refined models of Met6pA in complex with Hcy, Met, Gln, and 5-methyl-THF-Glu_3 have been deposited in the PDB with entry codes 4L5Z, 4L61, 4L6O, and 4L64, respectively. The models of Met6pA in a ternary complex with 5-methyl-THF-Glu_3 and Met or MTX-Glu_3 and Hcy have entry codes, 4L65 and 4L6H, respectively. A list of solved and deposited structures can be found in Table 2.1.

Table 2.1 Deposited structures of the fungal Met6p enzyme

Organism	Author	Condition	PDB ID
Candida albicans	Ubhi/ Robertus	Met6pA (+Zn)	3PPG
		Met6pA (-Zn)	3PPF
		Met6pT (-Zn)	3PPH
		Met6pY (+Zn)	3PPC
		Met6pA with Hcy (+Zn), pH 7.4	4L5Z
		Met6pA with Met (+Zn), pH 7.4	4L61
		Met6pA with Gln (+Zn), pH 7.4	4L6O
		Met6pA with 5-methyl-THF-GLu3 (+Zn), pH 7.4	4L64
		Met6pA with Met and 5-methyl-THF-Glu3 (+Zn), pH 7.4	4L65
		Met6pA with Hcy and MTX-Glu3 (+Zn), pH 7.4	4L6H

CHAPTER 3: RESULTS AND DISCUSSION

The Structures of three Met6p variants crystallized using SER

We undertook the SER engineering of *C. albicans* Met6p because we were unable to crystallize the wild-type protein. Our engineering focused on an elongated surface loop, initially identified by the SERp server. Residues 103-112 in the fungal enzyme lengthen a surface loop common to all members of the family (Figure 3.1). Three variants were constructed by site-directed mutagenesis: Met6pA, Met6pT and Met6pY. Protein was purified for all three and tested for activity using the absorbance based kinetic assay. The catalytic activity of the mutant proteins was indistinguishable from the wild-type protein, showing that the surface mutations had not affected enzyme function (data are summarized in Table 3.1). All three proteins formed well-diffracting crystals which allowed us to collect data at 2.0 - 2.8 Å resolution. Crystallographic statistics are given in Table 3.2.

The Met6pA protein crystallized in spacegroup $P2_12_12_1$ with one monomer in the asymmetric unit. The N-terminally His-tagged Met6pA consists of 789 amino acids, of which 740 were modeled into the electron density. The histidine tag, residues within the engineered loop (106-110; see Figure 3.1) and four loops connecting α-helices and β-strands in the C-terminal domain were disordered and left un-modeled. The final model includes Met6p residues 1-105, 111-659, 663-679, 689-702, 710-740, 744-767, one Zn^{2+} ion and 501 water molecules.

Analysis of crystal packing supports an important role of the mutated residues in forming crystal contacts. The engineered loop is arranged as an extended β-hairpin with the main-chain atoms of residues at the base of the loop (101-103 and 112-114) forming two short antiparallel strands. Although the tip of the loop is disordered, it projects towards the interface of the two symmetry-related molecules and directly facilitates

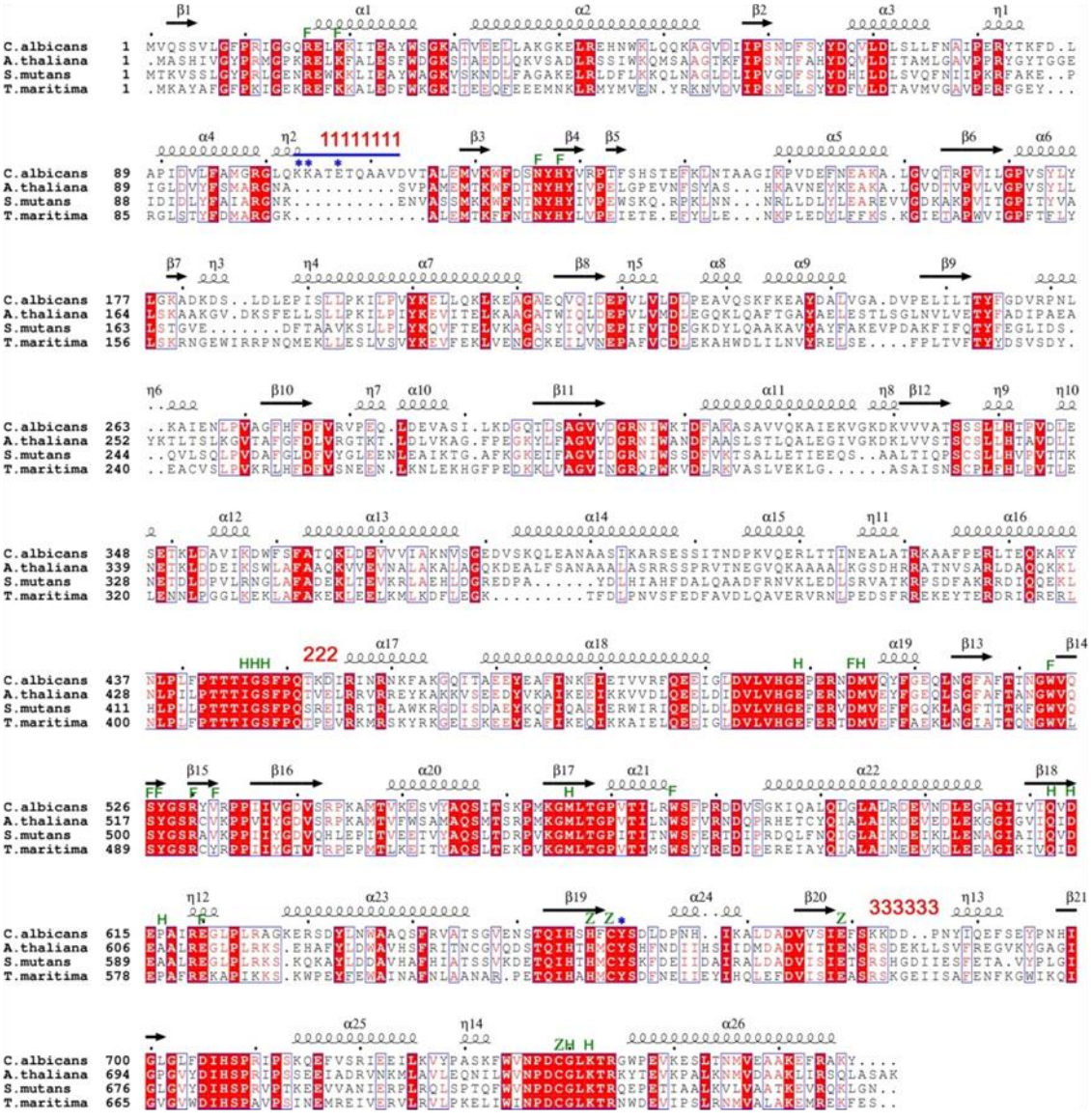

Figure 3.1 Sequence alignment of Met6p homologs. The *C. albicans* Met6p is aligned with homologs from *A. thaliana*, *S. mutans*, *T. maritima* and *E. coli*. The elongated loop is marked by a blue line and the mutated SER residues are identified by blue asterisks. Disordered regions are designated by red dashes. The Zn ligands are identified with a green 'Z', and residues in the Hcy and folate pocket are designated by a 'H' and 'F', respectively. Figure taken from Ubhi, Kavanagh et al. 2011.

Table 3.1 The activity of wild-type Met6p and engineered SER mutants is shown as μM product formed. Table taken from Ubhi, Kavanagh et al. 2011.

Protein sample	[5,10-Methenyl THF] (μM)
Met6p wildtype[a]	13.81 ± 0.45
Met6pA[a]	13.38 ± 0.54
Met6pY[a]	13.34 ± 0.58
Met6pT[b]	14.49 ± 0.71

[a] Proteins were stored at −80 °C and thawed prior to use.
[b] Protein was freshly purified.

Table 3.2 X-ray data collection and refinement of SER mutants. Table adapted from Ubhi, Kavanagh et al. 2011.

Space group	Met6pY + Zn $P2_12_12_1$	Met6pT C2	Met6pA + Zn $P2_12_12_1$	Met6pA $P2_12_12_1$
Cell dimensions				
a, b, c (Å)	77.7, 92.7, 191.0	163.6, 98.1, 162.6	77.2, 99.2, 100.8	76.9, 98.8, 100.8
αβγ (°)	90, 90, 90	90, 131.1, 90	90, 90, 90	90, 90, 90
Resolution (Å)[a]	50-2.2 (2.32-2.20)	50-2.8 (2.95-2.80)	50-2.0 (2.01-1.98)	50-2.3 (2.34-2.30)
R_{merge} (%)	0.097 (0.43)	0.109 (0.659)	0.084 (0.629)	0.087 (0.545)
$\langle I/\sigma_I \rangle$	13.2 (3.2)	9.2 (1.9)	10.1 (3.4)	9.9 (3.8)
Completeness (%)	96.5 (82.7)	99.8 (99.9)	100 (100)	99.9 (99.3)
Unique reflections	68,226	47,736	54,885	35,447
Redundancy	6.4	3.6	10	6.4
$R_{working}$	0.182	0.217	0.178	0.181
R_{free}	0.231	0.278	0.220	0.253
Average B factor for protein atoms (Å^2)	19.0	57.8	37.5	33.7
Average B factor for solvent atoms (Å^2)	17.2	38.2	37.5	33.4
Rms deviation from ideality				
Bond length (Å)	0.018	0.008	0.007	0.007
Bond angle (°)	1.506	1.156	0.982	1.047

[a] Highest resolution data is shown in parenthesis.

crystal packing (Figures 3.2). Ala103 and Ala104 have van der Waals contacts with Glu511, Gln512, Leu513 and Asn514 of a symmetry-related molecule. Analysis by PISA shows that this interaction buries 88 Å² of surface area for Ala103-Ala104 and 75 Å² for amino acids 511-514 (Krissinel and Henrick 2007). This contact would not be

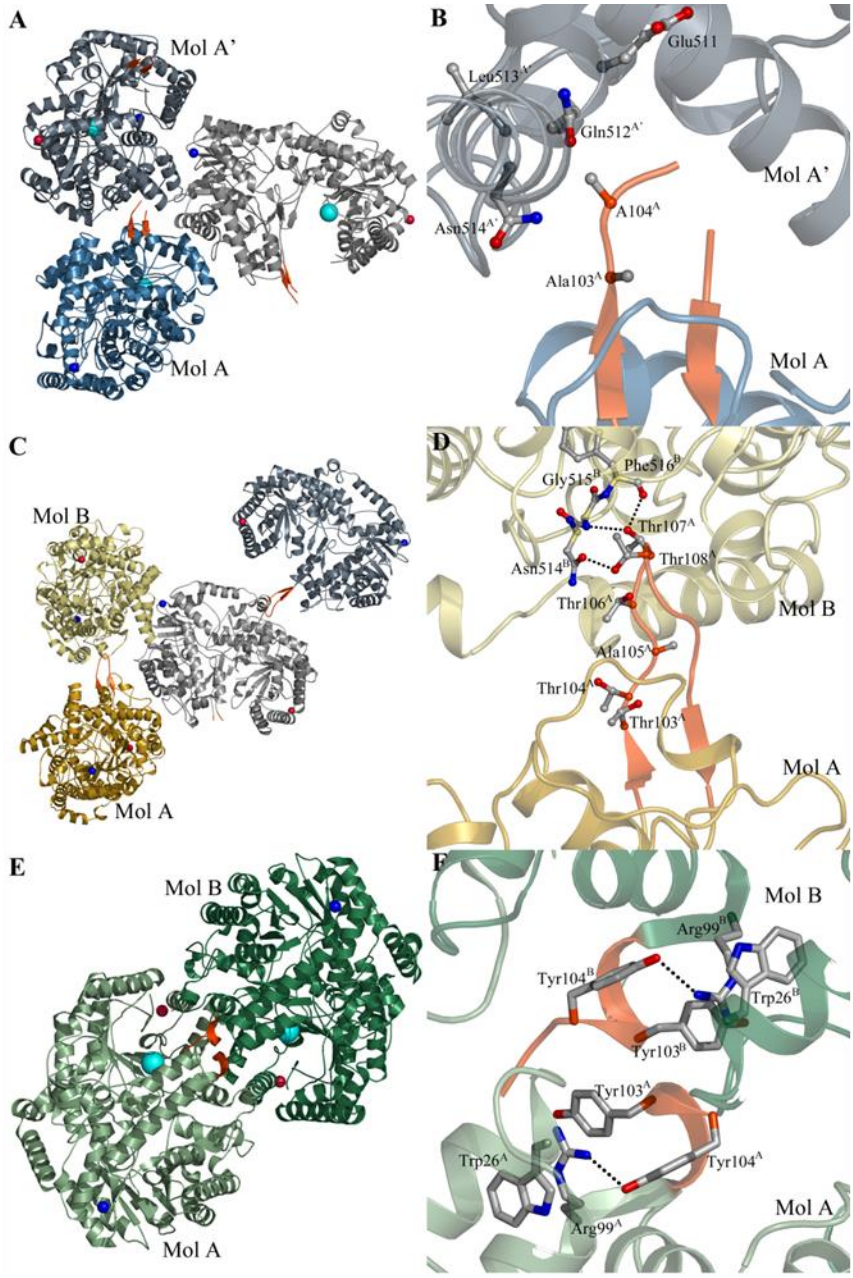

Figure 3.2 Crystal packing interactions observed for each SER variant. The zinc is shown as a cyan sphere and the N and C termini are marked by blue and red spheres, respectively. The mutated loop is shown in orange. A & B) The Met6pA in the ASU is shown in blue and two symmetry-related molecules are shown in grey. C & D) The two molecules in the ASU of Met6pT are shown in yellow and the symmetry related mate is shown in grey. E & F) The two molecules in the ASU of Met6pY are shown in green. Figure taken from Ubhi, Kavanagh et al. 2011.

possible for the wild-type loop since the elongated and highly mobile Lys103 and Lys104 would sterically interfere with this packing. Although residues 106-110 are disordered, there is plenty of space at the interface to accommodate different conformations of the loop.

The zinc-depleted Met6pA crystal structure closely resembles its zinc-containing counterpart with an RMSD value of 0.45 Å over 739 equivalent Cα (calculated with SSM) (Krissinel and Henrick 2004). The loss of Zn^{2+} allows a disulfide bridge to form between two of the Zn^{2+}-ligating residues, Cys659 and Cys739. Both Met6pA structures, with and without Zn^{2+}, have the same unit cell dimensions as well as identical crystal packing.

The Met6pT mutant protein crystallized in spacegroup C2 with two molecules in the asymmetric unit. As observed in Met6pA, the protein also lost Zn^{2+} during crystallization and a disulfide bond is formed between Cys659 and Cys739. As can be seen from figure 3.2 (A & C), the crystal packing of Met6pT is similar to the packing for the Met6pA variant. When molecule A of Met6pT is superimposed onto Met6pA, the orientation of the Met6pT B molecule is related to a Met6pA symmetry molecule (denoted Mol A') by a ~7° rotation and ~11 Å translation. This slight rearrangement is enough to shift the spacegroup from $P2_12_12_1$ to C2. Disordered residues in molecules A and B include the N-terminal His tag and loops connecting βα motifs in the C-terminal domain. In particular, residues 661-662, 705-712 and 767 could not be modeled in molecule A and molecule B is missing electron density for residues 103-113, 661-662 and 705-711. An important difference between the monomers is that the SER loop for molecule A is well ordered with all residues defined by electron density, while residues 103-113 are mobile and disordered in molecule B. The final model for Met6pT includes 1502 protein residues and 50 water molecules.

The introduced Thr residues participate in crystal packing in only one of the monomers in the asymmetric unit. The SER loop from molecule A is again in an extended β-hairpin conformation and interacts with a cavity on molecule B (Figure 3.2). Thr103A and Thr104A are not directly involved in crystal packing although Thr103A does stabilize the antiparallel β structure at the base of the loop. Engineered Thr107A donates a hydrogen bond to the carbonyl of Phe516B and accepts one from the amide nitrogen of Gly515B. This Gly515-Phe516 region is remarkably close to the loop-interaction area for the Met6pA mutant (residues 511-514).

The Met6pY variant crystallized in spacegroup $P2_12_12_1$ with two monomers in the asymmetric unit. Like Met6pA and Met6pT, the disordered regions include the N-terminal His tag, portions of the SER loop and loops between the βα motifs in the C-terminal domain. In molecule A residues 107-114, 413, 452-454 and 682-685 are disordered while molecule B lacks density for residues 105-114, 453-468 and 682-688. The final model includes 1485 protein residues, two Zn^{2+} ions, eight chloride ions (located by their anomalous signal), and 432 waters.

The Met6pY crystal lattice is distinct from the other two lattices in that the engineered SER loop forms a more compact structure and participates in crystal contacts which bury more surface area. As shown in Figure 3.2, the engineered Tyr103 and Tyr104 at the base of the loop form a helical structure. The introduced tyrosines interact with other residues within the monomer to create a surface for intermolecular contacts. Some of these interactions are shown in Figure 3.2 whereby Tyr103 joins an aromatic stack with Arg99 and Trp26. The side chain of Tyr104 sits roughly perpendicular to that stack, making non-polar contacts, while the hydroxyl of Tyr104 accepts a hydrogen bond from Arg99. This patch within each molecule is then utilized to interact with an adjacent

molecule. Formation of this intermolecular dimer buries ~1300 Å^2, and packing of the engineered loops contributes 415 Å^2 of buried surface area.

Crystal packing properties of Met6pA, Met6pT, and Met6pY

All three SER variants crystallized using the loop to create new packing interfaces. Of the three variant proteins, Met6pY crystals have the lowest solvent content with a Matthews coefficient (Vm) of 1.94 and 37% solvent content. Crystal contacts bury 4792 Å^2 of the surface area for the two molecules in the asymmetric unit. The Met6pA and Met6pT crystals are not as densely packed. The Met6pA crystal form has Vm = 2.17 and 43% solvent content with 1108 Å^2 buried surface area. Met6pT has the highest solvent content with Vm = 2.77 and 56% solvent content and only 2082 Å^2 of buried surface area for the two molecules in the asymmetric unit.

The overall Structure of the fungal Met6p enzyme

C. albicans Met6p has a distinct two-domain structure that is similar to other cobalamin-independent methionine synthases for which structures have been determined. Each domain is a $(\beta\alpha)_8$ barrel with extended βα loops; the barrels are arranged face to face and the extended βα loops form the interface. The active site lies between the two barrels, and has binding sites for both the folate methyl doner and the Hcy. In *C. albicans* Met6p the N-terminal domain contains residues 1-398, and a linker of 5 residues separates it from the C-terminal domain comprised of residues 405-767. Using the program SSM, the Cα positions for 648 aligned residues between Met6pA and *A. thaliana* MetE superimpose with an RMSD of 1.75 Å (Krissinel and Henrick 2004). The resemblance can be clearly seen in Figure 3.3 which shows the superposition of the backbone of Met6pA (3PPG) with that of methionine synthase from *A. thaliana* (1U1H), *S. mutans* (3L7S) and *T. maritima* (3BQ5).

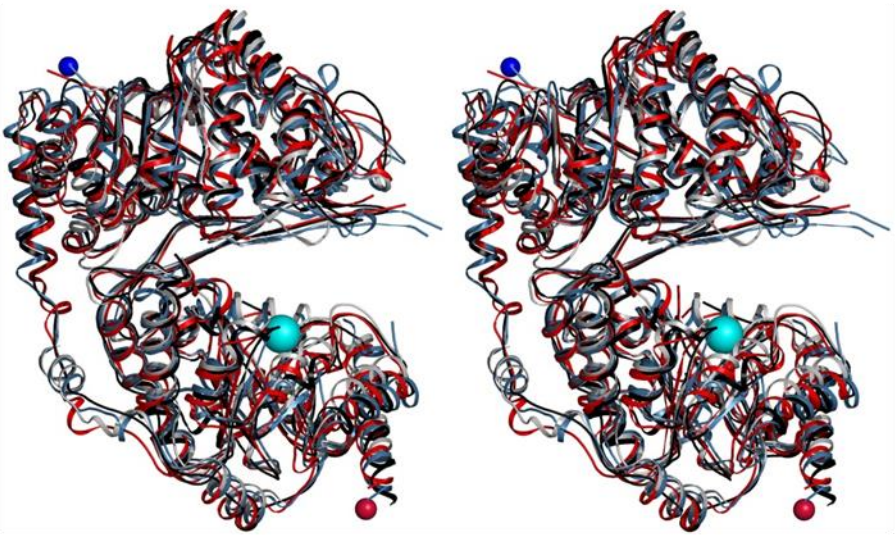

Figure 3.3 Overaly of Met6pA with structural homologs shown in stereo. Met6pA (3PPG, blue) is superimposed with MetE from *A. thaliana* (1U1H, black), *S. mutans* (3L7S, red) and *T. maritima* (3BQ5, grey). The N and C termini are marked by blue and red spheres, respectively, and the zinc from Met6pA is displayed as a cyan sphere. Figure taken from Ubhi, Kavanagh et al. 2011.

Methionine synthase transfers a methyl group from a folate cofactor to Hcy through a Zn^{2+} mediated alkylation reaction. The residues which secure Hcy, folate, and zinc in structures of methionine synthase from *A. thaliana* and *T. maritima* align well with their counterparts in our substrate-free Met6pA structure. Figure 3.1 shows that despite an overall sequence homology of <50%, residues that bind the 5-methyl-THF-Glu_3, Hcy, and Zn^{2+} (Trp576, Asp504, Asp614, Glu499, Ser448, His657, Cys659, Glu679, and Cys739) are highly conserved.

The zinc coordination site in Met6pA and Met6pY

To activate Hcy for catalysis Met6p uses a Zn^{2+} ion that is bound in the C-terminal domain and is ligated by three conserved residues; His657, Cys659, and Cys739.

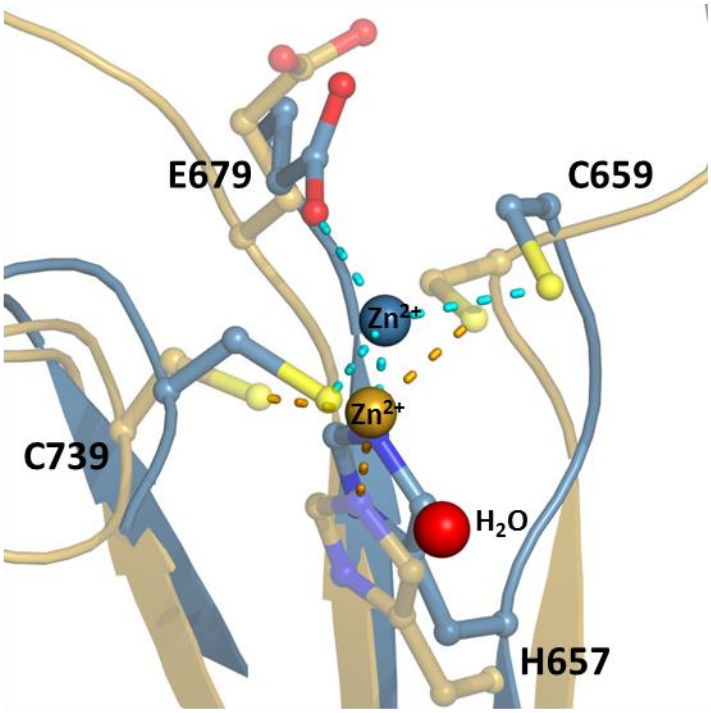

Figure 3.4 Zinc coordination site in the SER variants. Overaly of the zinc coordination site from the Met6pA (3PPG, blue) and Met6pY (3PPC, golden) structures. The Zinc-ligand interactions are shown in cyan for Met6pA and in orange for Met6pY. A single water is present in the Met6pY structure (red sphere).

Zinc typically has tetrahedral coordination and analysis of our apo protein structures shows that Glu679 is the fourth ligand for Met6pA while Met6pY has trigonal planar geometry with a distant axial water (Figure 3.4). Variations in Zn^{2+} coordination are also seen in other methionine synthases: in addition to the His and two Cys ligands, Ferrer et al. observed water to be the fourth ligand in the *A. thaliana* enzyme, while in the *S. mutans* structure (2L7S, unpublished) and in the substrate free *T. maritima* enzyme glutamate is the fourth ligand (Ferrer, Ravanel et al. 2004, Pejchal and Ludwig 2005). According to EXAFS experiments and a few ligand bound homologs, the entry of Hcy is expected to invert the tetrahedral geometry but the Hcy-replete structure from *T.*

maritima exhibit trigonal bipyrimidal geometry with relatively long distances for the axial ligands (Peariso 1998, Pejchal and Ludwig 2005). Although the implications of these zinc coordination differences for methionine synthase activity are unclear at the moment, structural reorganization of ligands surrounding a metal ion are also observed in zinc-dependent alcohol dehydrogenases and are proposed to be a necessary component of catalysis (Baker, Britton et al. 2009).

Ligand bound Met6pA structures

We soaked pre-formed crystals of the fungal Met6pA (PDB ID: 3PPG) with substrate and products or their analogs, as well as an inhibitor, at pH 7.4. Binary complexes include Hcy, Met and Gln (Glutamine) to map the methyl-receptor binding site, and 5-methyl-THF-Glu_3 to map the folate site. Ternary complexes include 5-methyl-THF-Glu_3 and Met, or Methotrexate-Glutamate$_3$ (MTX-Glu_3) and Hcy. Soaking experiments with both substrates, 5-methyl-THF-Glu_3 and Hcy, cracked the crystals and could not be observed. Crystallographic statistics are given in Table 3.3. The overall structure of all the complexes is similar and also closely resembles the open configuration previously observed in other homologs. Figure 3.5 shows a model of the complex with 5-methyl-THF-Glu_3 and Met; it shows the overall folding and domain pattern as well as the two substrate binding areas and the position of the active site Zn^{2+} ion.

Complexes with substrates and analogs have been seen previously for the enzyme from *A. thaliana*, and *Thermotoga maritima* under pH conditions ranging from 4.6 to 8.5 (33,34,39) (Ferrer, Ravanel et al. 2004, Pejchal and Ludwig 2005, Koutmos, Pejchal et al. 2008). Enzymes from each homolog are found in an open configuration, where the distance between substrates is too large for methyl transfer, and it is assumed that the enzymes must have an as yet unobserved closed form that brings these compounds closer

Table 3.3 X-ray data collection and refinement of ligand-bound Met6pA.

Structures	Hcy	Met	Gln	5-methyl-THF-Glu_3	Met + 5-methyl-THF-Glu_5	Hcy + MTX-Glu_3
Cell dimensions						
a, b, c (Å)	77.1, 97.7, 98.2	77.5, 97.2, 97.9	77.3, 97.2, 97.9	76.9, 99.1, 100.7	76.9, 98.9, 100.9	77.1, 99.0, 102.0
αβγ (°)	90, 90, 90	90, 90, 90	90, 90, 90	90, 90, 90	90, 90, 90	90, 90, 90
Resolution (Å)[a]	49.2-2.2 (2.22-2.18)	49.0-2.1 (2.17-2.13)	43.8-1.9 (1.91-1.88)	49.6-2.18 (2.22-2.18)	49.5-2.3 (2.37-2.33)	33.9-1.75 (1.78-1.75)
R_{merge} (%)	0.089 (0.556)	0.097 (0.570)	0.072 (0.761)	0.083 (0.564)	0.066 (0.549)	0.069 (0.548)
$\langle I/\sigma_I \rangle$	8.5 (3.3)	8.7 (3.1)	10.8 (2.1)	8.6 (3.0)	11.0 (3.0)	11.2 (3.0)
Completeness (%)	100 (100)	100 (100)	100 (98.6)	100 (100)	100 (100)	100 (100)
Unique reflections	39,077	42,001	59,860	40,901	34,134	78,948
Redundancy	7.3	7.3	10	7.3	7.2	7.2
$R_{working}$	0.173	0.187	0.169	0.181	0.205	0.185
R_{free}	0.234	0.241	0.213	0.243	0.275	0.231
Average B factor for protein atoms ($Å^2$)	39.4	41.5	36.9	43.6	60.5	28.2
Average B factor for solvent atoms ($Å^2$)	37.7	37.1	36.9	41.0	49.0	33.3
Average B factor for ligand atoms ($Å^2$)	35.2	40.4	50.9	64.1	75.3	45.1
Rms deviation from ideality						
Bond length (Å)	0.016	0.016	0.019	0.016	0.013	0.018
Bond angle (°)	1.679	1.726	1.913	1.701	1.572	1.821

[a] Highest resolution data is shown in parenthesis.

together. Hcy binds deep in the C terminal domain near the active site Zn^{2+} ion, while the folate lies atop the N terminal domain but has interactions with both domains (Figure 3.5). The available structures also suggest a flexible metal binding site with the Zn^{2+} readily changing ligands and coordination geometries (Koutmos, Pejchal et al. 2008).

Hcy/Met specificity pocket in the C-terminal barrel

The available apo and ligand bound structures of methionine synthases from *A. thaliana* and *T. maritima* crystallize in an open configuration with a flexible metal binding site and a fairly rigid Hcy/Met binding pocket. In these structures, the essential residues in the Hcy/Met binding site are ideally positioned for bonding in the Zn^{2+}-replete structures and the entry of either ligand appears to have no significant effect on the overall protein structure.

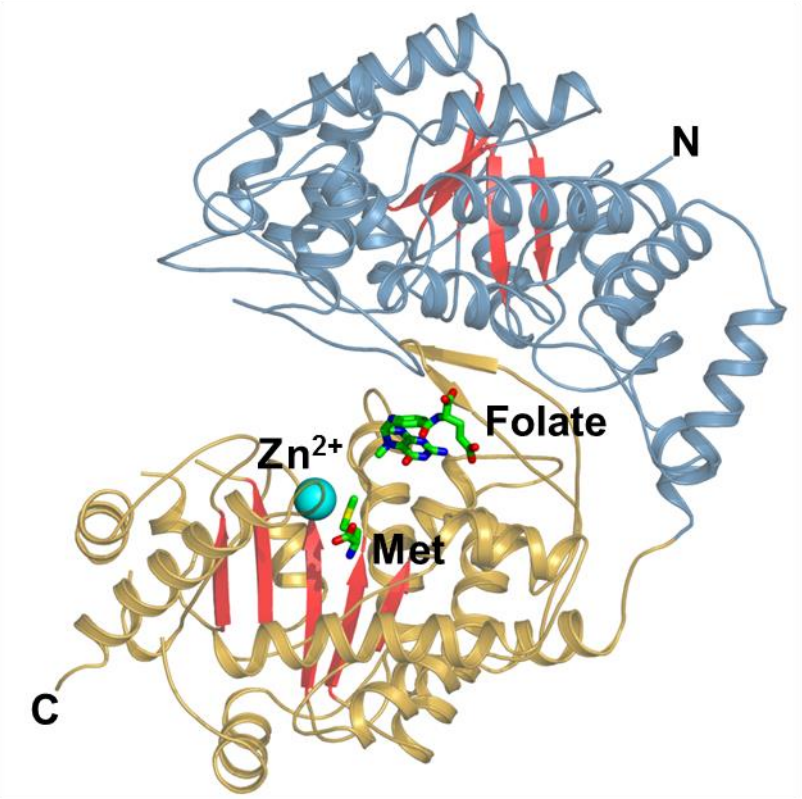

Figure 3.5 The ternary Met6p complex. The overall configuration of Met6pA in complex with 5-methyl-THF-Glu_3 (Folate) and Methionine (Met). The zinc is shown as a cyan sphere and both ligands are shown as green sticks. The distance between the N5 methyl and the Met sulfur is ~ 7 Å.

We collected datasets of the fungal Met6pA bound with Hcy, Met, or Gln at 2.18 Å, 2.13 Å, and 1.88 Å, respectively. In each ligand bound structure, strong Fo-Fc density was observed on the surface of the C-terminal barrel adjacent to the Zn^{2+} and in place of loops otherwise disordered in the Met6pA search model.

Both the Hcy substrate and Met product are anchored into the same pocket by their amino and carboxyl groups (Figure 3.6). The amino group ion pairs with the side chains of Asp614 and Glu499, and donates a hydrogen bond to the backbone carbonyl of Ile446; we previously used site directed mutagenesis to show that Asp614 is essential for

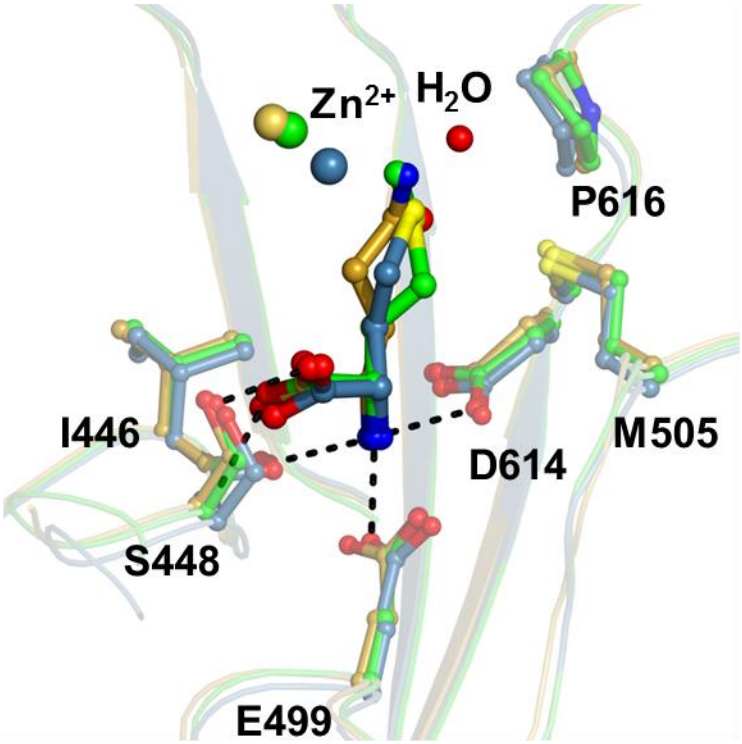

Figure 3.6 The Met6pA substrate binding site. The Hcy (blue), Met (green), and Gln (golden) bound structures are superimposed and each active site zinc is shown as a sphere and colored in the same shade as each secondary structure. A water molecule found only in the Gln bound complex is shown as a red sphere.

enzyme activity and that conversion to Ala or even to Asn leaves no detectable activity (Prasannan, Suliman et al. 2009). The importance of Glu499 has not been tested by mutagenesis. The Hcy or Met carboxylate forms hydrogen bonds with the side chain and backbone amide of Ser448. A Ser448Ala mutant was shown to retain 67% enzyme activity with growth on minimal media. The side chains of Hcy or Met are sequestered from the solvent by the surrounding hydrophobic residues Met505 and Pro616. The free thiol in Hcy coordinates with the active site Zn^{2+}, however the sulfur of Met is too far away at 3.65 Å to form a bond. Structural analysis by the program PDBePISA shows

that these interactions bury 100% of the solvent accessible surface area of Hcy and 95% of Met (Krissinel and Henrick 2007).

We further investigated the Hcy/Met pocket for its ability to bind an alternative ligand containing an amino acid backbone. We soaked Met6pA crystals with the polar amino acid Gln. Gln is similar in size to the natural ligands and exhibited a binding mode which was essentially indistinguishable from the natural substrate/product (Figure 3.6). The amine group forms the same ion pairs, and the carboxylate makes the same hydrogen bonds. The side-chain is sandwiched between the adjacent zinc coordination site and the side chains of Met505 and Pro616. The Gln side chain accepts a hydrogen bond from a neighboring water molecule. According to PDBePISA, these interactions bury 88.96 % of the solvent accessible surface area of Gln (Krissinel and Henrick 2007).

We superimposed the ligand-bound (Hcy) and apo Met6pA structures using the program SSM in order to identify any ligand induced changes in the substrate/product pocket (Krissinel and Henrick 2004). The Cα positions for 736 aligned residues superimposed with an RMSD of < 1 Å, which suggests two nearly identical structures. A closer look at the substrate pocket, shown in Figure 3.7, shows a well aligned polypeptide backbone with mostly fixed and a few mobile active site residues. Of the latter, the two most noticeable residues are His657 and Asp614. In the apo structure, the backbone amide of His657 donates a 2.9 Å hydrogen bond to the side-chain carboxylate of Asp614. This interaction is also secured by a hydrogen bond between the Asp614 $O_{\delta 2}$ atom and Gln612. Upon ligand (Hcy, Gln, or Met) entry, the Asp614 side chain rotates away from His657 and makes a 2.7 Å ionic bond with the Hcy backbone amine. In the process, Asp614 breaks the hydrogen bond between $O_{\delta 2}$ and Gln612 and remakes another between its $O_{\delta 1}$ and Gln612. As a result, His657 protrudes into the space vacated by Asp614. The active site Zn^{2+}, coordinated by the side chain of His657, also travels in the direction of

Hcy. In both structures, residues Glu499, Ser448, Met505, and Pro616 are almost perfectly aligned and form nearly equivalent interactions with the substrate. The hydrogen bond between the backbone carbonyl of Ile446 and the Hcy amine is only observed in the substrate bound structure.

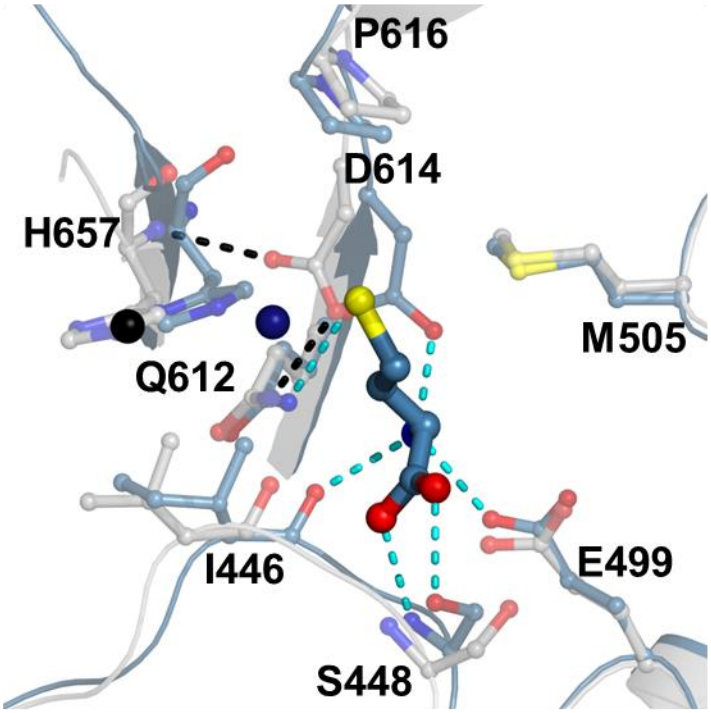

Figure 3.7 Overlay of a substrate-free and Hcy-bound Met6pA. The apo structure is shown in grey (zinc is a black sphere) and the Hcy-bound structure in shown in blue (zinc is a blue sphere). Bonds between the substrate and residues of the Hcy-bound structure are highlighted in cyan. A few notable interactions in the apo structure are shown in black.

Zinc coordination in the ligand bound C-terminal barrel

The cobalamin-independent and dependent enzymes require a Zn^{2+} to orient and activate the Hcy thiol. Ligand bound Met6pA homologs from *A. thaliana* and *T.*

maritima were crystallized at pH 4.6 or 6.5, respectively; the distance between Zn^{2+} and the Hcy sulfur is too long in each case to form a reasonable bond. At a higher pH, however, the equilibrium favors the thiolate form of Hcy and in *T. maritima* structures solved at pH 8.5, the Zn^{2+}-S bond is 2.36 Å. We evaluated the metal site as well as the overall configuration of the C-terminal barrel in Met6pA crystals soaked with Hcy, Met or Gln at a physiologically relevant pH of 7.4.

In the ligand-free Met6pA structure, zinc is tetrahedrally coordinated by four conserved residues His657, Cys659, Cys739, and Glu679 with the N_{657}- Zn^{2+}, S_{659}- Zn^{2+}, S_{739}- Zn^{2+}, and O_{679}- Zn^{2+} distances of 2.3, 2.7, 2.4, and 2.3 Å, respectively. In a Hcy-complex structure, the zinc migrates 3.69 Å away from Glu679 and towards the Hcy side chain thiol, clearly inverting the tetrahedral geometry observed in the apo enzyme (Figure 3.8). In this configuration, the bond lengths between N_{657}- Zn^{2+}, S_{659}- Zn^{2+}, S_{739}- Zn^{2+} and S_{Hcy}- Zn^{2+} are 2.16 Å, 2.64 Å, 2.32 Å, and 2.27 Å, respectively.

When a methyl transfer reaction converts Hcy to Met, an electron-rich ligand like sulfur is converted to a relatively inert thioether. Nevertheless, when Met is soaked into the crystals, the O_{679}- Zn^{2+} interaction is broken, zinc moves 2.17 Å towards the product, resting in between the apo and Hcy metal positions, the bond to Glu679 is broken, and a water molecule replaces it as a ligand (Figure 3.8). Zinc coordinates with His657, Cys659, Cys739 and a water with bond lengths of 2.22 Å, 2.44 Å, 1.93 Å, and 2.18 Å, respectively, and retains the tetrahedral geometry observed in the apo structure. The amino acid Gln binds in essentially the same manner as Met (Figure 3.8). The zinc in the Gln complex is less than 0.5 Å from the Met induced position, and both are about 1.7 Å from the position in the Hcy complex. The bond lengths between N_{657}- Zn^{2+}, S_{659}- Zn^{2+}, S_{739}- Zn^{2+} and O_{water}- Zn^{2+} are 2.32 Å, 2.52 Å, 2.28 Å, and 1.89 Å, respectively.

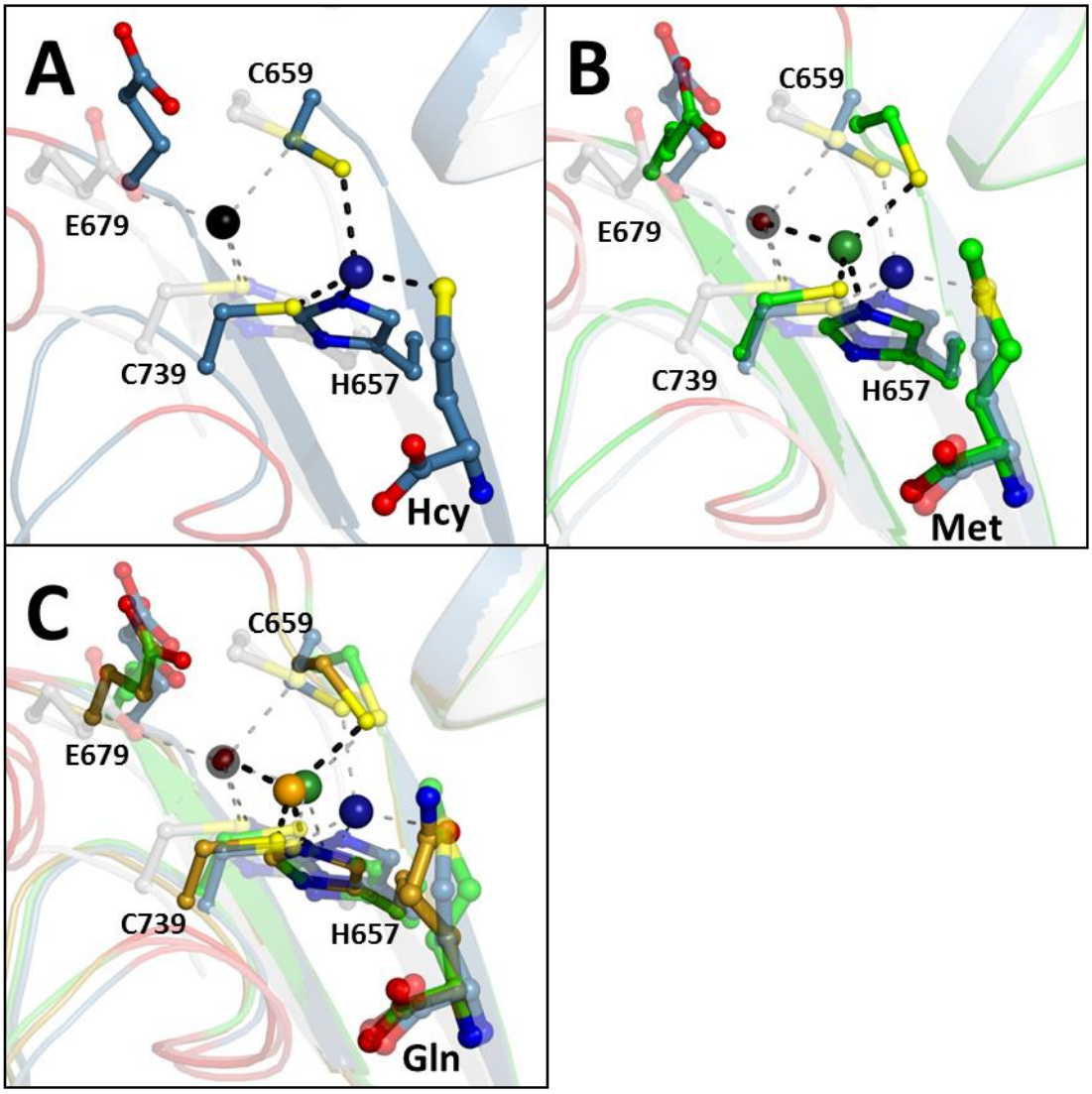

Figure 3.8 Overlay of the ligand-bound and free Met6pA zinc binding site. A) The zinc coordination site in the apo (grey) and Hcy bound (blue) structures with the zinc displayed as a black (apo) and blue (Hcy-bound) sphere. B) The zinc coordination site in the Met bound (green) enzyme is superimposed with the structures in panel A. The zinc in shown as a green sphere. C) The zinc coordination site in the Gln bound (golden) enzyme is superimposed with the structures in panel B. The zinc is shown as an orange sphere. The water molecule in the Met and Gln bound structures is shown as a red sphere (aligns with the apo zinc). The ordered βα-loops are shown in red.

In the apo structure the catalytic Zn^{2+} is coordinated by four strong ligands but the entry of a weak (Gln/Met) or strong (Hcy) ligand impacts Zn^{2+} coordination. The thioether causes at least a 1.93 Å displacement of Zn^{2+} and disrupts the O_{679}- Zn^{2+} interaction while a strong thiolate ligand pulls the Zn^{2+} another 1.8 Å. The binding of a ligand like Gln, which lacks a sulfur in the side chain, is very informative. It suggests that the Hcy pocket has evolved to recognize and strongly interact with an amino acid backbone. The binding of the amino acid amine and carboxylates orients the side chain toward the active site Zn^{2+} of the enzyme. This must trigger a conformational change and initiate the inversion of the Zn^{2+} coordination which goes to completion only in the presence of Hcy.

The four Zn^{2+} ligands, His657, Cys659, Cys739, and Glu679 are located near the ends of three β-strands in the C-terminal barrel. In the apo structure the loops that connect these strands to their following α-helices are disordered while in the Hcy, Met and Gln bound structures, the loops in question: residues 660-662, 680-688, 703-709 and 741-743 are almost completely ordered. Residues at positions 660, 681, 705-709, and 741-743 are highly conserved. The resolved loops, shown in red in Figure 3.9, surround the Zn^{2+} coordination site located at the top of the C-terminal barrel.

A flexible C-terminal barrel with a key role for Tyr660

The entry of Hcy, Met or Gln into the C-terminal barrel triggers conformational changes in the βα loops surrounding the Zn^{2+} coordination site. However one highly conserved residue, Tyr660, remains in a disordered state in this open enzyme structure. We evaluated the importance of Tyr660 by creating three mutants in which the tyrosine is replaced by Ala (Tyr660Ala), Gln (Tyr660Gln), or Phe (Tyr660Phe) and tested each variant using the fluorescence activity assay. The first two mutants have no detectable

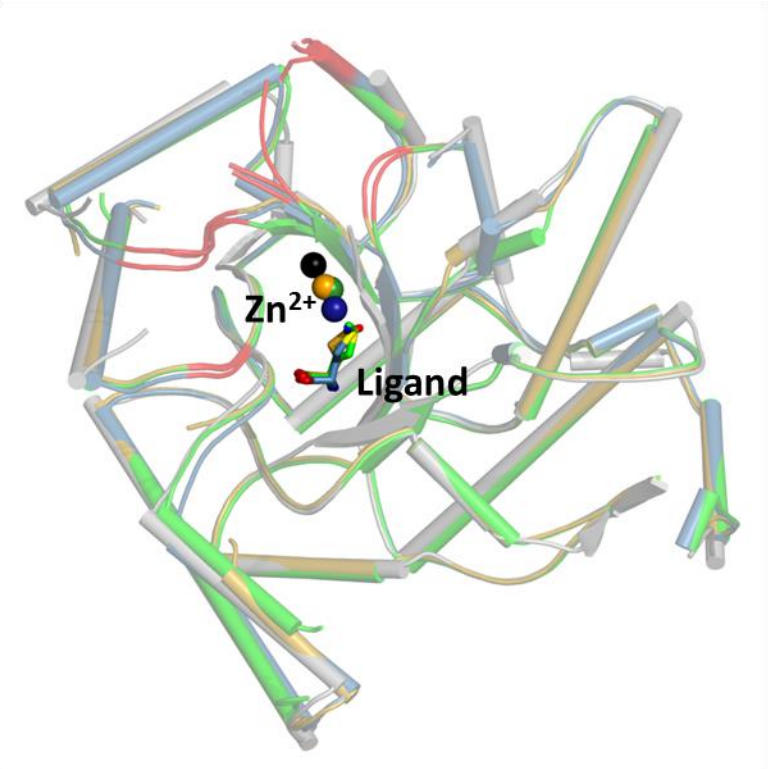

Figure 3.9 Overlay of the apo and ligand-bound C-terminal barrel. The apo structure is shown in grey (black zinc), the Hcy-bound structure is in blue (blue zinc), the Met-bound structure is shown in green (green zinc), and the Gln bound structure is in goldenrod (orange zinc). The ordered βα-loops are found in the ligand bound structures and shown in red.

activity but the Tyr660Phe mutant appears to be fully active (Table 3.4). The Gln side chain is long with a flat polar amide that could mimic many of the Tyr contacts, but clearly this did not happen. On the other hand, Phe, which cannot form hydrogen bonds, is fully active indicating that Tyr660 has a hydrophobic role. We hypothesize that Tyr660 is an important part of a system that detects Hcy binding and triggers a conformation change that facilitates catalysis. We predict that Tyr660 does this by making important hydrophobic interactions that link the C and N terminal barrels and stabilizes the as yet unseen closed conformation. By doing so, it would contribute to the

Table 3.4 Enzyme activity of Met6pA mutants. The % activity of four mutants relative to Met6pA.

Protein sample	% Activity
M6pA	100 ± 0
M6pA_Y660F	93 ± 2
M6pA_Y660Q	14 ± 2
M6pA_Y660A	0 ± 2
M6pA_N126A	14 ± 4

hydrophobic environment known to exist in the ternary complex that supports folate activation by protonation (Taurog and Matthews 2006). Ultimately, the putative closed configuration of Met6p is necessary to bring the methyl donor and acceptor into proximity for catalysis.

The folate-bound binary and ternary complexes

The structures of Met6pA bound with 5-methyl-THF-Glu_3 and with both 5-methyl-THF-Glu_3 and Met were solved at a resolution of 2.18 Å and 2.31 Å respectively. We observed difference density for the pterin and p-aminobenzoic acid (PABA) moieties as well as the first glutamyl residue of the polyglutamate tail. In both structures, the folate is bound at the inter-domain interface through interactions with residues from each domain. These residues are either located on the loops decorating the face of each barrel or on an extended loop of 38 residues (512-549) which protrudes out of the C-terminal domain and appears to envelop the substrate (Figure 3.5).

Figure 3.10 shows the binding of folate from the ternary and binary complex. In both superimposed structures, the folate pterin stacks on the indole side chain of Trp576 and is oriented with the N^5 methyl pointing towards the Met/Hcy pocket. However, only in the ternary complex does the folate make specific hydrogen bonds between the substrate amines and enzyme residues Asn126 and Asp504. N^1 of THF is a hydrogen

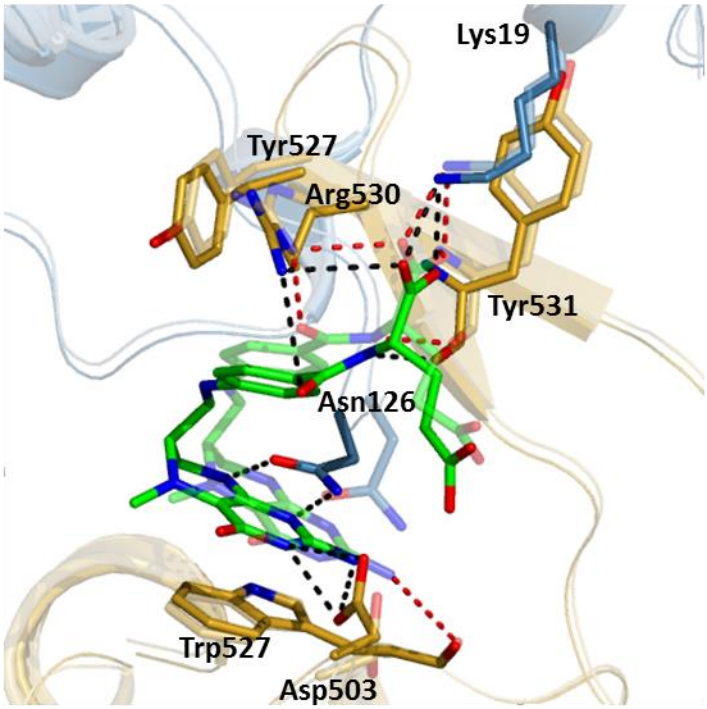

Figure 3.10 The folate binding pocket bound with 5-methyl-THF-Glu_3. Both the binary and ternary folate bound complexes are superimposed with the more prominent structure corresponding to the ternary structure (with Met and 5-methyl-THF-Glu_3). In this structure, many specific interactions secure the folate and are shown in black. The contacts observed in the binary structure are represented by red dashes.

bond acceptor; it receives a bond from the $N_{\delta 2}$ of Asn126. N^8 of THF is a hydrogen bond donor and it donates to $O_{\delta 1}$ of Asn126. The acceptor/donor pair of Asn126 matches that of the reduced substrate. Asp504 accepts a hydrogen bond from both the N^3 and the exocyclic amine of THF (Oefner, D'Arcy et al. 1988, Davies, Delcamp et al. 1990). In the binary structure, the pterin ring stacks on the side-chain of Trp576, but is rotated slightly and the pattern of hydrogen bonds is disrupted. No bonds are formed directly to Asn126, although a water molecule bridges between it and N^8 of THF. The N^2

(exocyclic) amine of THF donates one hydrogen bond to the backbone carbonyl of Trp576. The side chain of Asp504 is oriented toward the substrate amines but remains too far to form a hydrogen bond.

We believe the folate binding described above for the ternary complex reflects the interactions of a productive substrate complex. In particular, residues involved in making specific hydrogen bonding interactions were shown to be important by mutagenesis. We mutated Asn126 to Ala and found that the mutant protein had negligible enzyme activity (Table 3.4). Site directed mutagenesis shows Asp504 is essential for activity and converting it to Ala reduced catalysis by 25-fold (Prasannan, Suliman et al. 2009). The differences between the binary and ternary complex suggest that the hydrophobic stacking interaction is the primary binding force for folate binding, but it is non-directional. The specific hydrogen bonding interactions are not particularly strong and can be cancelled by other subtle forces that are difficult to quantify.

In both binary and ternary complexes, the PABA moiety of THF appears to make an edge to face hydrophobic interactions with the side-chain of Tyr527; the Tyr side chain swings into this position upon substrate binding, but the orientation suggests it is a rather weak interaction compared to an ideal aromatic edge to face bonding (Burley and Petsko 1985). A key interaction is the formation of a short ion pair between the α-carboxylate of the first glutamate and the side chains of Lys19; interaction with the side chain of Arg530 is observed in some, but not all folate complexes. In addition the α-amino nitrogen donates a hydrogen bonds to the carbonyl of Tyr531. These interactions are specific to the first glutamate residue and are invariant, independent of the number of glutamates in the tail. The side chain carboxylate of the first glutamate does not make any specific interactions with this open form of the protein structure. This is the side to

which additional glutamates would be condensed in a poly-glutamate tail, but we have not observed any density for these longer tails in the open Met6p conformation.

Methotrexate-Glutamate$_3$ and Hcy ternary complex

Methotrexate is a well-known anti-folate, frequently used in the treatment of cancer. It is thought to function by binding to the folate site of dihydrofolate reductase and interfering with nucleotide synthesis. Structurally, it closely resembles 5-methyl-THF-Glu$_3$; however the pterin ring is aromatic and flat, and the drug has two exocyclic amines at positions 2 and 4. We carried out kinetic measurements that show MTX-Glu$_3$ inhibits Met6p activity, and soaked both MTX-Glu$_3$ and Hcy into Met6pA crystals to form a ternary complex which diffracts to 1.75 Å.

MTX-Glu$_3$ binds to the folate site of Met6pA and makes generally similar contacts observed with 5-methyl-THF-Glu$_3$. We solved several complexes with MTX-Glu$_3$, and each showed electron density that was consistent with a mixture of states (Figure 3.11). In the predominant mode, the fully aromatic pterin stacks against the Trp576 side chain. Asn126 does not hydrogen bond to the oxidized pteridine ring since the donor/acceptor pattern is disrupted. However, $O_{\delta 2}$ of Asp504 receives a hydrogen bond from the exocyclic N^4 and the backbone carbonyl of Trp576 receives a hydrogen bond from the exocyclic N^2. These interactions are possible because the oxidized pteridine is positioned closer to Trp576 and Asp504. Only the natural, reduced, substrate induces Asp126 to rotate and Asp504 to move into position to make their specific interactions. In the second MTX-Glu$_3$ configuration, the pteridine ring is flipped. It still stacks over Trp576, but is rotated so that N^2 forms a hydrogen bond with the backbone carbonyl of Trp576 and N^4 donates a hydrogen bond to a neighboring water molecule. Asp504 is too far away to make a useful hydrogen bond. In both orientations, the

benzene ring of the PABA moiety makes a face to edge interaction with Tyr527, and the first glutamate retains the hydrogen bond and ion pair with Tyr531 and Lys19, respectively.

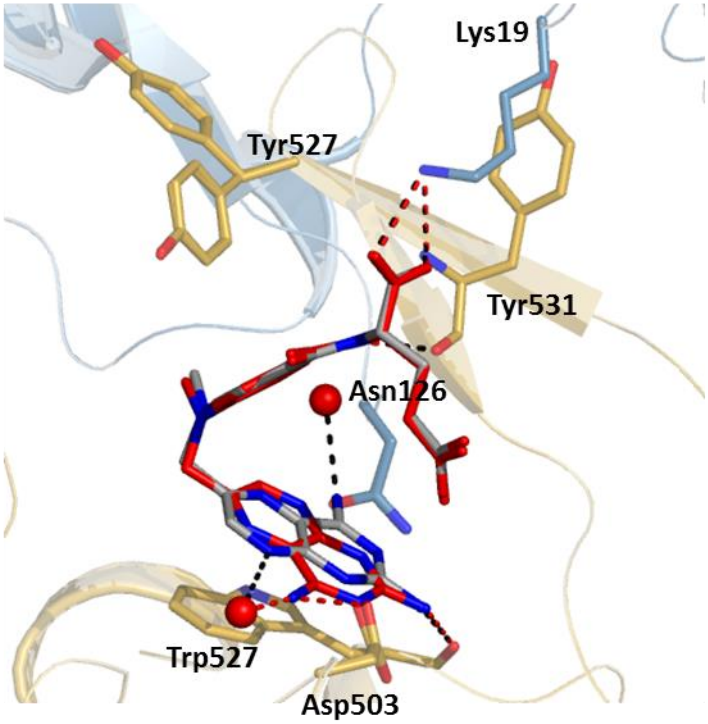

Figure 3.11 The folate pocket bound with MTX-Glu_3. MTX-Glu_3 has two possible orientations, shown in red and grey with respective interactions shown in red and black dashes. Waters are shown as red spheres.

Enzyme inhibition by MTX-Glu_3 was tested using the fluorescence activity assay. The dose-response curve in Figure 3.12 shows that MTX-Glu_3 inhibits with an IC_{50} of 4 ± 1.4 mM and has a Hill coefficient of 1.4 ± 0.1. The kinetic data is consistent with the observed 1:1 binding stoichiometry to the enzyme. The IC_{50} is modest, but consistent with a freely rotating and weakly bound pteridine moiety. MTX-Glu_3 is one of the many

available anti-folates, which can now be screened by crystallography and an activity assay. The only other anti-folates that bind and inhibit catalysis were first identified in the bacterial homolog MetE, and at minimum required an oxidized or reduced pterin connected by a PABA moiety to two glutamates (Whitfield and Weissbach 1970).

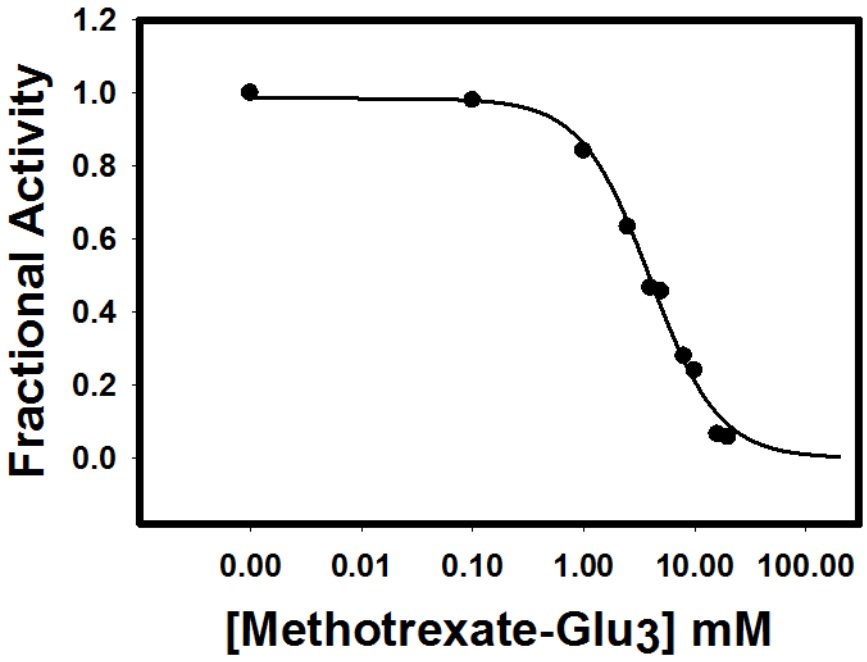

Figure 3.12 Inhibitor dose-response curve. The enzyme activity was tested in the presence of 0-20 mM MTX-Glu_3 with [S] = 2x[Km]. The data corresponds to an IC_{50} of 4 ± 1.4 mM with a Hill coefficient of 1.4 ± 0.1.

S-adenosyl homocysteine (SAH) bound Met6pA

So far, the various substrate, product, and inhibitor-bound or free Met6pA structures have been crystallized in an 'open' configuration. In this form, Met6p has two distinct substrate binding pockets which are separated by ~7 Å. The two pockets and the

region in between could potentially be spanned by a single, Met6p specific bi-dentate analog. Prior to entering the rigorous process of design and synthesis, I searched the Sigma-Aldrich website (among other vendors) for a bi-substrate analog with an amino acid backbone, a linker, and a heterocyclic ring. The commercially available S-adenosyl homocysteine (SAH) was a potential candidate with a free amino acid backbone of Hcy linked via a ribose sugar to an adenine base (Figure 1.9). The overall length of SAH was ideal and could place the amino acid and adenine in the appropriate substrate pockets, but the bulky sugar linker did raise some steric concerns.

The rationale behind using SAH is based on the ability of the C-terminal barrel to recognize and strongly interact with an amino acid backbone, and the ability of the folate pocket to accommodate simple aromatic or reduced heterocyclic rings. In a Met6pA crystal soaked with SAH, we observed excellent Fo-Fc density that spanned both substrate pockets (Figure 3.13). The crystallographic statistics are shown in Table 3.5. An entire molecule of SAH was successfully modeled in this 'open' Met6p structure (Figure 3.13). As expected, the amino acid backbone is the only component of SAH to make specific hydrogen and ionic interactions. The amino group is secured through ionic interactions with Glu499 and Asp614, and hydrogen bonds with the backbone carbonyl of Ile446. The carboxylate forms hydrogen bonds with the backbone amine and side chain hydroxyl of Ser448.

The rest of SAH, including the ribose sugar and adenine ring form non-specific hydrophobic or stacking interactions. The space between the Hcy/Met pocket and the folate site is mostly solvent exposed except for a few hydrophobic residues which line the top of the C-terminal barrel. This hydrophobic patch of residues includes Met505, Pro616 and Trp576. The side-chains of Met505 and Pro616 form hydrophobic interactions with the side chain of Hcy and the ribose sugar. The face of the sugar ring

Table 3.5 X-ray data collection and refinement of SAH bound Met6pA.

Structures	SAH
Cell dimensions	
a, b, c (Å)	77.1, 99.2, 102.0
αβγ (°)	90, 90, 90
Resolution (Å)[a]	38.6-2.3 (2.35-2.31)
R_{merge} (%)	0.100 (0.363)
$\langle I/\sigma_I \rangle$	9.5 (5.4)
Completeness (%)	97 (95.2)
Unique reflections	33,963
Redundancy	7.0
$R_{working}$	0.183
R_{free}	0.244
Average B factor for protein atoms (Å^2)	15.7
Average B factor for solvent atoms (Å^2)	25.5
Average B factor for ligand atoms (Å^2)	34.5
Rms deviation from ideality	
Bond length (Å)	0.014
Bond angle (°)	1.652

[a] Highest resolution data is shown in parenthesis.

packs against the hydrophobic patch while the 2' and 3' hydroxyls are rotated away in the direction of solvent. The adenine base forms non-specific stacking interactions with the side chain of Trp576, reminiscent of the interactions made by folates. The exocyclic and endocyclic amines at position C^6 and N^1, respectively, form hydrogen bonds with a neighboring water molecule.

SAH makes specific or non-specific interactions with residues located exclusively in the C-terminal barrel and this triggers conformational changes in the barrel in the same way as Hcy, Gln and Met. An overlay of the apo and the four ligand bound structures is shown in figure 3.14; the four ligands align in the same pocket and make the same contacts via the amino acid backbones. The amino acid side chain of SAH contains a thioether, like Met, instead of the free thiol found in the natural substrate (Hcy). As a

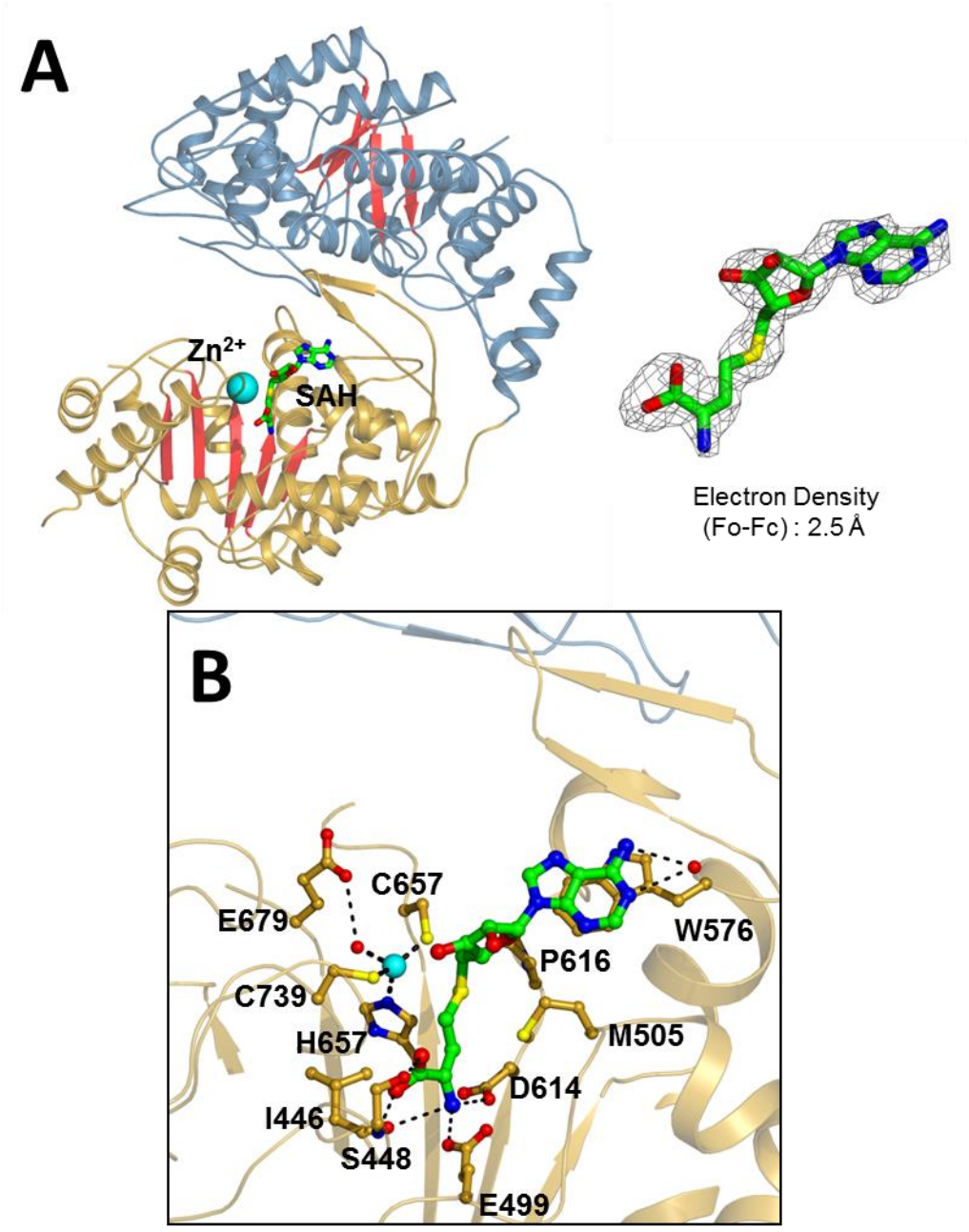

Figure 3.13 SAH bound Met6pA. A) The N and C terminal domains are shown in blue and golden, respectively. The bound SAH is shown in green and the active zinc is shown as a cyan sphere. B) The hydrogen bond and ionic interactions in the Zn^{2+} binding pocket and the adjacent SAH binding pocket are shown. Waters are shown as red spheres and the active site zinc is shown as a cyan sphere.

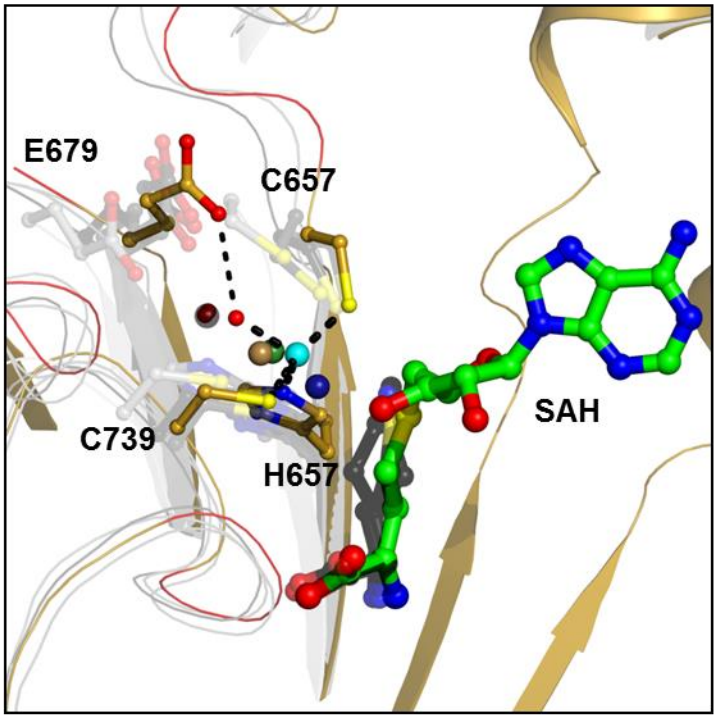

Figure 3.14 Overlay of the Zn^{2+} coordination site. The ligand-free, Hcy, Met, and Gln bound Met6pA structures are shown in grey and each respective zinc is shown as a grey, blue, green, and golden sphere, respectively. The SAH bound structure is shown in gold with the SAH in green and the zinc sphere in cyan. The ordered βα loops surrounding the metal coordination site are in red.

result, the zinc coordination geometry in the SAH-replete structure closely resembles the geometry observed in the Met and Gln bound structures. That is, the Zn^{2+} ion moves toward the ligand, breaking the interaction with Glu679 and forming a new bond with water. Zinc coordinates with His657, Cys659, Cys739, and the water with bond lengths of 2.15 Å, 2.04 Å, 2.39 Å, and 2.09 Å, respectively. SAH binding pulls the Zn^{2+} 2.8 Å from the apo position, compared to 2.1 Å for the thioether in the Met complex. The SAH induced displacement places the Zn^{2+} in between the metal positions for the Met and Hcy

complexes. The βα loops which surround the Zn^{2+} coordination site are also mostly ordered in the SAH bound structure.

SAH is the first bi-substrate analog to successfully bind both substrate pockets and will be used as a template to design and synthesize highly specific and potent Met6p inhibitors. One of the most important features of SAH is the amino acid backbone; it anchors the SAH into the Hcy site and allows the adenine to form a stable but non-specific stacking interaction with Trp576. In the solvent exposed folate pocket, the side chain of Trp576 behaves as a hydrophobic anchor, and is used to attract and non-specifically bind a variety of pterins. Residues Asp504 and Asn126 correctly orient the natural substrate 5-methyl-THF-Glu_3 and could also be recruited by the right substituted heterocyclic ring. The folate pocket is lined with a few more hydrophobic (Tyr527) and basic (Arg530, Lys19) residues which help bind the PABA moiety and polyglutamate tail, and could also be exploited by the right Met6p inhibitors.

Development of a fluorescence-based Met6p activity assay

The enzyme activity of the wild-type or any mutant Met6p can be evaluated by using the existing absorbance assay; however this detection method cannot be used to test inhibitors that resemble anti-folates like methotrexate. The absorbance based method was introduced by Drummond and Matthews in 1995 as an alternative to the existing radioactive assay (Drummond, Jarrett et al. 1995). This group introduced a chemical and heat treatment step to stop the enzymatic reaction and convert the product THF-Glu_3 into methenyl-THF-Glu_3, which absorbs at a wavelength of 350 nm. Many available anti-folates also absorb near 350 nm. The natural substrate, 5-methyl-THF-Glu_3 does not get derivatized or absorb at this wavelength and generally produces a signal in the range of

Table 3.6 Background signals in Absorbance Based Assay. Absorbance measurements of various folates, anti-folates, and pteroic acid taken at 350 nm.

Ligand (500 µM)	Absorbance 350 nm
5-Methyl-THF-Glu_1	0.206
5-Methyl-THF-Glu_3	0.148
Folic Acid	0.747
Methotrexate-Glu_1	1.621
Methotrexate-Glu_3	1.626
Folinic Acid	1.653
Pteroic Acid	0.865

0.1-0.2 AU. In contrast, when the various anti-folates and pteroic acid are tested in the absorbance assay, they have an absorbance signal (Table 3.6).

The fluorescence based assay takes advantage of the commercially available probe, Measure-iT^{TM} (2',7'-difluoro-4'-(2-(5-((dimethalyaminophenyl)azo)pyridyl) dithiopropionylaminometyl) fluorescein), which selectively reacts with the free thiol in Hcy and generates a quantitative fluorescence signal. This probe is 400 times more sensitive than the widely used Ellman's reagent, with excitation/emission maxima near 490/520 nm. Folates like folic acid and anti-folates like MTX-Glu_3 absorb light near 300-400 nm and emit near 350-500 nm. These compounds are not expected to react with the Measure-iT^{TM} thiol quantitation reagent or produce a fluorescence signal with the 490/520 filters. A concentration gradient of MTX-Glu_3 was tested and did not produce a fluorescence signal alone or in the presence of the Measure-iT thiol quantitation reagent (Figure 3.15). A significant and linear increase in fluorescence was only observed for Hcy over a range of 0 to 200 uM (Figure 3.15).

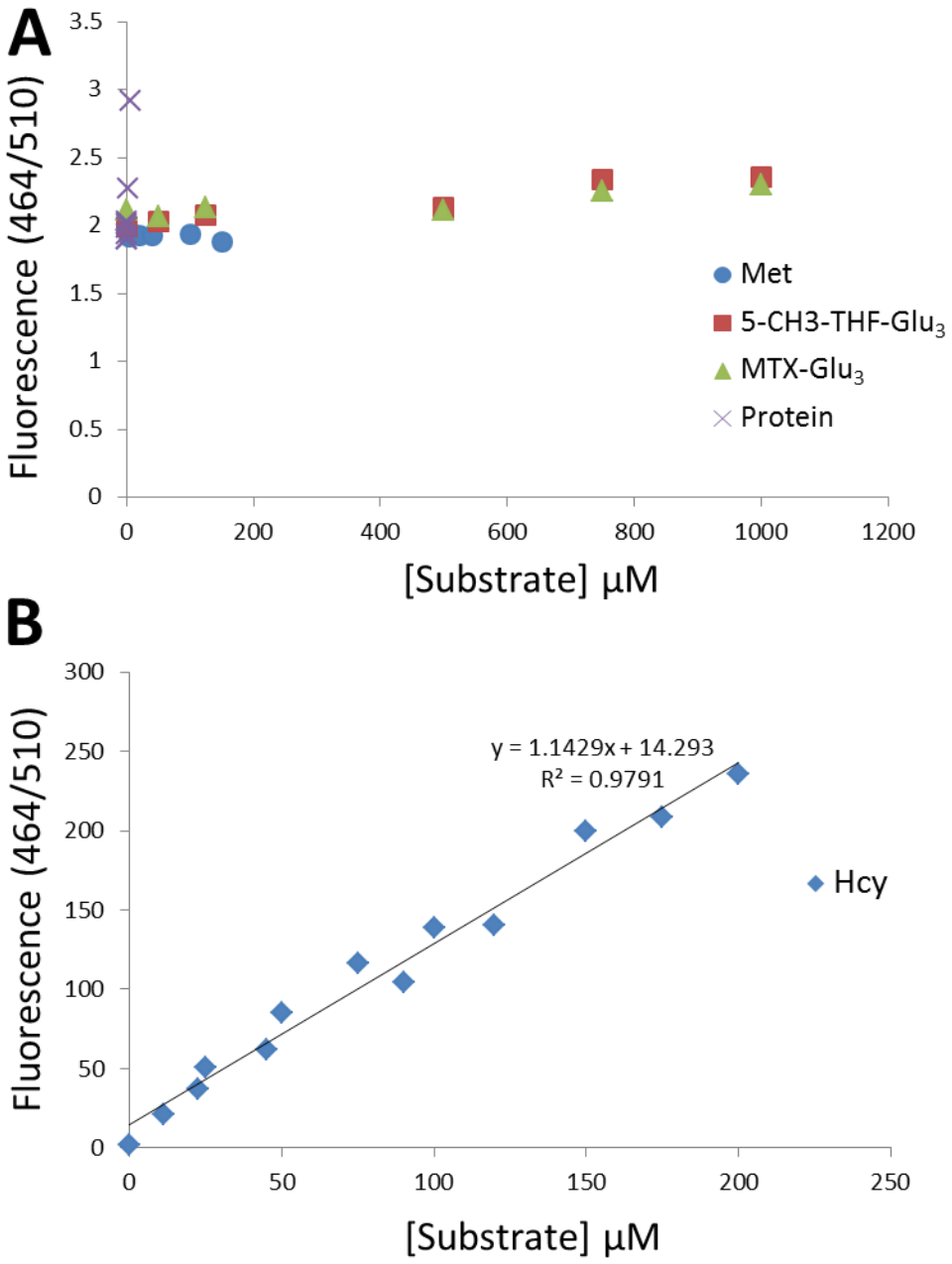

Figure 3.15 Development of the fluorescence based activity assay. The fluorescence signal (at excitation/emission wavelengths of 464/510 nm) generated by substrates, products, and inhibitors. A) The fluorescence vs. concentration gradients of Met (0-150 µM), 5-methyl-THF-Glu_3 (0-1 mM), MTX-Glu_3 (0-1 mM) and protein (0-6 µM). B) The fluorescence vs concentration gradient with Hcy (0-200 µM).

The fluorescence assay was developed by slightly modifying the reaction conditions used in the absorbance assay and completely replacing the heat and chemical treatment steps previously required for methenyl-THF-Glu_3 synthesis. Overall, the enzyme reaction conditions remain the same, but all reducing agents were omitted because the thiol quantitation reagent reacts with DTT, BME and TCEP. Instead, all reagents and samples are flushed with N_2 gas and when necessary protected from light and/or air. The final reaction volume is also scaled down from the 380 µL used in the absorbance assay to 10 µL. The reaction is stopped by an incubation step in ice and the substrate Hcy is quantified by adding saturating concentrations of the Measure-iT™ reagent. The reaction between the free thiol and the reagent is proprietary. This reaction goes to completion in 2-3 minutes at room temperature. Fluorescence measurements are taken using the Roche LightCycler® 480 RT-PCR instrument using the available excitation/emission filters of 464/510 nm.

Once the enzyme reaction and detection steps were successfully combined, steady state kinetics experiments were done to determine the substrate K_Ms and the k_{cat}. The steady state concentration of the enzyme (110 nm) was determined from an activity vs. protein concentration plot shown in Figure 3.16. I carried out steady state kinetics and measured the K_M of 25 ± 16 µM and k_{cat} of 25 ± 5/min for Hcy, and the K_M of 87 ± 31 uM and k_{cat} of 29 ± 2/min for 5-methyl-THF-Glu_3. The k_{cat} and K_M parameters for each substrate closely resemble the values previously reported by the absorbance assay (Figure 3.17).

The steady state parameters were used to establish a standard, single time point activity assay which can be used to efficiently test the wild-type enzyme, and to evaluate any Met6p mutants. We tested a few interesting mutants located in the folate pocket (Asn126Ala) and at the inter-domain interface (Tyr660Ala, Tyr660Asn, Tyr660Phe). A

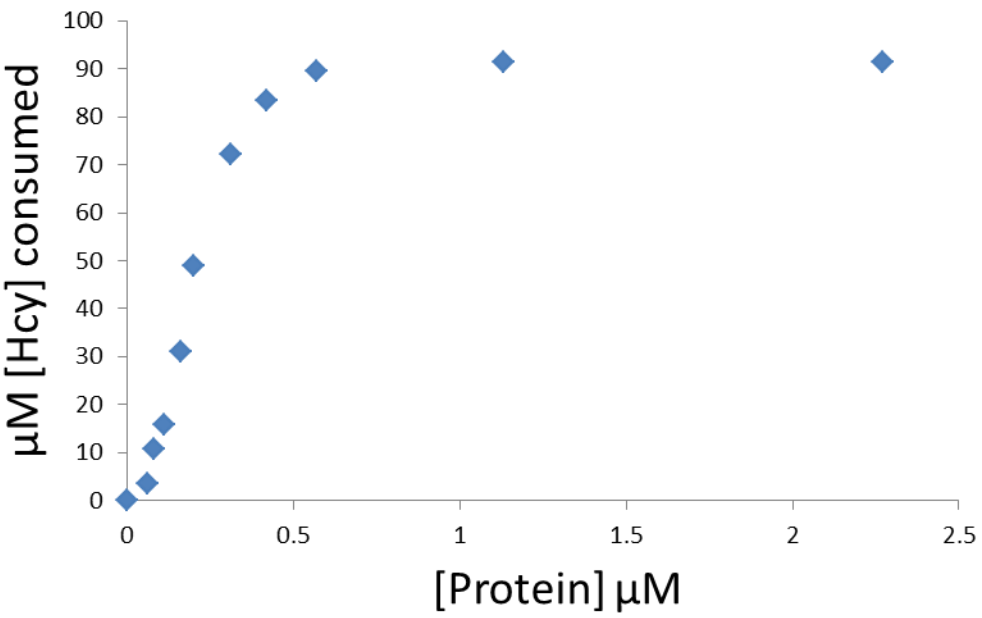

Figure 3.16 Development of the fluorescence based activity assay. The steady state protein concentration used in the fluorescence-based activity assay was established by testing a protein concentration gradient (0-2.27 µM) in the presence of saturating concentrations of Hcy (100 µM) and 5-methyl-THF-Glu_3 (500 µM). The reaction was stopped after 10 minutes and the fluorescence (464/510 nm) was converted to µM Hcy consumed.

few of these mutants, including Asn126Ala, Tyr660Ala and Tyr660Asn had no detectable activity in the standard assay. The standard assay contains saturating substrate and steady state protein concentrations. Although the initial results clearly support an essential role of Tyr660 and Asn126, we also tested and reported the enzyme activities at saturating enzyme concentrations (Table 3.4). The standard assay was also used to test the activity of the wild-type Met6p in the presence of the methyl source 5-methyl-THF-Glu_1, or with a protein pre-incubation step of 5 minutes with 500 µM EDTA. Zero enzyme activity was observed with either test condition (results not shown).

An inhibition study with the anti-folate MTX-Glu_3 was also done using a slightly modified standard assay. We reduced the substrate concentrations to 2x the K_M values in

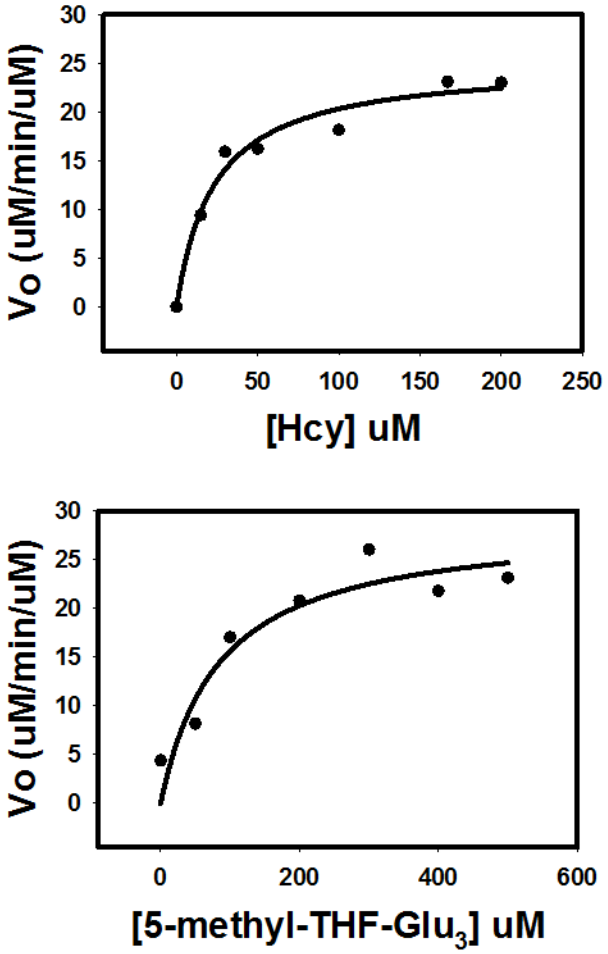

Figure 3.17 Steady state kinetics. The steady state parameters for Hcy and 5-methyl-THF-Glu_3 were experimentally determined using the fluorescence based kinetic assay. Shown on top is the steady state curve for Hcy with a Km of 25 ± 16 µM and Kcat of 25 ± 5/min, and shown on the bottom is the steady state curve for 5-methyl-THF-Glu_3 with a Km of 87 ± 31 µM and Kcat of 29 ± 2/min.

order to give competitive inhibitors a chance to bind. Data from a 20 minute time course experiment with S = 2x[K_M] and steady state protein concentration is shown in figure 3.18. The raw fluorescence readings for each sample (Hcy, reaction background, and

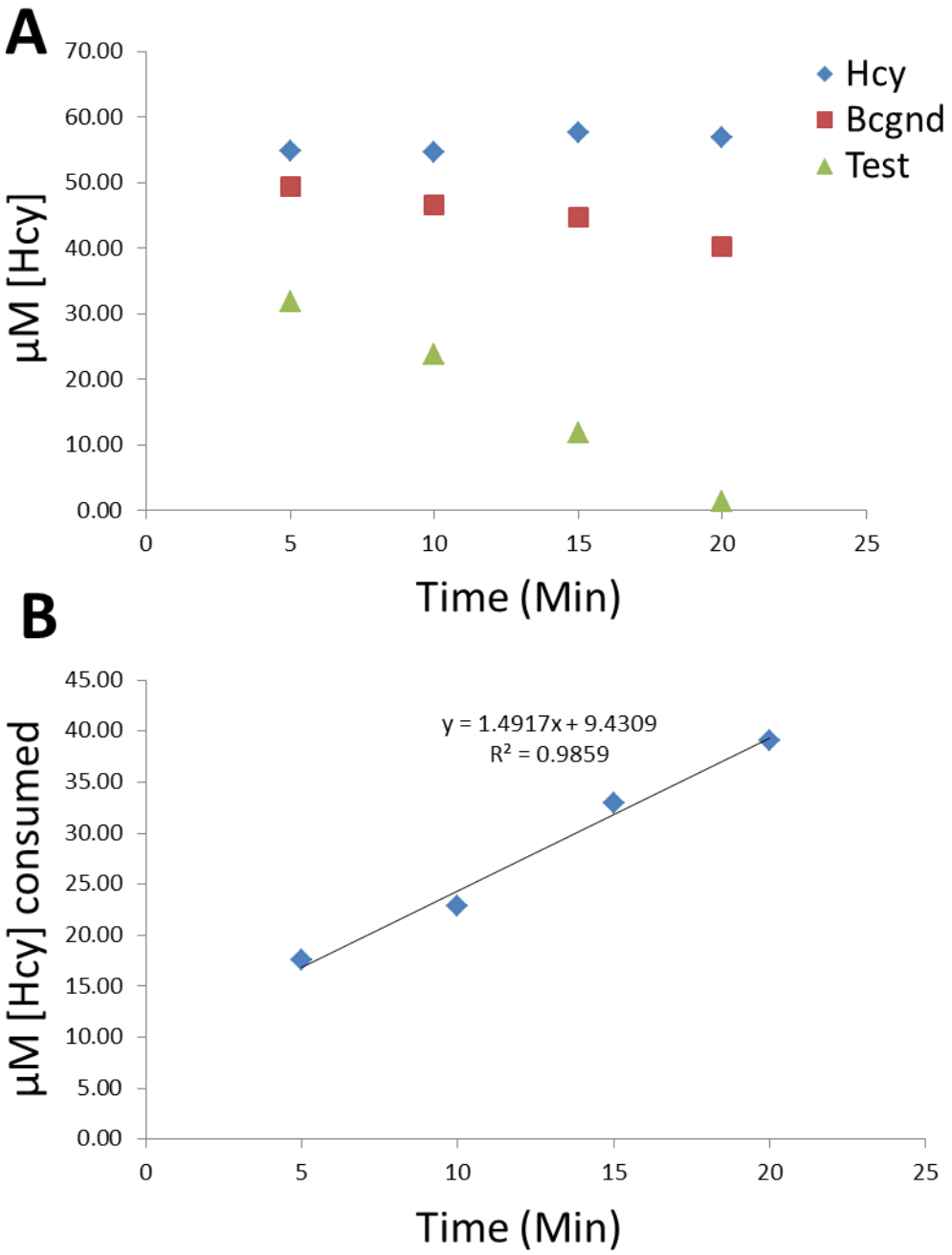

Figure 3.18 Fluorescence based assay over a 20 minute time course. The assay was done with S=2x[Km], and 100 nM protein. A) The raw fluorescence readings for each sample were converted to uM [Hcy] and plotted over time. B) The uM [Hcy] consumed was calculated as the difference between the Test and Background (Bcgnd) samples and plotted over time. The data points were fit to a linear function.

test) were converted to μM Hcy and plotted against time. The μM Hcy consumed at each time point was determined by calculating the difference between the background, or "blank rate" and the test sample. The data points from the entire time course were fit to a linear function with an R^2 of 1. This experiment was repeated at a single time point of 10 minutes in the presence of 0-20 mM MTX-Glu_3 and the resulting dose-response curve is shown in Figure 3.12.

The Development of a high-throughput DSF assay

Differential scanning fluorimetry (DSF) is a popular biophysical method which can be used to screen ligands that bind and stabilize protein (Niesen, Berglund et al. 2007). This method is inexpensive, high-throughput, and requires low quantities of protein, a special fluorescent dye, and an RT-PCR instrument. The protein is heated in the presence of a fluorescent dye, and as the protein unfolds, the dye binds to the exposed hydrophobic regions and fluoresces. The instrument is used to control the temperature gradient (usually 25 °C to 100 °C), and as the protein melts, the instrument records the fluorescence vs. temperature protein melting curve. The inflection point in this curve is the Tm, or the temperature at which half the protein population is denatured. In the presence of a stabilizing ligand the Tm is expected to increase, generating a positive Tm shift.

A high-throughput DSF method was successfully developed (described in materials and methods) for the fungal Met6p enzyme. The final 25 μL reaction includes 750 nM protein, 5X Sypro Orange dye, and ≤ 2% DMSO buffered by 20 mM Hepes, 150 mM NaCl, pH 7.5. The Tm for Met6p alone (negative control) was 71 ± 0.07 °C. In the presence of Hcy (positive control), a Tm shift of 1.5 ± 0.07 °C was observed. The product Met and substrate 5-methyl-THF-Glu_3 shift the Tm by 0.7 °C ± 0.07 °C and 0.8 ±

0.05 °C, respectively. The inhibitor MTX-Glu_3 shifts the Tm by 0.7 °C ± 0.02 °C. The melting curves for the negative and positive controls are shown in Figure 3.19. The standard deviation for the negative and positive control was consistently ≤ 0.07 °C (across 96 wells) and any compound which could bind and shift the Tm by at least 0.3 °C (3 times the standard deviation) was considered a hit.

Three distinct libraries were screened using DSF in order to identify compounds (tested at 100 μM final concentration), which bound and increased the Tm of Met6p. The entire NIH clinical collection of 731 compounds consists of FDA approved drug-like molecules which are well characterized, soluble and commercially available. The second library from Chembridge consists of 7,000 small fragments (MW < 300) which are highly soluble, pure and have excellent physicochemical properties. The third set of 11,000 molecules from Chembridge is a kinase inhibitor-biased library called KINASet. This library is enriched with ligands containing heterocyclic rings.

Out of the 731 compounds in the NIH clinical collection (NCC), 26 were found to increase the protein Tm by ≥ 0.3 °C. False positives were removed by retesting freshly purchased compounds and reduced the number of hits to just 13. These hits were further validated using the absorbance based enzyme activity assay at a single inhibitor concentration of 500 μM. Only 3 molecules inhibited the enzyme and reduced the activity from the 100% observed in wild-type to 40-60%, while two potential candidates, Benidipine and Pterostillbene, could not be further evaluated due to their high background signals at 350 nm. Triclabendazole could not be purchased and remains to be tested, however, dose-response experiments were done using Triclosan, PD81723, and Phenothiazine over the range of 0-1 mM (Figure 3.20). When possible, the data points were fit to a 3 parameter logistic equation, or evaluated by eye in order to determine the IC_{50}, defined as the concentration of inhibitor required for 50% inhibition. Triclosan and

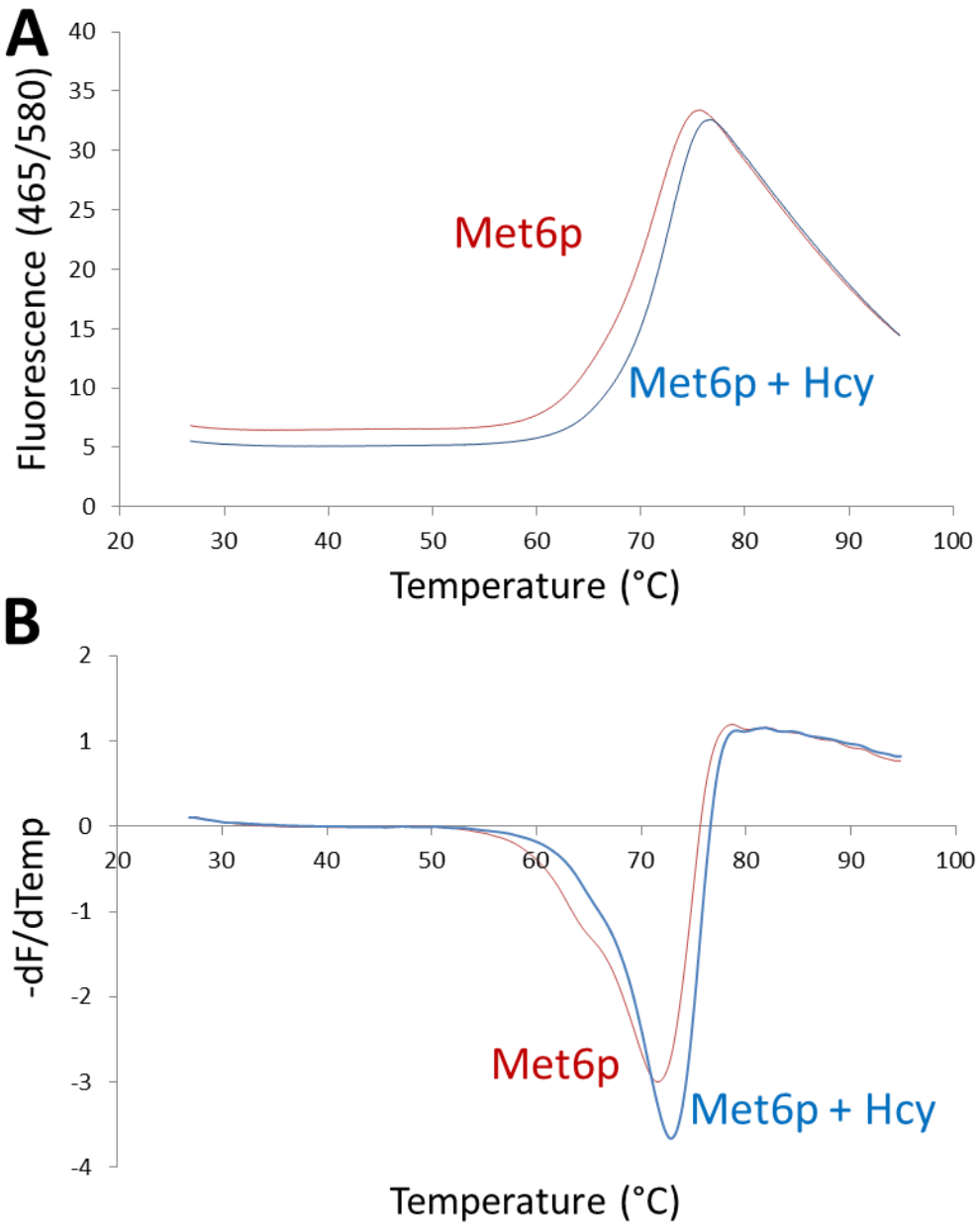

Figure 3.19 Melting curves with the DSF assay. Melting curves are shown for the ligand-free and Hcy-bound Met6pA. A) The fluorescence vs. temperature curves are shown for the ligand-free (red) and Hcy-bound (blue) Met6p enzyme. B) The protein melting curves are calculated by taking the first derivative of the fluorescence as a function of temperature. The Tm is the point of inflection. Met6p has a Tm of 71 ≤ 0.07 °C and Met6p+Hcy has a Tm of 72.5 ≤ 0.07 °C.

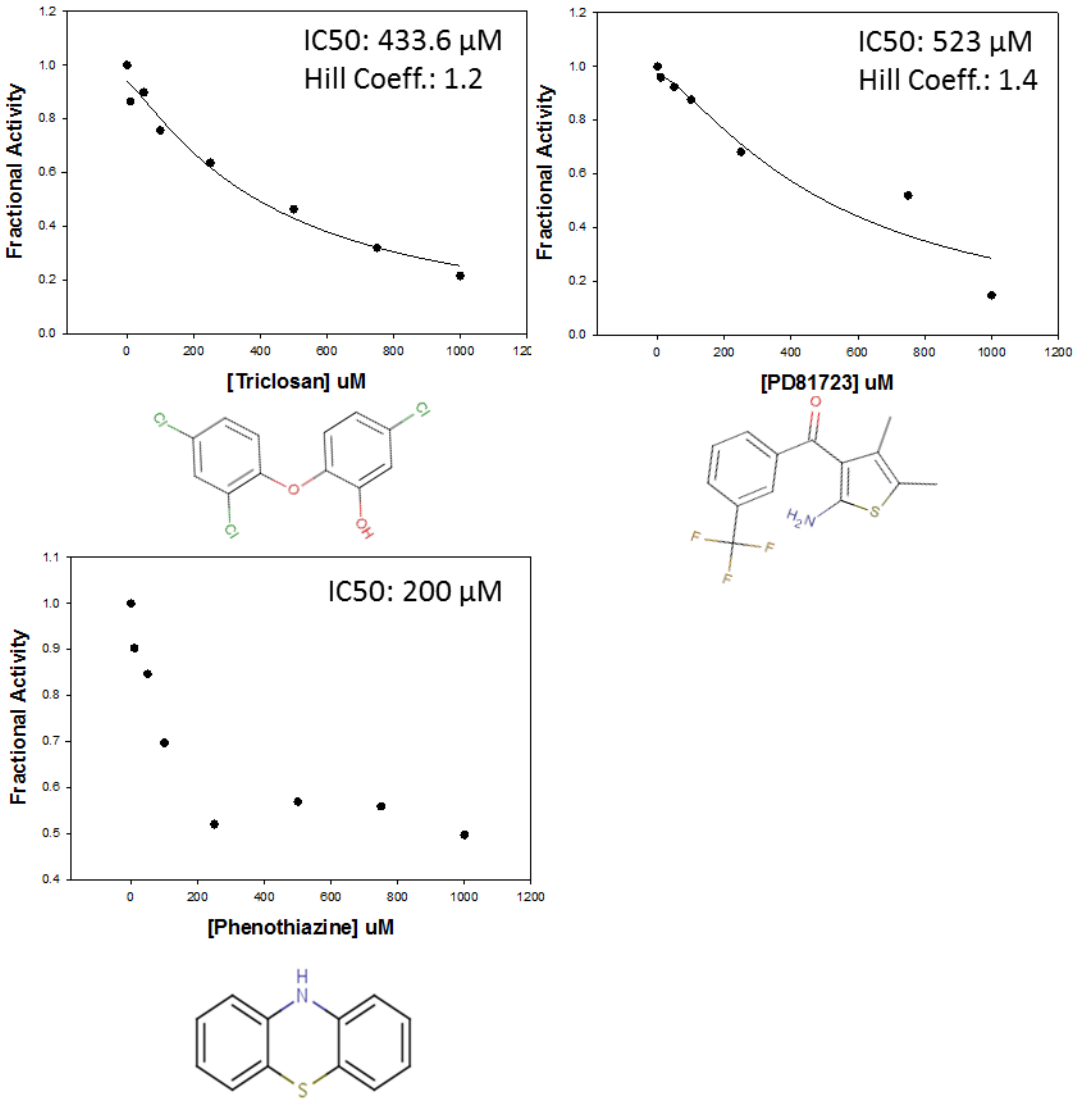

Figure 3.20 Dose-response curves for compounds from the NCC. The apparent IC_{50}s and Hill coefficients are listed for each compound. Phenothiazine precipitates out of solution at ~250 µM.

PD81723 have apparent IC_{50} values of roughly 434 and 523 µM, respectively, with Hill coefficients of roughly 1. Phenothiazine precipitates out of solution at ~250 µM and its IC_{50} was estimated by eye as 200 uM.

Out of the first 4,000 compounds in the Fragment library, 13 increased the protein Tm by ≥ 0.3 °C. Ten out of the thirteen were successfully retested and shifted the Tm ≥ 0.3 °C. These hits were further validated by the absorbance based activity assay in which four compounds, 5214970, 5376760, 5303077 and 5279826, reduced the enzyme activity to 0-30% (relative to wild-type) when tested at 500 µM. Dose-response experiments were done for all four compounds, but the IC_{50} values could only be measured for two because at higher concentrations compounds 5214970 and 5376760 absorbed at 350 nm. The apparent IC_{50} values for 5303077 and 5279826 were 191 µM and 84 µM, respectively, and Hill coefficients were roughly equal to 1 (Figure 3.21).

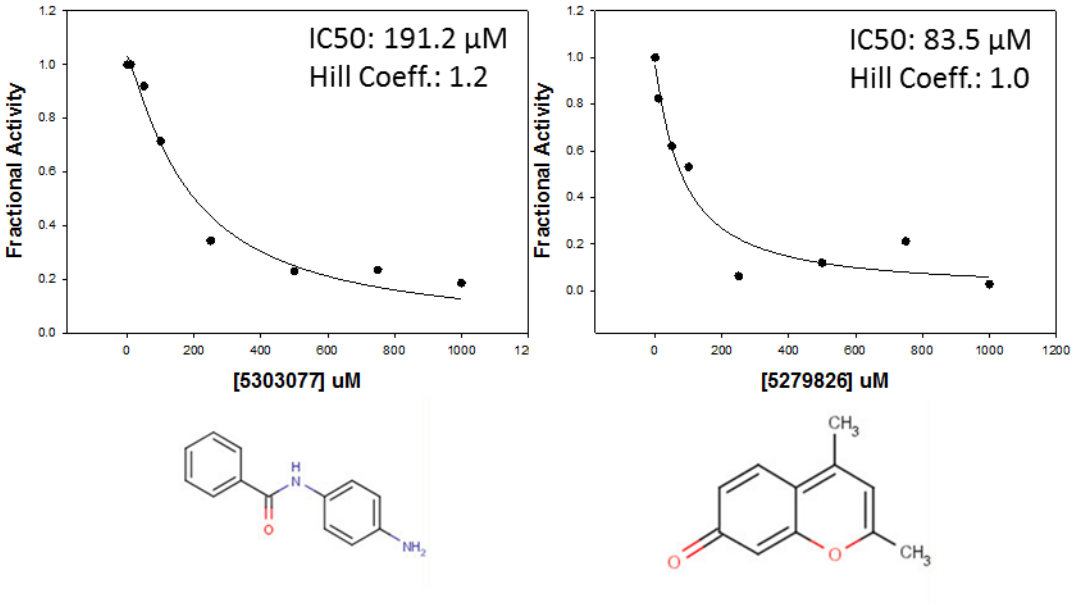

Figure 3.21 Dose-response curves for compounds from the Fragment library. The apparent IC_{50}s and Hill coefficients are listed for each compound. .

Out of the first 4,000 compounds in the KINAset library, 20 shifted the Tm by ≥ 0.3 °C. Sixteen out of the twenty were successfully retested. These hits were further

validated using the absorbance based activity assay in which 12 compounds reduced the enzyme activity to 6-63% (relative to wild-type) when tested at 500 μM. Only 10 out of the 12 were tested further because compounds 5848343 and 6385797 could not be purchased. Dose-response experiments were successfully done with 7 compounds which had apparent IC_{50}s ranging from 57-328 μM, and Hill coefficients close to 1 (Figure 3.22). The IC_{50} values for compounds 6215005, 7014609, and 7031899, could not be determined due to the high background signals at 350 nm.

The DSF and the absorbance based kinetic assays were successfully used to identify 3 potential Met6p inhibitors from the NIH clinical collection, 2 from the fragment library, and 7 from the KINAset library. These compounds are enriched with aromatic and/or reduced rings. Our experience with MTX-Glu_3, 5-methyl-THF-Glu_3, folinic acid, folic acid, and SAH has shown that an otherwise solvent exposed folate pocket has a tendency to form non-specific stacking or hydrophobic interactions with heterocyclic rings. In order to understand the mode of binding, Met6pA crystals were soaked with saturating concentrations of each compound (5 mM). With some of these compounds, we observed patches of density near the solvent exposed side of Trp576 (folate pocket). Unfortunately, the density is consistently weak and incomplete, making it difficult to dock and/or rationalize the mode of binding. Co-crystallization experiments have also been done, but were unsuccessful. These compounds should be retested using the fluorescence based activity assay and co-crystallized and/or soaked using the Met6pT or Met6pY proteins. However, based on the drug screening, kinetic, and structural work done so far, this strategy has failed.

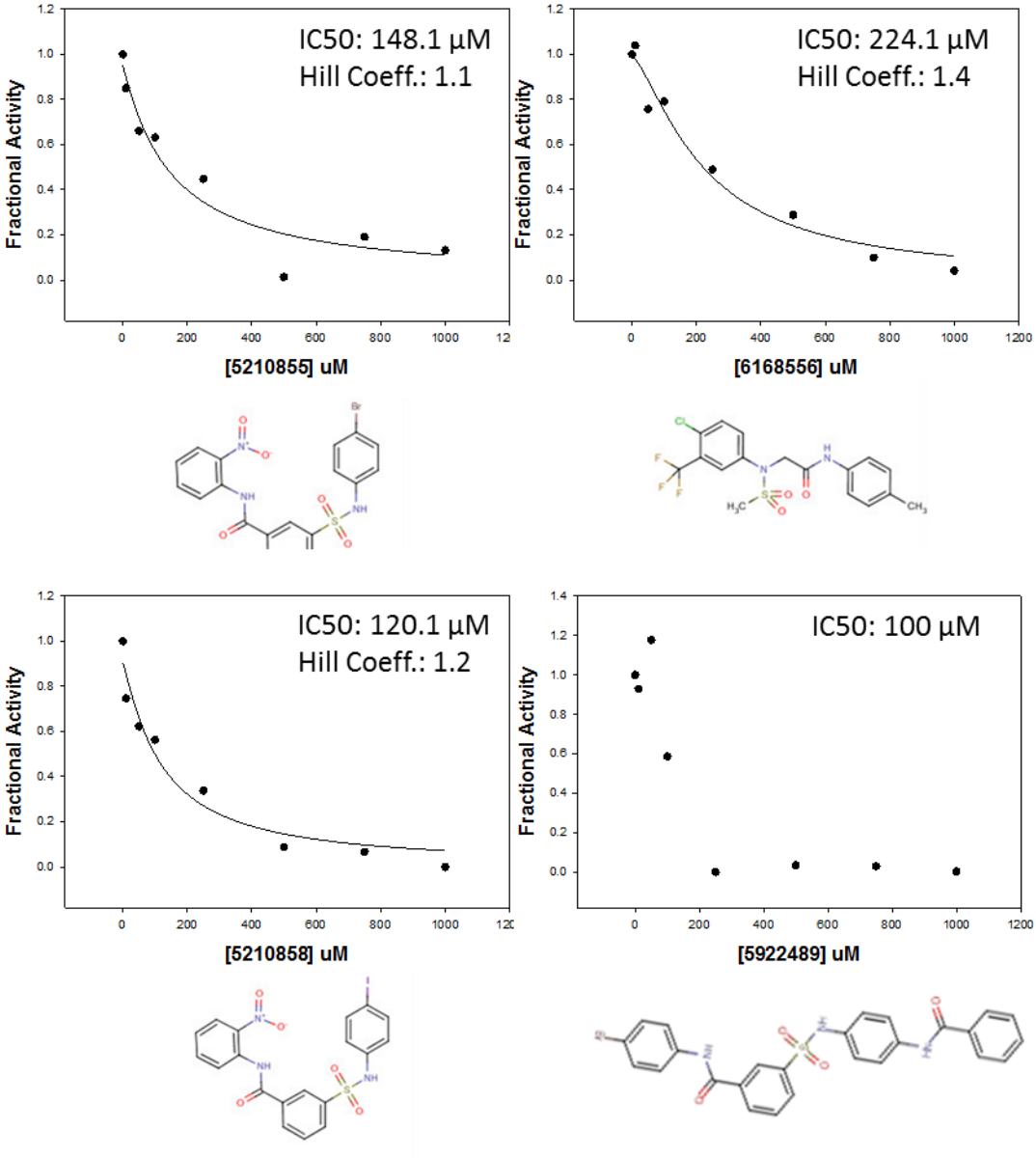

Figure 3.22 Dose-response curves for compounds from the KINAset library. The apparent IC_{50}s and Hill coefficients are listed for each compound.

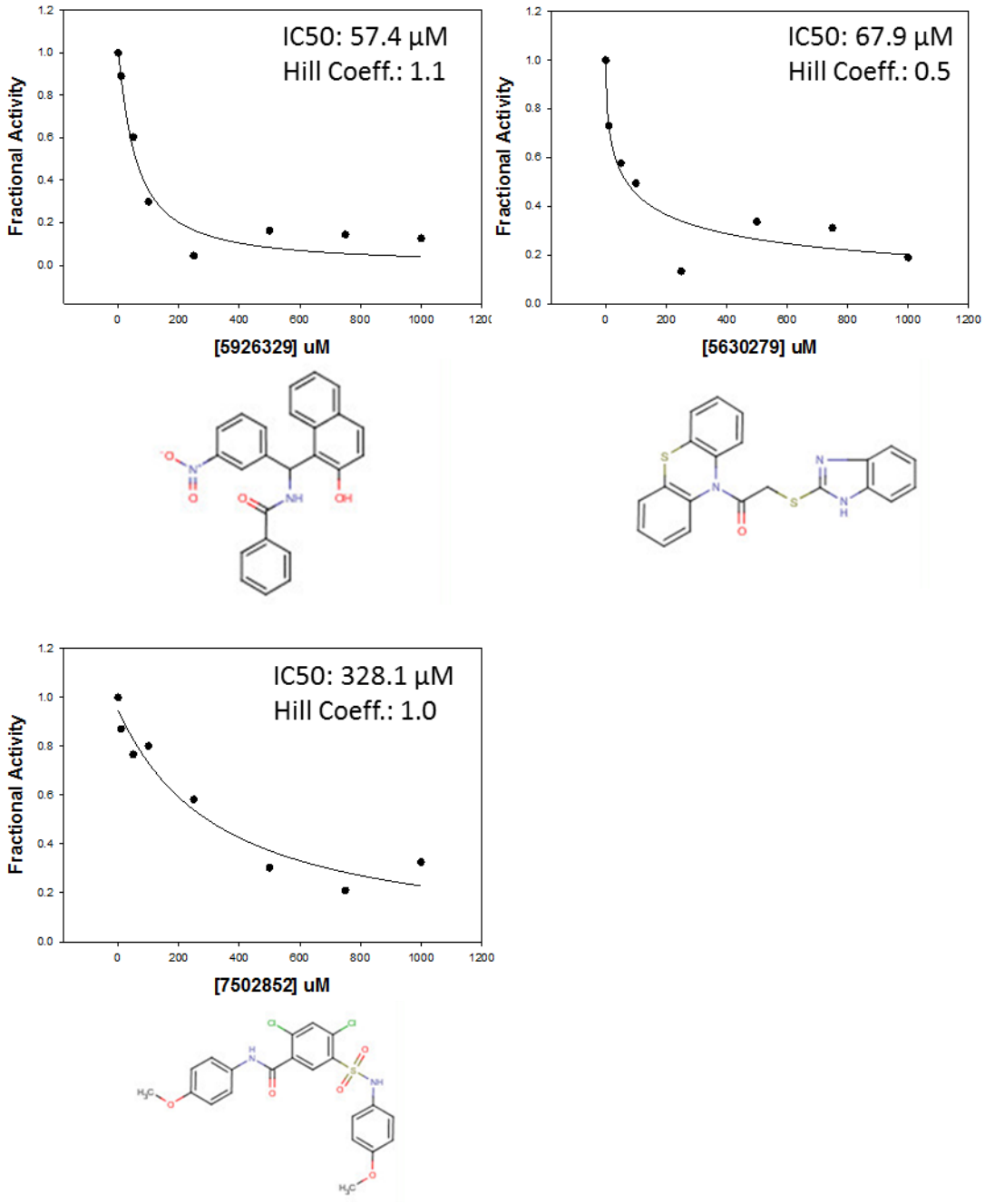

Figure 3.22 continued. Dose-response curves for compounds from the KINAset library. The apparent IC_{50}s and Hill coefficients are listed for each compound.

Conclusion

Candidemia is a serious health concern which afflicts millions and results in considerable mortality. Fungal infections are often serious medical problems and difficult to treat due to the similarity of most human and fungal enzymes. It would be useful to find a novel fungal target which is present in a broad range of fungi; methionine synthase is such a target. The *Candida albicans* species is the most prevalent cause of candidemia and has been the focus of previous studies which identified an essential *C. albicans* gene, MET6. This gene encodes the zinc-dependent fungal enzyme cobalamin-independent methionine synthase (Met6p) which synthesizes methionine by directly transferring a methyl group from 5-methyl-tetrahydrofolate (5-methyl-THF) to L-homocysteine (Hcy). This 88 kDa protein is structurally and mechanistically different from the modular 140 kDa cobalamin-dependent methionine synthase (MetH) used by mammals.

The overall goal of this project was to characterize the structure and action of Met6p and to discover a variety of drug-like scaffolds. I used the SER strategy to initially crystallize three variants of the wild-type enzyme, Met6pA, Met6pT and Met6pY, all of which crystallized in the 'open' configuration and retained full enzyme activity.

Crystals of the Met6pA variant were soaked with natural substrate, products, anti-folates (MTX-Glu_3) and substrate analogs (Gln) in order to characterize the Zn^{2+}, Hcy, and 5-methyl-THF-Glu_3 binding pockets. Structural studies were accompanied with site-directed mutagenesis and mutants were tested by a novel fluorescence based activity assay. We uncovered key roles for two active site residues, Tyr660 and Asn126, not previously implicated in Met6p activity.

Other groups have previously characterized the Hcy pocket by using the natural substrate and product, however, we are the first to capture a Gln bound Met6p and to show that it was the binding of the amino acid backbone that triggered an ordering of active site loops and the movement of the catalytic Zn^{2+} towards the substrate. Hcy, Met and Gln all bind at the top of the C-terminal barrel through an identical amino acid backbone and all three ligands stabilize the 'open' configuration by ordering the flexible loops in the C-terminal barrel.

Other groups have previously characterized the folate pocket by using the natural substrate and product; however, we are the first to capture a MTX-Glu_3 bound Met6p and to observe a productive ternary complex. The folate pocket was able to form non-specific stacking interactions between the conserved side chain of Trp576 and an oxidized or reduced pterin. However, the aromatic 2,4-diaminopteridine of MTX-Glu_3 was found to easily rotate and performed as a modest inhibitor with an IC_{50} of ~4 mM. On the other hand, THF with its three distinguishable endocyclic nitrogens, a carbonyl group and an exocyclic amine made numerous specific contacts. Asn126 was especially interesting; the acceptor/donor pair on its side-chain aligned with the donor/acceptor pair at position N^8 and N^1 in 5-methyl-THF-Glu_3. The two available hydrogen donors on the otherwise oxidized pyrimidine ring donated hydrogen bonds to the side chain of Asp504.

The extensive structural characterization has made rational drug design a feasible strategy. It was successfully implemented in identifying the bi-substrate analog SAH. Although SAH is not an ideal folate-Hcy analog, it contains the basic components we initially found to be important for binding in each substrate pocket: the amino acid backbone and a heterocyclic ring. This compound successfully bound the 'open' configuration of Met6p by using the amino acid backbone to anchor into the Hcy/Met site, the Hcy side-chain and ribose sugar for hydrophobic interactions with M505 and

Pro616, and the aromatic adenine ring to form non-specific stacking interactions with the conserved residue Trp576.

Thousands of compounds were screened using an optimized high-throughput DSF assay, and a few were successfully tested by the absorbance based activity assay with reported IC_{50} values in the micromolar range. However, these inhibitors have failed to bind the Met6pA crystals by soaking or co-crystallization experiments. Since similar methods were successfully used for substrate, MTX-Glu_3, and SAH, it is possible that compounds in the NIH clinical collection, Fragment library and KINAset library do not bind the 'open' configuration. A stable 'closed' methionine synthase structure remains to be seen, however, for now; the 'open' configuration can be successfully targeted using rational drug design.

Appendix A

Abbreviations	
B_{12}	Cobalamin (Vitamin)
BHMT	Betaine homocysteine methyltransferase
BME	β-Mercaptoethanol
Cys	Cysteine
DHF	Dihydrofolate (Glutamate$_{1-3}$)
DHFR	Dihdrofolate reductase
DSF	Differential Scanning Fluorimetry
DTNB	Ellman's reagent
DTT	Dithiothreitol
EXFAS	Extended X-ray absorption fine structure
GARFT	Glycinamide ribonucleotide formyltransferase
Gln	Glutamine
Hcy	L-Homocysteine
HMT	S-methylmethionine Hcy S-methyltransferase
Met	Methionine
MetE	Cobalamin-independent methionine synthase (bacteria and plants)
MetH	Cobalamin-dependent methionine synthase
Met6p	Cobalamin-independent methionine synthase (yeast)
Met6pA	^{103}AlaAlaAlaThrAla^{107}
Met6pY	^{103}TyrTyrAlaThrTyr^{107}
Met6pT	^{103}ThrThrAlaThrThr^{107}
MS	Methionine synthase
MTHFR	5,10-Methylenetetrahydrofolate reductase
MTX-Glu$_3$	Methotrexate-Glutamate$_3$
PABA	Para-aminobenzoic acid
PDB	Protein Data Bank
Pteroyl-Glu$_5$	Pteroylglutamaic$_5$ acid (Folic Acid with polyanionic tail)
RMSD	Root mean square deviation
SAH	S-Adenosyl-L-homocysteine
SAM	S-Adenosyl methionine
SER	Surface Entropy Reduction
SHMT	Serine hydroxymethyltransferase
SMM	L-S-methylmethionine
THF	Tetrahydrofolate (Glutamate$_{1-3}$)
Tm	Protein melting temperature
TS	Thymidylate synthase
Zn	Zinc
5-methyl-THF-Glu$_n$	5-methyltetrahydrofolate-glutamate$_{1-3}$

Appendix B

Materials

Material	Manufacturer
Acetic Acid	Fisher Scientific, Fair Lawn, NJ
Agarose	Life technologies, Carlsbad, CA
β-Mercaptoethanol	Sigma Aldrich, St. Louis, MO
Centricon Filter (concentrator 30 kDa)	Millipore, Billerica, MA
Citric Acid	Sigma Aldrich, St. Louis, MO
Dithiothreitol	Sigma Aldrich, St. Louis, MO
DMSO	Fisher Scientific, Fair Lawn, NJ
DpnI	New England Biolabs, Ipswich, MA
DTNB	Thermo Scientific, Rockford, IL
Formaldehyde	Fisher Scientific, Fair Lawn, NJ
Formate	Fisher Scientific, Fair Lawn, NJ
Fragment library	ChemBridge, San Diego, CA
Glutamine	Sigma Aldrich, St. Louis, MO
HCl	Fisher Scientific, Fair Lawn, New Jersey
Hcy Thiolactone	Sigma Aldrich, St. Louis, MO
Hepes	Sigma Aldrich, St. Louis, MO
Imidazole	Acros organics, Morris, New Jersey
IPTG	Gold Biotechnology, St. Louis, MO
JCSG+ Suite	Qiagen, Bethesda, Maryland
Kanamycin	Sigma Aldrich, St. Louis, MO
KCl	Fisher Scientific, Fair Lawn, New Jersey
KH2PO4	Sigma Aldrich, St. Louis, MO
K2HPO4	Fisher Scientific, Fair Lawn, New Jersey
KINAset library	ChemBridge, San Diego, CA
KOD Hot Start DNA polymerase	Novagen, San Diego, CA
KSCN	Hampton Research, Aliso Viejo, CA
Measure-iT™ thiol quantitation reagent	Invitrogen, Oregon, CA
Methionine	Sigma Aldrich, St. Louis, MO
MgSO4	Fisher Scientific, Fair Lawn, NJ
MTX-Glu_3	Schircks Laboratories, Jona, Switzerland
Na2HPO4	EM Science, Cherry Hill, Jew Jersey
NaH2PO4	EM Science, Cherry Hill, Jew Jersey
NaOH	EM Science, Cherry Hill, Jew Jersey

Appendix B Continued

Materials

Material	Manufacturer
NaBH4	Sigma Aldrich, St. Louis, MO
NaBH4	Sigma Aldrich, St. Louis, MO
NaI	Fisher Scientific, Fair Lawn, New Jersey
NIH clinical collection	Evotec, South San Francisco, CA
Ni-NTA beads	Novagen, San Diego, CA
One Shot BL21 (DE3) cells	Invitrogen, Carlsbad, CA
Pb(NO3)2	Sigma Aldrich, St. Louis, MO
PD10 Column	GE Healthcare, Buckinghamshire, UK
PEG/Ion HT	Hampton Research, Aliso Viejo, CA
PEG-MME 2000	Hampton Research, Aliso Viejo, CA
PEG 400	Hampton Research, Aliso Viejo, CA
PEG 3350	Hampton Research, Aliso Viejo, CA
Protease Inhibitors	Roche Applied Science, Mannheim, Germany
Pteroyl-Glu_3	Schircks Laboratories, Jona, Switzerland
S-Adenosylhomocysteine	Sigma Aldrich, St. Louis, MO
SDS	Sigma Aldrich, St. Louis, MO
Size Exclusion Column (S200 16/60)	GE healthcare, Stockholm, Sweden
Sypro® Orange dye	Invitrogen, Oregon, CA
Temed	Sigma Aldrich, St. Louis, MO
Trizma HCl	Sigma Aldrich, St. Louis, MO
Tryptone peptone	Difco Laboratories, Detroit, MI
VDX (24 well) plate	Hampton Research, Aliso Viejo, CA
Zeba^{Tm} Micro spin desalting column (7K)	Thermo Scientific, Rockford, IL
ZnSO4	Acros organics, Morris, New Jersey
5-methyl-THF-Glu_3	Schircks Laboratories, Jona, Switzerland
96 well Intelli-plate	Hampton Research, Aliso Viejo, CA
96 Well polypropylene plate	Roche Applied Science, Mannheim, Germany

References

Adams, P. D., P. V. Afonine, G. Bunkoczi, V. B. Chen, I. W. Davis, N. Echols, J. J. Headd, L. W. Hung, G. J. Kapral, R. W. Grosse-Kunstleve, A. J. McCoy, N. W. Moriarty, R. Oeffner, R. J. Read, D. C. Richardson, J. S. Richardson, T. C. Terwilliger and P. H. Zwart (2010). "PHENIX: a comprehensive Python-based system for macromolecular structure solution." Acta Crystallogr D Biol Crystallogr 66(Pt 2): 213-221.

Alberts, I. L., K. Nadassy and S. J. Wodak (1998). "Analysis of zinc binding sites in protein crystal structures." Protein Sci 7(8): 1700-1716.

Andreini, C., I. Bertini and G. Cavallaro (2011). "Minimal functional sites allow a classification of zinc sites in proteins." PLoS One 6(10): e26325.

Appling, D. R. (1991). "Compartmentation of folate-mediated one-carbon metabolism in eukaryotes." FASEB J 5(12): 2645-2651.

Auld, D. S. (2001). "Zinc coordination sphere in biochemical zinc sites." Biometals 14(3-4): 271-313.

Baker, P. J., K. L. Britton, M. Fisher, J. Esclapez, C. Pire, M. J. Bonete, J. Ferrer and D. W. Rice (2009). "Active site dynamics in the zinc-dependent medium chain alcohol dehydrogenase superfamily." Proc Natl Acad Sci U S A 106(3): 779-784.

Banerjee, R. (1997). "The Yin-Yang of cobalamin biochemistry." Chem Biol 4(3): 175-186.

Banerjee, R. V., V. Frasca, D. P. Ballou and R. G. Matthews (1990). "Participation of cob(I) alamin in the reaction catalyzed by methionine synthase from Escherichia coli: a steady-state and rapid reaction kinetic analysis." Biochemistry 29(50): 11101-11109.

Banerjee, R. V. and R. G. Matthews (1990). "Cobalamin-dependent methionine synthase." FASEB J 4(5): 1450-1459.

Basavanna, S., S. Chimalapati, A. Maqbool, B. Rubbo, J. Yuste, R. J. Wilson, A. Hosie, A. D. Ogunniyi, J. C. Paton, G. Thomas and J. S. Brown (2013). "The effects of methionine acquisition and synthesis on Streptococcus pneumoniae growth and virulence." PLoS One 8(1): e49638.

Basu, P. and S. J. Burgmayer (2011). "Pterin chemistry and its relationship to the molybdenum cofactor." Coord Chem Rev 255(9-10): 1016-1038.

Blakley, R. L. (1969). The Biochemistry of Folic Acid and Related Pteridines, North-Holland

Brand, U., M. Rombach, J. Seebacher and H. Vahrenkamp (2001). "Functional modeling of cobalamine-independent methionine synthase with pyrazolylborate-zinc-thiolate complexes." Inorg Chem 40(24): 6151-6157.

Brosnan, J. T. and M. E. Brosnan (2006). "The sulfur-containing amino acids: an overview." J Nutr 136(6 Suppl): 1636S-1640S.

Burley, S. K. and G. A. Petsko (1985). "Aromatic-aromatic interaction: a mechanism of protein structure stabilization." Science 229(4708): 23-28.

Castro, C., A. A. Gratson, J. C. Evans, J. Jiracek, M. Collinsova, M. L. Ludwig and T. A. Garrow (2004). "Dissecting the catalytic mechanism of betaine-homocysteine S-methyltransferase by use of intrinsic tryptophan fluorescence and site-directed mutagenesis." Biochemistry 43(18): 5341-5351.

Cathou, R. E. and J. M. Buchanan (1963). "Enzymatic synthesis of the methyl group of methionine. V. Studies with 5, 10-methylenetetrahydrofolate reductase from Escherichia coli." J Biol Chem 238: 1746-1751.

Chabner, B. A., C. J. Allegra, G. A. Curt, N. J. Clendeninn, J. Baram, S. Koizumi, J. C. Drake and J. Jolivet (1985). "Polyglutamation of methotrexate. Is methotrexate a prodrug?" J Clin Invest 76(3): 907-912.

Collaborative Computational Project, N. (1994). "The CCP4 suite: programs for protein crystallography." Acta Crystallogr D Biol Crystallogr 50(Pt 5): 760-763.

Cooper, D. R., T. Boczek, K. Grelewska, M. Pinkowska, M. Sikorska, M. Zawadzki and Z. Derewenda (2007). "Protein crystallization by surface entropy reduction: optimization of the SER strategy." Acta Crystallogr D Biol Crystallogr 63(Pt 5): 636-645.

Copeland, R. A. (2005). Evaluation of Enzyme Inhibitors in Drug Discovery, John Wiley & Sons.

Coyle, P., J. C. Philcox, L. C. Carey and A. M. Rofe (2002). "Metallothionein: the multipurpose protein." Cell Mol Life Sci 59(4): 627-647.

Das, I., P. Nightingale, M. Patel and P. Jumaa (2011). "Epidemiology, clinical characteristics, and outcome of candidemia: experience in a tertiary referral center in the UK." Int J Infect Dis 15(11): e759-763.

Daubner, S. C., J. L. Schrimsher, F. J. Schendel, M. Young, S. Henikoff, D. Patterson, J. Stubbe and S. J. Benkovic (1985). "A multifunctional protein possessing glycinamide ribonucleotide synthetase, glycinamide ribonucleotide transformylase, and aminoimidazole ribonucleotide synthetase activities in de novo purine biosynthesis." Biochemistry 24(25): 7059-7062.

Davies, J. F., 2nd, T. J. Delcamp, N. J. Prendergast, V. A. Ashford, J. H. Freisheim and J. Kraut (1990). "Crystal structures of recombinant human dihydrofolate reductase complexed with folate and 5-deazafolate." Biochemistry 29(40): 9467-9479.

Dixon, M. M., S. Huang, R. G. Matthews and M. Ludwig (1996). "The structure of the C-terminal domain of methionine synthase: presenting S-adenosylmethionine for reductive methylation of B12." Structure 4(11): 1263-1275.

Drennan, C. L., S. Huang, J. T. Drummond, R. G. Matthews and M. L. Lidwig (1994). "How a protein binds B12: A 3.0 A X-ray structure of B12-binding domains of methionine synthase." Science 266(5191): 1669-1674.

Drennan, C. L., R. G. Matthews and M. L. Ludwig (1994). "Cobalamin-dependent methionine synthase: the structure of a methylcobalamin-binding fragment and implications for other B12-dependent enzymes." Curr Opin Struct Biol 4(6): 919-929.

Drummond, J. T., J. Jarrett, J. C. Gonzalez, S. Huang and R. G. Matthews (1995). "Characterization of nonradioactive assays for cobalamin-dependent and cobalamin-independent methionine synthase enzymes." Anal Biochem 228(2): 323-329.

Eadsforth, T. C., S. Cameron and W. N. Hunter (2012). "The crystal structure of Leishmania major N(5),N(10)-methylenetetrahydrofolate dehydrogenase/cyclohydrolase and assessment of a potential drug target." Mol Biochem Parasitol 181(2): 178-185.

Eckermann, C., J. Eichel and J. Schroder (2000). "Plant methionine synthase: new insights into properties and expression." Biol Chem 381(8): 695-703.

Edmond, M. B., S. E. Wallace, D. K. McClish, M. A. Pfaller, R. N. Jones and R. P. Wenzel (1999). "Nosocomial bloodstream infections in United States hospitals: a three-year analysis." Clin Infect Dis 29(2): 239-244.

Eichel, J., J. C. Gonzalez, M. Hotze, R. G. Matthews and J. Schroder (1995). "Vitamin-B12-independent methionine synthase from a higher plant (Catharanthus roseus). Molecular characterization, regulation, heterologous expression, and enzyme properties." Eur J Biochem 230(3): 1053-1058.

Ellman, G. L. (1959). "Tissue sulfhydryl groups." Arch Biochem Biophys 82(1): 70-77.

Emsley, P. and K. Cowtan (2004). "Coot: model-building tools for molecular graphics." Acta Crystallogr D Biol Crystallogr 60(Pt 12 Pt 1): 2126-2132.

Evans, J. C., D. P. Huddler, M. T. Hilgers, G. Romanchuk, R. G. Matthews and M. L. Ludwig (2004). "Structures of the N-terminal modules imply large domain motions during catalysis by methionine synthase." Proc Natl Acad Sci U S A 101(11): 3729-3736.

Evans, J. C., D. P. Huddler, J. Jiracek, C. Castro, N. S. Millian, T. A. Garrow and M. L. Ludwig (2002). "Betaine-homocysteine methyltransferase: zinc in a distorted barrel." Structure 10(9): 1159-1171.

Falagas, M. E., N. Roussos and K. Z. Vardakas (2010). "Relative frequency of albicans and the various non-albicans Candida spp among candidemia isolates from inpatients in various parts of the world: a systematic review." Int J Infect Dis 14(11): e954-966.

Ferrer, J. L., S. Ravanel, M. Robert and R. Dumas (2004). "Crystal structures of cobalamin-independent methionine synthase complexed with zinc, homocysteine, and methyltetrahydrofolate." J Biol Chem 279(43): 44235-44238.

Finer-Moore, J. S., D. V. Santi and R. M. Stroud (2003). "Lessons and conclusions from dissecting the mechanism of a bisubstrate enzyme: thymidylate synthase mutagenesis, function, and structure." Biochemistry 42(2): 248-256.

Fontecave, M., M. Atta and E. Mulliez (2004). "S-adenosylmethionine: nothing goes to waste." Trends Biochem Sci 29(5): 243-249.

Fontecilla-Camps, J. C., Bugg, C.E., Temple, C., Rose, J.D., Montgomery, J.A., Kisliuk, R.L. (1979). "Absolute configuration of biological tetrahydrofolates. A crystallographic determination." Journal of the American Chemical Society 101(20): 6114-6115.

Fu, T. M., J. Almqvist, Y. H. Liang, L. Li, Y. Huang and X. D. Su (2011). "Crystal structures of cobalamin-independent methionine synthase (MetE) from Streptococcus mutans: a dynamic zinc-inversion model." J Mol Biol 412(4): 688-697.

Fujita, Y., E. Ukena, H. Iefuji, Y. Giga-Hama and K. Takegawa (2006). "Homocysteine accumulation causes a defect in purine biosynthesis: further characterization of Schizosaccharomyces pombe methionine auxotrophs." Microbiology 152(Pt 2): 397-404.

Garg, D., S. Henrich, O. M. Salo-Ahen, H. Myllykallio, M. P. Costi and R. C. Wade (2010). "Novel approaches for targeting thymidylate synthase to overcome the resistance and toxicity of anticancer drugs." J Med Chem 53(18): 6539-6549.

Gillespie, R. J., Robinson, E.A. (1998). Advances in Molecular Structure Research, JAI Press LTD.

Goldschmidt, L., D. R. Cooper, Z. S. Derewenda and D. Eisenberg (2007). "Toward rational protein crystallization: A Web server for the design of crystallizable protein variants." Protein Sci 16(8): 1569-1576.

Gonzalez, B., M. A. Pajares, M. Martinez-Ripoll, T. L. Blundell and J. Sanz-Aparicio (2004). "Crystal structure of rat liver betaine homocysteine s-methyltransferase reveals new oligomerization features and conformational changes upon substrate binding." J Mol Biol 338(4): 771-782.

Gonzalez, J. C., R. V. Banerjee, S. Huang, J. S. Sumner and R. G. Matthews (1992). "Comparison of cobalamin-independent and cobalamin-dependent methionine

synthases from Escherichia coli: two solutions to the same chemical problem." Biochemistry 31(26): 6045-6056.

Gonzalez, J. C., K. Peariso, J. E. Penner-Hahn and R. G. Matthews (1996). "Cobalamin-independent methionine synthase from Escherichia coli: a zinc metalloenzyme." Biochemistry 35(38): 12228-12234.

Goulding, C. W., D. Postigo and R. G. Matthews (1997). "Cobalamin-dependent methionine synthase is a modular protein with distinct regions for binding homocysteine, methyltetrahydrofolate, cobalamin, and adenosylmethionine." Biochemistry 36(26): 8082-8091.

Gruber, K. and C. Kratky (2001). Cobalamin-Dependent Methionine Synthase. Handbook of Metalloproteins., John Wiley & Sons, Ltd.

Hall, D. A., T. C. Jordan-Starck, R. O. Loo, M. L. Ludwig and R. G. Matthews (2000). "Interaction of flavodoxin with cobalamin-dependent methionine synthase." Biochemistry 39(35): 10711-10719.

Hatanaka, H., N. Ariga, J. Nagai and H. Katsuki (1974). "Accumulation of a sterol intermediate during reaction in the presence of homocysteine with cell-free extract of yeast." Biochem Biophys Res Commun 60(2): 787-793.

Hatzios, S. K. and C. R. Bertozzi (2011). "The regulation of sulfur metabolism in Mycobacterium tuberculosis." PLoS Pathog 7(7): e1002036.

Herbig, K., E. P. Chiang, L. R. Lee, J. Hills, B. Shane and P. J. Stover (2002). "Cytoplasmic serine hydroxymethyltransferase mediates competition between folate-dependent deoxyribonucleotide and S-adenosylmethionine biosyntheses." J Biol Chem 277(41): 38381-38389.

Ho, T. L., H. C. Ho and L. D. Hamilton (1978). "Biochemical significance of the hard and soft acids and bases principle." Chem Biol Interact 23(1): 65-84.

Holmes, W. B. and D. R. Appling (2002). "Cloning and characterization of methenyltetrahydrofolate synthetase from Saccharomyces cerevisiae." J Biol Chem 277(23): 20205-20213.

Huffnagle, G. B. and M. C. Noverr (2013). "The emerging world of the fungal microbiome." Trends Microbiol 21(7): 334-341.

Jakubowski, H. (1999). "Protein homocysteinylation: possible mechanism underlying pathological consequences of elevated homocysteine levels." FASEB J 13(15): 2277-2283.

Kacprzak, M. M., I. Lewandowska, R. G. Matthews and A. Paszewski (2003). "Transcriptional regulation of methionine synthase by homocysteine and choline in Aspergillus nidulans." Biochem J 376(Pt 2): 517-524.

Kallen, R. G. and W. P. Jencks (1966). "The dissociation constants of tetrahydrofolic acid." J Biol Chem 241(24): 5845-5850.

Kaur, S. and P. Mishra (1991). "Amino acid uptake as a function of differentiation in Candida albicans: studies of a non-germinative variant." FEMS Microbiol Lett 66(3): 341-344.

Kim, B. S., Y. S. Jeon and J. Chun (2013). "Current Status and Future Promise of the Human Microbiome." Pediatr Gastroenterol Hepatol Nutr 16(2): 71-79.

Kim, Y. G. and S. Maas (2000). "Multiple site mutagenesis with high targeting efficiency in one cloning step." Biotechniques 28(2): 196-198.

Kleifeld, O., A. Frenkel, J. M. Martin and I. Sagi (2003). "Active site electronic structure and dynamics during metalloenzyme catalysis." Nat Struct Biol 10(2): 98-103.

Kohls, D., T. Sulea, E. O. Purisima, R. E. MacKenzie and A. Vrielink (2000). "The crystal structure of the formiminotransferase domain of formiminotransferase-cyclodeaminase: implications for substrate channeling in a bifunctional enzyme." Structure 8(1): 35-46.

Koutmos, M., S. Datta, K. A. Pattridge, J. L. Smith and R. G. Matthews (2009). "Insights into the reactivation of cobalamin-dependent methionine synthase." Proc Natl Acad Sci U S A 106(44): 18527-18532.

Koutmos, M., R. Pejchal, T. M. Bomer, R. G. Matthews, J. L. Smith and M. L. Ludwig (2008). "Metal active site elasticity linked to activation of homocysteine in methionine synthases." Proc Natl Acad Sci U S A 105(9): 3286-3291.

Krcmery, V. and A. J. Barnes (2002). "Non-albicans Candida spp. causing fungaemia: pathogenicity and antifungal resistance." J Hosp Infect 50(4): 243-260.

Krissinel, E. and K. Henrick (2004). "Secondary-structure matching (SSM), a new tool for fast protein structure alignment in three dimensions." Acta Crystallogr D Biol Crystallogr 60(Pt 12 Pt 1): 2256-2268.

Krissinel, E. and K. Henrick (2007). "Inference of macromolecular assemblies from crystalline state." J Mol Biol 372(3): 774-797.

Krupenko, S. A. (2009). "FDH: an aldehyde dehydrogenase fusion enzyme in folate metabolism." Chem Biol Interact 178(1-3): 84-93.

Kwon, K., C. Cao and J. T. Stivers (2003). "A novel zinc snap motif conveys structural stability to 3-methyladenine DNA glycosylase I." J Biol Chem 278(21): 19442-19446.

Lai, C. C., C. K. Tan, Y. T. Huang, P. L. Shao and P. R. Hsueh (2008). "Current challenges in the management of invasive fungal infections." J Infect Chemother 14(2): 77-85.

Laity, J. H., B. M. Lee and P. E. Wright (2001). "Zinc finger proteins: new insights into structural and functional diversity." Curr Opin Struct Biol 11(1): 39-46.

Lee, Y. M. and C. Lim (2008). "Physical basis of structural and catalytic Zn-binding sites in proteins." J Mol Biol 379(3): 545-553.

Leslie, A. G. W. (1992). Joint CCP4 and ESF-EACMB Newsletter on Protein Crystallography(27): 7.

Lindskog, S. (1997). "Structure and mechanism of carbonic anhydrase." Pharmacol Ther 74(1): 1-20.

Liptak, M. D., S. Datta, R. G. Matthews and T. C. Brunold (2008). "Spectroscopic study of the cobalamin-dependent methionine synthase in the activation conformation: effects of the Y1139 residue and S-adenosylmethionine on the B12 cofactor." J Am Chem Soc 130(48): 16374-16381.

Litwach, G. (2008). Folic acid and Folates, Elsevier Inc.

Lovell, S. C., I. W. Davis, W. B. Arendall, 3rd, P. I. de Bakker, J. M. Word, M. G. Prisant, J. S. Richardson and D. C. Richardson (2003). "Structure validation by Calpha geometry: phi,psi and Cbeta deviation." Proteins 50(3): 437-450.

Maden, B. E. (2000). "Tetrahydrofolate and tetrahydromethanopterin compared: functionally distinct carriers in C1 metabolism." Biochem J 350 Pt 3: 609-629.

Maret, W. and Y. Li (2009). "Coordination dynamics of zinc in proteins." Chem Rev 109(10): 4682-4707.

Matthews, R. G. and C. W. Goulding (1997). "Enzyme-catalyzed methyl transfers to thiols: the role of zinc." Curr Opin Chem Biol 1(3): 332-339.

Matthews, R. G., A. E. Smith, Z. S. Zhou, R. E. Taurog, V. Bandarian, J. C. Evans and M. Ludwig (2003). "Cobalamin-Dependent and Cobalamin-Independent Methionine Synthases: Are there two solutions to the same chemical problem?" Helvetica Chimica Acta 86(12): 3939-3954.

Maurer-Stroh, S., S. Washietl and F. Eisenhaber (2003). "Protein prenyltransferases." Genome Biol 4(4): 212.

Mayer, F. L., D. Wilson and B. Hube (2013). "Candida albicans pathogenicity mechanisms." Virulence 4(2): 119-128.

McCall, K. A., C. Huang and C. A. Fierke (2000). "Function and mechanism of zinc metalloenzymes." J Nutr 130(5S Suppl): 1437S-1446S.

McCoy, A. J., Grosse-Kunstleve, R.W., Adams, P.D., Winn, M.D., Storoni, L.C., Read, R.J. (2007). "Phaser crystallographic software." Journal of Applied Crystallography 40: 16.

McCully, K. S. (2009). "Chemical pathology of homocysteine. IV. Excitotoxicity, oxidative stress, endothelial dysfunction, and inflammation." Ann Clin Lab Sci 39(3): 219-232.

McGuire, J. J. and J. C. Rabinowitz (1978). "Studies on the mechanism of formyltetrahydrofolate synthetase. The Peptococcus aerogenes enzyme." J Biol Chem 253(4): 1079-1085.

Millian, N. S. and T. A. Garrow (1998). "Human betaine-homocysteine methyltransferase is a zinc metalloenzyme." Arch Biochem Biophys 356(1): 93-98.

Moyes, D. L. and J. R. Naglik (2011). "Mucosal immunity and Candida albicans infection." Clin Dev Immunol 2011: 346307.

Murshudov, G. N., A. A. Vagin and E. J. Dodson (1997). "Refinement of macromolecular structures by the maximum-likelihood method." Acta Crystallogr D Biol Crystallogr 53(Pt 3): 240-255.

Niesen, F. H., H. Berglund and M. Vedadi (2007). "The use of differential scanning fluorimetry to detect ligand interactions that promote protein stability." Nat Protoc 2(9): 2212-2221.

Oefner, C., A. D'Arcy and F. K. Winkler (1988). "Crystal structure of human dihydrofolate reductase complexed with folate." Eur J Biochem 174(2): 377-385.

Otwinowski, Z. (1997). "Processing of X-ray Diffraction Data Collected in Oscillation Mode." Methods in Enzymology 276: 20.

Pajares, M. A. and D. Perez-Sala (2006). "Betaine homocysteine S-methyltransferase: just a regulator of homocysteine metabolism?" Cell Mol Life Sci 63(23): 2792-2803.

Parks, L. W. and W. M. Casey (1995). "Physiological implications of sterol biosynthesis in yeast." Annu Rev Microbiol 49: 95-116.

Pascon, R. C., T. M. Ganous, J. M. Kingsbury, G. M. Cox and J. H. McCusker (2004). "Cryptococcus neoformans methionine synthase: expression analysis and requirement for virulence." Microbiology 150(Pt 9): 3013-3023.

Peariso, K., Goulding, C.W., Huang, S., Matthews, R.G., Penner-Hahn, J.E. (1998). "Characterization of the Zinc Binding Site in Methionine Synthase Enzymes of Escherichia coli: The Role of Zinc in the Methylation of Homocysteine." Journal of The American Chemical Society 120(33): 8410-8416.

Peariso, K., Z. S. Zhou, A. E. Smith, R. G. Matthews and J. E. Penner-Hahn (2001). "Characterization of the zinc sites in cobalamin-independent and cobalamin-dependent methionine synthase using zinc and selenium X-ray absorption spectroscopy." Biochemistry 40(4): 987-993.

Pejchal, R. and M. L. Ludwig (2005). "Cobalamin-independent methionine synthase (MetE): a face-to-face double barrel that evolved by gene duplication." PLoS Biol 3(2): e31.

Pfaller, M. A., R. N. Jones, G. V. Doern, H. S. Sader, R. J. Hollis and S. A. Messer (1998). "International surveillance of bloodstream infections due to Candida species: frequency of occurrence and antifungal susceptibilities of isolates collected in 1997 in the United States, Canada, and South America for the SENTRY Program. The SENTRY Participant Group." J Clin Microbiol 36(7): 1886-1889.

Picot, D., G. Ohanessian and G. Frison (2008). "The alkylation mechanism of zinc-bound thiolates depends upon the zinc ligands." Inorg Chem 47(18): 8167-8178.

Plener, L., P. Boistard, A. Gonzalez, C. Boucher and S. Genin (2012). "Metabolic adaptation of Ralstonia solanacearum during plant infection: a methionine biosynthesis case study." PLoS One 7(5): e36877.

Prasannan, P., H. S. Suliman and J. D. Robertus (2009). "Kinetic analysis of site-directed mutants of methionine synthase from Candida albicans." Biochem Biophys Res Commun 382(4): 730-734.

Rajilic-Stojanovic, M. (2013). "Function of the microbiota." Best Pract Res Clin Gastroenterol 27(1): 5-16.

Ranocha, P., F. Bourgis, M. J. Ziemak, D. Rhodes, D. A. Gage and A. D. Hanson (2000). "Characterization and functional expression of cDNAs encoding methionine-sensitive and -insensitive homocysteine S-methyltransferases from Arabidopsis." J Biol Chem 275(21): 15962-15968.

Rao, N. A., R. Talwar and H. S. Savithri (2000). "Molecular organization, catalytic mechanism and function of serine hydroxymethyltransferase--a potential target for cancer chemotherapy." Int J Biochem Cell Biol 32(4): 405-416.

Rees, D. C., M. Lewis, R. B. Honzatko, W. N. Lipscomb and K. D. Hardman (1981). "Zinc environment and cis peptide bonds in carboxypeptidase A at 1.75-A resolution." Proc Natl Acad Sci U S A 78(6): 3408-3412.

Rizzetto, L. and D. Cavalieri (2011). "Friend or foe: using systems biology to elucidate interactions between fungi and their hosts." Trends Microbiol 19(10): 509-515.

Roe, A. J., C. O'Byrne, D. McLaggan and I. R. Booth (2002). "Inhibition of Escherichia coli growth by acetic acid: a problem with methionine biosynthesis and homocysteine toxicity." Microbiology 148(Pt 7): 2215-2222.

Sardi, J. C., L. Scorzoni, T. Bernardi, A. M. Fusco-Almeida and M. J. Mendes Giannini (2013). "Candida species: current epidemiology, pathogenicity, biofilm formation, natural antifungal products and new therapeutic options." J Med Microbiol 62(Pt 1): 10-24.

Savitsky, P., J. Bray, C. D. Cooper, B. D. Marsden, P. Mahajan, N. A. Burgess-Brown and O. Gileadi (2010). "High-throughput production of human proteins for crystallization: the SGC experience." J Struct Biol 172(1): 3-13.

Schnell, J. R., H. J. Dyson and P. E. Wright (2004). "Structure, dynamics, and catalytic function of dihydrofolate reductase." Annu Rev Biophys Biomol Struct 33: 119-140.

Scott, J. M. (1999). "Folate and vitamin B12." Proc Nutr Soc 58(2): 441-448.

Selhub, J. (1999). "Homocysteine metabolism." Annu Rev Nutr 19: 217-246.

Seong, K., Z. Hou, M. Tracy, H. C. Kistler and J. R. Xu (2005). "Random Insertional Mutagenesis Identifies Genes Associated with Virulence in the Wheat Scab Fungus Fusarium graminearum." Phytopathology 95(7): 744-750.

Smith, A. E. and R. G. Matthews (2000). "Protonation state of methyltetrahydrofolate in a binary complex with cobalamin-dependent methionine synthase." Biochemistry 39(45): 13880-13890.

Solomon, P. S., P. S. Nielsen, A. J. Clark and R. P. Oliver (2000). "Methionine synthase, a gene required for methionine synthesis, is expressed in planta by Cladosporium fulvum." Mol Plant Pathol 1(5): 315-323.

Sophianopoulou, V. and G. Diallinas (1995). "Amino acid transporters of lower eukaryotes: regulation, structure and topogenesis." FEMS Microbiol Rev 16(1): 53-75.

Stover, P. J. and M. S. Field (2011). "Trafficking of intracellular folates." Adv Nutr 2(4): 325-331.

Suliman, H. S., D. R. Appling and J. D. Robertus (2007). "The gene for cobalamin-independent methionine synthase is essential in Candida albicans: a potential antifungal target." Arch Biochem Biophys 467(2): 218-226.

Suliman, H. S., G. M. Sawyer, D. R. Appling and J. D. Robertus (2005). "Purification and properties of cobalamin-independent methionine synthase from Candida albicans and Saccharomyces cerevisiae." Arch Biochem Biophys 441(1): 56-63.

Szegedi, S. S., C. C. Castro, M. Koutmos and T. A. Garrow (2008). "Betaine-homocysteine S-methyltransferase-2 is an S-methylmethionine-homocysteine methyltransferase." J Biol Chem 283(14): 8939-8945.

Takahashi, H., S. Kopriva, M. Giordano, K. Saito and R. Hell (2011). "Sulfur assimilation in photosynthetic organisms: molecular functions and regulations of transporters and assimilatory enzymes." Annu Rev Plant Biol 62: 157-184.

Tannock, G. W. (1995). Normal Microflora: An introduction to Microbes inhabiting the Human Body, Chapman & Hall.

Taurog, R. E., H. Jakubowski and R. G. Matthews (2006). "Synergistic, random sequential binding of substrates in cobalamin-independent methionine synthase." Biochemistry 45(16): 5083-5091.

Taurog, R. E. and R. G. Matthews (2006). "Activation of methyltetrahydrofolate by cobalamin-independent methionine synthase." Biochemistry 45(16): 5092-5102.

Thanbichler, M., B. Neuhierl and A. Bock (1999). "S-methylmethionine metabolism in Escherichia coli." J Bacteriol 181(2): 662-665.

Thomas, D. and Y. Surdin-Kerjan (1997). "Metabolism of sulfur amino acids in Saccharomyces cerevisiae." Microbiol Mol Biol Rev 61(4): 503-532.

Tibbetts, A. S. and D. R. Appling (2010). "Compartmentalization of Mammalian folate-mediated one-carbon metabolism." Annu Rev Nutr 30: 57-81.

Ubhi, D., K. L. Kavanagh, A. F. Monzingo and J. D. Robertus (2011). "Structure of Candida albicans methionine synthase determined by employing surface residue mutagenesis." Arch Biochem Biophys 513(1): 19-26.

Uerre, J. A. and C. H. Miller (1966). "Preparation of L-homocysteine from L-homocysteine thiolactone." Anal Biochem 17(2): 310-315.

Vallee, B. L. and D. S. Auld (1990). "Zinc coordination, function, and structure of zinc enzymes and other proteins." Biochemistry 29(24): 5647-5659.

Wang, G., C. Strang, P. J. Pfaffinger and M. Covarrubias (2007). "Zn2+-dependent redox switch in the intracellular T1-T1 interface of a Kv channel." J Biol Chem 282(18): 13637-13647.

Weissbach, H. and N. Brot (1991). "Regulation of methionine synthesis in Escherichia coli." Mol Microbiol 5(7): 1593-1597.

Whitfield, C. D., E. J. Steers, Jr. and H. Weissbach (1970). "Purification and properties of 5-methyltetrahydropteroyltriglutamate-homocysteine transmethylase." J Biol Chem 245(2): 390-401.

Whitfield, C. D. and H. Weissbach (1970). "Binding of the folate substrate to 5-methyltetrahydropteroyltriglutamate-homocysteine transmethylase." J Biol Chem 245(2): 402-409.

Wilker, J. J. and S. J. Lippard (1997). "Alkyl Transfer to Metal Thiolates: Kinetics, Active Species Identification, and Relevance to the DNA Methyl Phosphotriester Repair Center of Escherichia coli Ada." Inorg Chem 36(6): 969-978.

Wipf, D., U. Ludewig, M. Tegeder, D. Rentsch, W. Koch and W. B. Frommer (2002). "Conservation of amino acid transporters in fungi, plants and animals." Trends Biochem Sci 27(3): 139-147.

Wright, D. L. and A. C. Anderson (2011). "Antifolate agents: a patent review (2006 - 2010)." Expert Opin Ther Pat 21(9): 1293-1308.

Yeo, E. J. and C. Wagner (1992). "Purification and properties of pancreatic glycine N-methyltransferase." J Biol Chem 267(34): 24669-24674.

Zeh, M., G. Leggewie, R. Hoefgen and H. Hesse (2002). "Cloning and characterization of a cDNA encoding a cobalamin-independent methionine synthase from potato (Solanum tuberosum L.)." Plant Mol Biol 48(3): 255-265.

Zhang, J. H., T. D. Chung and K. R. Oldenburg (1999). "A Simple Statistical Parameter for Use in Evaluation and Validation of High Throughput Screening Assays." J Biomol Screen 4(2): 67-73.

Zhou, Z. S., K. Peariso, J. E. Penner-Hahn and R. G. Matthews (1999). "Identification of the zinc ligands in cobalamin-independent methionine synthase (MetE) from Escherichia coli." Biochemistry 38(48): 15915-15926.

Zimny, J., M. Sikora, A. Guranowski and H. Jakubowski (2006). "Protective mechanisms against homocysteine toxicity: the role of bleomycin hydrolase." J Biol Chem 281(32): 22485-22492.

Vita

Devinder Kaur Ubhi was born in 1984 in Jalandhar, Punjab, India. She emigrated to the United States of America in 1992 with her family. In 2002 she entered the University of California at Davis and completed her Bachelor of Arts in German with honors and Bachelor of Science in Genetics with honors. As an undergraduate she completed a summer lab internship at Chiron Corporation in 2005 and at Novozymes in 2006. Upon graduating in 2006, she was hired as an Associate I in the QC Analytical Technology Department at Novartis Incorporated. In Fall of 2008 she entered graduate school at the University of Texas at Austin. Research has resulted in one publication and one in preparation:

Ubhi, D., K. L. Kavanagh, A. F. Monzingo and J. D. Robertus (2011). "Structure of Candida albicans methionine synthase determined by employing surface residue mutagenesis." Arch Biochem Biophys 513(1): 19-26.

Ubhi, D., G. Kago, A. F. Monzingo and J. D. Robertus (2013). "Structural analysis of the fungal methionine synthase with substrates and inhibitors." (in preparation).

Permanent email: dkubhi@gmail.com

This dissertation was typed by the author.